

**Spin Crossover Behavior of 1,3,4-Oxadiazole Based  
Dinuclear Iron(II) Complexes**

und

**Functionalized Phosphonates as Bridging Ligands in  
Inorganic-Organic Hybrid-Materials**

**Dissertation**

zur Erlangung des Grades  
"Doktor der Naturwissenschaften"  
im Promotionsfach Chemie

am Fachbereich Chemie, Pharmazie und Geowissenschaften  
der Johannes Gutenberg-Universität in Mainz

vorgelegt von

**Christian Köhler**

geboren in Berlin

Mainz, 2016



Die vorliegende Arbeit wurde in der Zeit vom April 2013 bis Mai 2016 im Institut für Anorganische Chemie und Analytische Chemie der Johannes Gutenberg-Universität Mainz unter Anleitung von [REDACTED] angefertigt.

Ich versichere, dass ich diese Arbeit selbstständig verfasst und keine anderen als die angegebenen Quellen und Hilfsmittel benutzt habe.

Mainz, den 11.05.2016

Dekan: [REDACTED]

Erster Berichterstatter: [REDACTED]

Zweiter Berichterstatter: [REDACTED]



## Acknowledgment

Before all others, I want to thank my supervisor, [REDACTED], for letting me become part of her group and spent my time there as a doctoral candidate. I appreciate the trust she put in me, when she enabled me to work independently, and the encouragement and guidance she offered when things were not going smoothly.

I want to thank [REDACTED] for the enlightening and helpful conversation regarding X-ray structure analysis and [REDACTED] and [REDACTED] for the Mössbauer measurements. I kindly acknowledge [REDACTED] for the support during NMR measurements, and [REDACTED] for X-ray diffraction measurements.

Especially I want to thank the current members of the [REDACTED] group as well as the people who have finished recently and a little while ago. I enjoyed every barbeque we had, every field trip we made (especially the seminar in the shack), the occasional and spontaneous get-together and all the other great stuff we did and laughed about. It was a real great pleasure to work with you and getting to know you all.

I am really grateful for meeting all the people, who accompanied me during my time as a (PhD) student. You really ensured, that the time I spent at the university became truly memorable! No matter how demanding or boring lectures and learning was, you made everything somehow become fun. Even the time during lab courses felt like hanging out. A special thanks to [REDACTED]

I would like to express my deep gratitude to my parents, sisters, grandparents, uncle and aunt, who supported me in every thinkable way, who always stood by my side no matter what, and who never doubted me. Thank you!

Finally, I want to thank [REDACTED] not only for her never ending support during rough times, but also for the beautiful times we had and are about to have.



---

# Contents

<b>I. 1,3,4-Oxadiazole Based Spin Crossover Compounds</b>	<b>1</b>
<b>1. Introduction</b>	<b>5</b>
1.1. Theory . . . . .	5
1.1.1. Ligand Field Theory . . . . .	5
1.1.2. Spin Crossover . . . . .	6
1.1.3. Characteristics of Spin Transition . . . . .	9
1.1.4. Cooperative Effects . . . . .	11
1.1.5. Solvent and Anion Effects . . . . .	12
1.1.6. Occurrence of Spin Transition . . . . .	14
1.1.7. Structural Considerations . . . . .	15
1.2. Detection of Spin Crossover . . . . .	16
1.2.1. Magnetic Measurements . . . . .	16
1.2.2. Single Crystal X-Ray Diffraction . . . . .	17
1.2.3. Mössbauer-Spectroscopy . . . . .	17
1.2.4. Other Methods . . . . .	18
1.3. Ligand Considerations . . . . .	19
1.4. Mono-, Di- and Polynuclear Compounds . . . . .	20
<b>2. Objective and Aims</b>	<b>22</b>
<b>3. Oxadiazole Based Spin Crossover Compounds</b>	<b>25</b>
3.1. Introduction . . . . .	25
3.2. Abstract . . . . .	27
3.3. Introduction . . . . .	27
3.4. Results and Discussion . . . . .	28
3.4.1. Syntheses . . . . .	28
3.4.2. Crystal Structures . . . . .	29

3.4.3. Magnetic Measurement and Mössbauer-spectroscopy . . . . .	34
3.5. Conclusion . . . . .	37
3.6. Experimental Section . . . . .	38
3.7. Acknowledgements . . . . .	40
3.8. References . . . . .	40
3.9. Supporting Information . . . . .	42
3.10. Summary . . . . .	53
<b>4. Further Investigations</b>	<b>55</b>
4.1. Modifications: Incorporation of Cobalt(II) . . . . .	55
4.2. Modifications: Coordinating Counterions . . . . .	57
4.3. Ligand Modifications: Blocking of H-Bonds . . . . .	59
<b>5. Summary and Outlook</b>	<b>61</b>
<b>II. Inorganic-Organic Hybrid Materials</b>	<b>65</b>
<b>6. Introduction</b>	<b>69</b>
6.1. Inorganic-Organic Hybrid-Materials . . . . .	69
6.2. Coordination Polymers . . . . .	71
6.3. Extended Inorganic Hybrids . . . . .	73
6.4. Mixed Inorganic-Organic Materials . . . . .	74
6.5. Applications of Hybrid-Materials . . . . .	76
6.6. Phosphonates in Hybrid-Materials . . . . .	76
6.6.1. Hydrothermal Synthesis . . . . .	77
6.6.2. Evolution of Phosphonate Compounds . . . . .	78
6.7. Recent Progress . . . . .	79
<b>7. Objectives and Aims</b>	<b>80</b>
<b>8. Phosphonate Based Inorganic-Organic Hybrid-Materials</b>	<b>82</b>
8.1. Introduction . . . . .	82
8.2. Abstract . . . . .	84
8.3. Introduction . . . . .	85



---

8.4. Results and Discussion . . . . .	86
8.4.1. Synthesis . . . . .	86
8.4.2. Crystal Structures . . . . .	88
8.4.3. Magnetic Properties . . . . .	95
8.5. Conclusion . . . . .	99
8.6. Experimental . . . . .	100
8.6.1. General methods and materials . . . . .	100
8.6.2. Synthesis . . . . .	101
8.7. Acknowledgements . . . . .	102
8.8. Notes and references . . . . .	103
8.9. Supporting Information . . . . .	107
<b>9. Further Investigations</b>	<b>116</b>
9.1. One-Dimensional Cobalt Chain . . . . .	116
9.2. Two-Dimensional Lanthanides . . . . .	119
9.2.1. Terbium Complex . . . . .	119
9.2.2. Dysprosium Complex . . . . .	122
9.3. Other Compounds . . . . .	125
9.3.1. Compound 13 . . . . .	126
9.3.2. Compounds 14, 15 and 16 . . . . .	127
<b>10. Summary and Perspective</b>	<b>129</b>
<b>11. Experimental Section</b>	<b>133</b>
11.1. Methods and Materials . . . . .	133
11.2. Syntheses . . . . .	135
11.2.1. Ligands . . . . .	135
11.2.2. Complexes . . . . .	137
11.2.2.1. Synthesis of $[\text{Co}_2(\mu_2\text{-L})_2](\text{ClO}_4)_4 \cdot 4\text{MeCN}$ (4) . . . . .	137
11.2.2.2. Synthesis of $[\text{NaL}_2]\text{BPh}_4$ (5) . . . . .	137
11.2.2.3. Synthesis of $[\text{Co}(\text{II})(\mu_2\text{-}\eta_2\text{-H}_3\text{L})_2]^*6\text{H}_2\text{O}$ (10) . . . . .	137
11.2.2.4. Synthesis of $[\text{Tb}(\mu_4\text{-H}_2\text{H}^{\text{M}})(\text{H}_2\text{O})_4]\text{Cl}_2 \cdot \text{H}_2\text{O}$ (11) . . . . .	138
11.2.2.5. Synthesis of $[\text{Dy}(\text{H}_2\text{H}^{\text{M}})_2]\text{ClHCl} \cdot 4\text{H}_2\text{O}$ (12) . . . . .	138

---

11.2.2.6. Synthesis of [Fe(II)(( <b>EtO</b> ) <sub>4</sub> <b>L</b> ) <sub>3</sub> ](BF <sub>4</sub> ) <sub>2</sub> (13)	138
11.2.2.7. Synthesis of [LaCo(III)( <b>H</b> <sub>2</sub> <b>L</b> ) <sub>3</sub> (H <sub>2</sub> O) <sub>3</sub> ]NaCl (14)	139
11.2.2.8. Synthesis of [GdCo(III)( <b>H</b> <sub>2</sub> <b>L</b> ) <sub>3</sub> (H <sub>2</sub> O) <sub>5</sub> ]NaCl (15)	139
11.2.2.9. Synthesis of [GdCo(III)( <b>H</b> <sub>2</sub> <b>L</b> ) <sub>3</sub> ] <sub>2</sub> (16)	139
<b>12. Bibliography</b>	<b>141</b>
<b>A. Abbreviations</b>	<b>151</b>
<b>B. NMR Spectra</b>	<b>153</b>
<b>C. Crystallographic Parameters</b>	<b>155</b>
<b>D. Curriculum Vitae</b>	<b>163</b>





## **Part I.**

# **Spin Crossover Behavior of 1,3,4-Oxadiazole Based Dinuclear Iron(II) Complexes**



## Kurzzusammenfassung

Die Fähigkeit einer Verbindung zwischen den elektronischen Zuständen *High-Spin* und *Low-Spin* zu wechseln wird Spin Crossover genannt. Der Wechsel des Zustandes kann durch eine Temperaturänderung, eine Druckänderung oder durch die Bestrahlung mit Licht hervorgerufen werden. Diese Schaltbarkeit ist in den meisten Fällen durch ein 3d Übergangsmetallion mit der Elektronenkonfiguration  $3d^4$  bis  $3d^7$  im oktaedrischen Ligandenfeld gegeben. Grundvoraussetzung stellt eine Koordinationsumgebung dar, die aufgrund geeigneter Ligandenfeldaufspaltung der d-Orbitale sowohl den *High-Spin* als auch den *Low-Spin* Zustand stabilisieren kann. Eines der am meisten untersuchten Metallionen ist in diesem Zusammenhang  $Fe^{2+}$ . Bei dem größten Teil dieser Verbindungen handelt es sich um einkernige Komplexe. Allerdings sind besonders dinukleare Verbindungen von großem Interesse, da zusätzlich zu intermolekularen auch intramolekulare Wechselwirkungen untersucht werden können. Zum Anderen ist neben dem reinen *HS* bzw. *LS* auch ein weiterer gemischter [*HS-LS*]-Zustand möglich.

Im Rahmen dieser Doktorarbeit wurde ein Ligand auf Basis eines symmetrischen 2,5-disubstituierten 1,3,4-Oxadiazols hergestellt und im Weiteren zur Komplexierung verschiedener Eisen(II)-Salze verwendet. Bei den so synthetisierten dinuklearen Verbindungen konnten durch Einkristall-Röntgendiffraktometrie, Mößbauer-Spektroskopie und magnetische Messungen die vielseitigen Spin Crossover Eigenschaften untersucht werden. Es wurde gezeigt, dass die zum Ladungsausgleich notwendigen Gegenionen das Übergangsverhalten durch klassische und nicht-klassische Wasserstoffbrücken maßgeblich beeinflussen können. Dabei ist nicht nur entscheidend, zu welcher Atomsorte des Gegenions Wasserstoffbrücken von einem Kation ausgebildet werden, sondern auch die Anzahl der Kontakte zwischen zwei benachbarten Kationen.

Weiterhin konnte der starke Einfluss von Flexibilität und Sterik des verwendeten Liganden aufgezeigt werden. Der Vergleich mit analogen Komplexen auf Basis von Thiadiazolen und Triazolen zeigt strukturelle Unterschiede sowie signifikant unterschiedliches Spin Crossover Verhalten. Beides ist auf die Substitution des Heteroatoms im Fünfring zurückzuführen. Die hier vorgestellten Verbindungen stellen somit ein ideales Modellsystem dar, um die Vielfältigkeit und Komplexität von Spin Crossover Verbindungen und die wichtige Rolle der intermolekularen Kontakte zu verdeutlichen.

## Abstract

The change between the electronic states *high-spin* and *low-spin* is called spin crossover or spin transition. The transition can be induced by a change in temperature, pressure, or the irradiation with light. The requirement for such properties is a 3d transition metal ion with the electronic configuration  $3d^4$  to  $3d^7$ . Crucial for the switchability is a coordination environment that can stabilize both, the *High-Spin* and *Low-Spin* state. Therefore, the ligand field has to have the appropriate strength to split the d-orbitals up to the point, where the preferred state is determined by the external stimuli. One of the most studied metal ions in this matter is probably iron(II) in an octahedral coordination geometry. Especially dinuclear compounds are of great interest because both, intermolecular and intramolecular interaction can be observed. Furthermore, a third mixed *[HS-LS]* state can occur.

Herein, several new compounds based on a symmetric 2,5-disubstituted 1,3,4-oxadiazole ligand are reported, that were synthesized using different iron(II) metal salts. With single crystal X-Ray diffraction, Mössbauer-spectroscopy and magnetic measurements, the spin crossover properties of the novel complexes were investigated. The measurements revealed a strong dependence on classical and non-classical hydrogen bonds between the complex cation and the counter ions: a change of the hydrogen bond acceptor at the counter ions results in a different spin crossover behavior. Additionally, the number of contacts between a cation and its next neighbors via hydrogen bonds mediated by the counterions has a strong influence on the nature of the spin transition. The steric hindrance and flexibility of the ligand has to be considered as well. Compared to analog complexes based on thiadiazole and triazole ligands, they differ not only on a structural level, but also significantly in their spin crossover characteristics. The origin for these changes is found in the substitution of the hetero atom in the five membered ring. This new family of oxadiazole based dinuclear iron(II) compounds is an ideal model system to illustrate the diversity and complexity of spin crossover compounds and pronounce the important part of intermolecular contacts.



# 1. Introduction

## 1.1. Theory

Spin crossover (SCO) or spin transition (ST) describes the change between the two electronic states *high-spin (HS)* and *low-spin (LS)* which is triggered by an external disturbance.<sup>[1,2]</sup> Since the first discovery of this phenomenon, the field has attracted a great deal of attention due to the broad variety of possible applications.<sup>[3]</sup> The unique properties of compounds showing SCO are attributed to several transformations which a molecule undergoes during that process.<sup>[4]</sup> The most prominent alterations between these states are the change of the magnetic moment, the switching of color and the contraction or enlargement of the complex due to changing bond lengths between ligand donor atom and metal ion.<sup>[5]</sup> In the following section the theoretical background and the origin of these features will be discussed in detail.

### 1.1.1. Ligand Field Theory

When a transition metal ion forms a complex by coordinating ligands, an electrostatic repulsion between the ligands and the metal ions electrons in the d-orbitals and is found. Depending on the coordination number and the geometry in which the ligands are approaching, the energy levels of the orbitals diverge in a specific pattern. In case of six donor atoms and an octahedral coordination geometry ( $O_h$ ), they split into two degenerated sets.<sup>[6]</sup> When ligands point directly towards an orbital, its energy level increases by  $0.6 \Delta_o$ . This is the case for the  $d_{x^2-y^2}$ - and  $d_{z^2}$ -orbitals, i.e. the  $e_g$ -orbitals, with antibonding character. The energy of the remaining  $t_{2g}$ -orbitals ( $d_{xy}$ -,  $d_{xz}$ - and  $d_{yz}$ -orbital) decreases in total by the same amount,  $0.4 \Delta_o$  for each one.<sup>[7]</sup> The difference in energy is the ligand field splitting  $\Delta_o$  (LFS) with a value of  $10 Dq$  and will be crucial for further SCO considerations.<sup>[8]</sup> The splitting is dependent on the repulsion between the electrons of the metal ion and the ligand. But a larger effective nuclear charge of a heavier element attracts a ligand more and forces the electrons of both

components into closer proximity. Therefore, heavier metal ions have a larger "natural" splitting.<sup>[9]</sup>

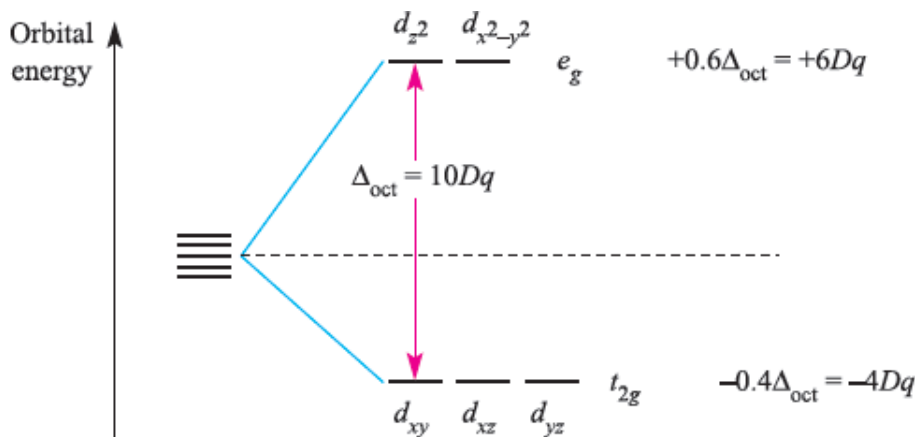


Figure 1.1.: Schematic representation of the d-orbital splitting in an octahedral ligand field.<sup>[9]</sup>

For up to three electrons, the metal orbitals can be filled in only one certain modification following Hund's rule. Any additional electron can occupy either the  $t_{2g}$ -orbitals as well or else the  $e_g$ -orbitals. In the first case, the system has to provide the spin-pairing energy  $P$ . This leads to the *low-spin*-state. In the second case, the  $e_g$ -orbitals are populated and the system loses energy by occupying antibonding orbitals, which results in the *high-spin*-state. By a comparison of  $P$  and the size of the LFS, the state of the system can be identified. Since the value of  $P$  is nearly constant, the LFS is the only variable which determines whether the *HS*-state or the *LS*-state is preferred.<sup>[7,8]</sup>

### 1.1.2. Spin Crossover

Only a small number of metal ions with certain electronic configurations can form compounds, where both states *high-spin* and *low-spin* can exist in an octahedral coordination environment. For obvious reasons, the main group metal ions can be ignored in that matter. The "natural" LFS of all transition metal ions apart from the 3d metal ions is very large, leaving nearly any system in the *low-spin*-state. Further more, the choice

between both states is only possible with an electronic configuration between  $3d^4$  and  $3d^7$ . In most cases the spin-state of a metal center in a given system is either *LS* or *HS* and will not undergo further changes. But if the LFS is at the threshold, where  $P$  is as large as the loss of energy by populating  $e_g$ -orbitals, it is possible to induce a transition of the spin-state with an external stimuli. This process is called spin crossover.

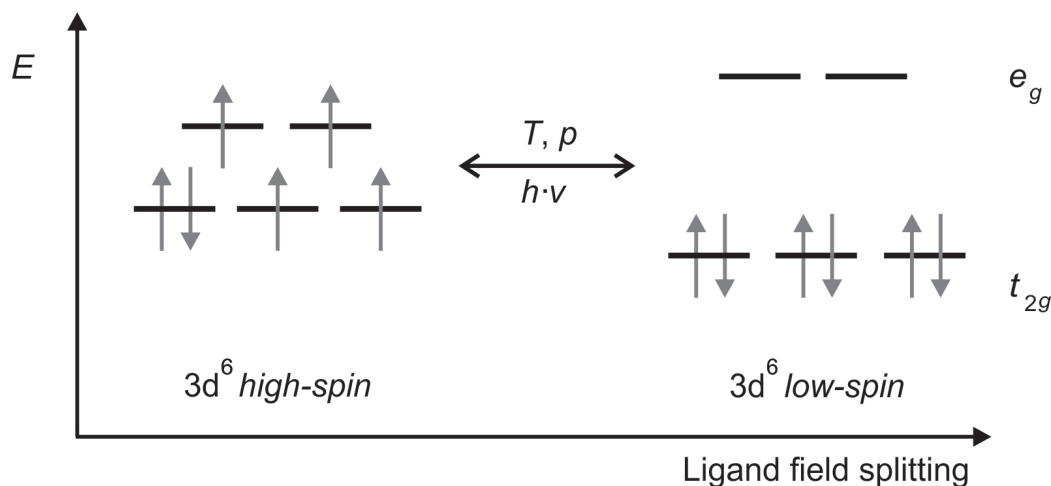


Figure 1.2.: Schematic representation of spin crossover for an iron(II) ion.

The magnitude of the d-orbital splitting is unique for every 3d metal ion and differs as well with the oxidation state of a metal. This becomes clear by a comparison of the two  $d^6$  metal ions Fe(II) and Co(III): both ions possess six d-electrons, but it is iron in the oxidation state +II dominating the field of spin crossover, whereas for cobalt in the oxidation state +III only a few reports are known.<sup>[10,11]</sup> Furthermore, a ligand system that allows spin-state switching in combination with an iron(II)-center will not do so with an cobalt(II)-center. As a consequence, the ligand environment must be specific for every metal in order to observe SCO.<sup>[12,13]</sup> Only then a transition can be triggered, either by a change in pressure, the irradiation with light or a change in temperature. Even though the effect of all three perturbations is the same, they all have a different origin. If hydrostatic pressure is applied on a sample, the distance between the ligands and the metal ion is reduced. By that, the electrostatic repulsion of the ligand and metal ions electrons increases, leading to a larger LFS. Additionally, the shortening of the bond lengths disfavors the occupancy of antibonding orbitals. Upon reaching a critical value,

the system will yield to the external constraints with a ST and the stabilization of the *LS*-state.

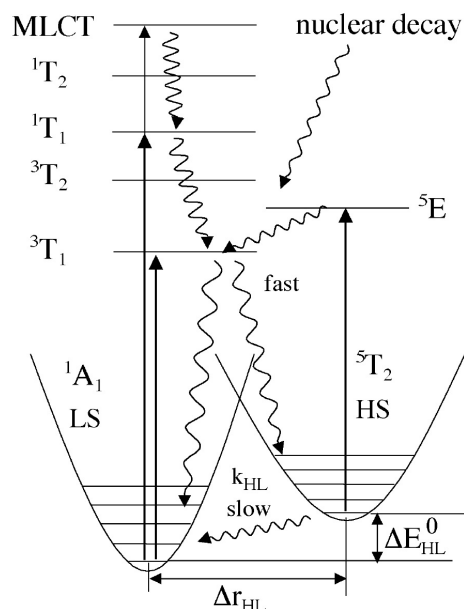


Figure 1.3.: Schematic representation of the electronic structure of an iron(II) center. Curly arrows indicate inter system crossing processes, illustrating the mechanism of LIESST and reverse-LIESST.<sup>[14]</sup>

If a compound is in the *LS*-state and provides the requirements to show spin transition properties, it is sometimes possible to observe the LIESST-effect (Light Induced Excited Spin State Trapping) upon radiation with light in the visible region as depicted in figure 1.3. Electrons from the ground state  ${}^1A_1$  ( $t_{2g}^6$ ) are promoted to an excited state  ${}^3T_1$  or  ${}^1T_1$  via a spin-allowed ligand-field transition. After two inter-system crossing processes the electronic  ${}^5T_2$ -state is reached, which represents the *HS*-state ( $t_{2g}^4e_g^2$ ). At low temperature, the energy barrier between the two states prevents a relapse into the *LS*-state. The most common perturbation to trigger SCO is of thermal origin.<sup>[5]</sup> In figure 1.4, the potential wells for both states are illustrated with the energy on the y-axis vs. the distance between metal center and ligand on the x-axis. In order to observe a thermal spin crossover, the energy difference  $\Delta E_{HL}^0$  has to be in the range of the thermal energy  $k_B T$ , which will lead to a stabilization of the *LS*-state at low temperatures.<sup>[15]</sup> When the temperature increases above a critical value  $T_{1/2}$  a transition to the *HS*-state

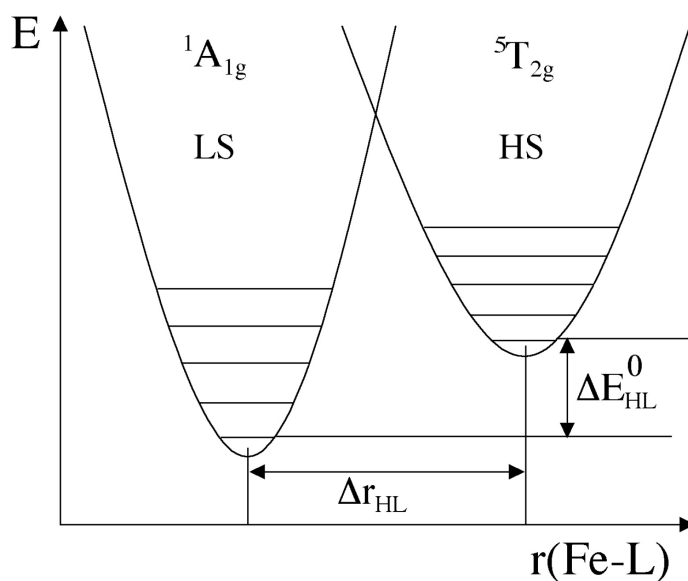


Figure 1.4.: Representation of the potential wells of the *HS* and the *LS*-state (left and right, respectively) of a metal ion with the electronic configuration  $d^6$ .<sup>[15]</sup>

is found. This process is entropy-driven and includes a vibrational and an electronic contribution: the first and by far larger one is attributed to the lower vibrational frequencies in the *HS*-state. The second contribution arises from the spin degeneracy upon switching to the *HS*-state and contributes about 25% to the total entropic gain. It can be calculated with the following formula.<sup>[16,17]</sup>

$$\Delta S_{mag} = R \cdot \ln \frac{(2S + 1)_{HS}}{(2S + 1)_{LS}} \quad (1.1)$$

In equation (1.2), the relation between the free energy  $\Delta G$  and the entropy  $\Delta S$  is given:

$$\Delta G = \Delta H - T\Delta S \quad (1.2)$$

At high temperatures, the entropic term in the Gibbs-Helmholtz-equation dominates, leading to a complete depopulation of the *LS*-state.

### 1.1.3. Characteristics of Spin Transition

Spin crossover compounds are a class of materials, which established a large platform for fascinating research due to the combination of several unique properties. Even if

these properties are regarded separately, they show great potential for applications. The following section will describe the common characteristics of spin-state switching materials based on iron(II) and where they are originating from.

The key feature of a SCO is the relocation of at least one electron to a different energy level within the d-orbitals. In case of the electronic configuration  $d^6$ , it is in general the population or depopulation of the antibonding  $e_g$ -orbitals, which has an influence on the bond lengths between the ligands and the metal center. In fact, one of the characteristics of a spin crossover in iron(II) compounds is the large change of the bond lengths, which can be up to 10%.<sup>[18]</sup> The magnitude of this effect differs with the oxidation state and the metal. Since its origin is found in the changing number of electrons in the  $e_g$ -orbitals, it is obvious that the effect is smaller for Co(II) where only one electron is relocated.

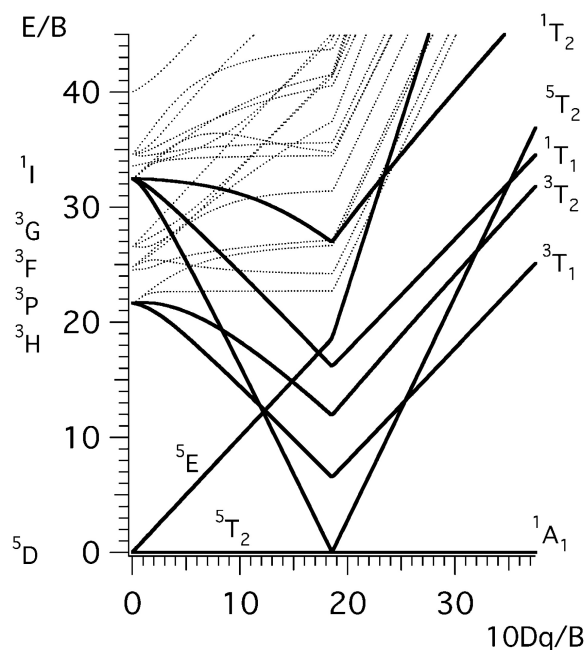


Figure 1.5.: Tanabe-Sugano diagram for the electronic configuration  $d^6$ . The y-axis shows the energy of the ligand-field states, the x-axis the ligand-field splitting  $10Dq$ . The unit of both axis is given in the Racah parameter  $B$ .<sup>[19]</sup>

Due to the pairing and unpairing of electrons during a SCO, the magnetic moment of the ion changes as well. A ST from the *LS*- to the *HS*-state leads to a population of

the previously empty  $e_g$ -orbitals with two electrons and results in an increasing paramagnetic behavior due to the larger number of unpaired electrons. In case of iron(II), the  $LS$ -state is even diamagnetic. In compounds with more than one metal center, it is additionally possible that cooperative magnetic ordering is observed. This can influence the magnetic and transition properties as well.

The third characteristic of a spin crossover is the thermochromism that accompanies every spin transition.<sup>[15]</sup> This phenomenon describes the change of color of a compound when the threshold between *low-spin* and *high-spin* is passed.<sup>[20–22]</sup> A Tanabe-Sugano diagram for a the electronic configuration  $d^6$  aids to comprehend the mechanism of thermochromism. The left side of figure 1.5 represents the *high-spin*-state with values for  $10Dq$  being between 0 B and 18.5 B. The only spin-allowed transition is found in the  $d-d$  transition  ${}^5T_2 \rightarrow {}^5E_g$  which is in the infrared region and appears therefore to be colorless for the naked eye. If the ligand field splitting increases, it will reach a critical value  $\Delta_{crit}$  and a spin transition can occur. More important, the ground state has switched from  ${}^5T_2$  to  ${}^1A_1$ . Now, the spin-allowed  $d-d$  transitions are  ${}^1A_1 \rightarrow {}^1T_1$  and  ${}^1A_1 \rightarrow {}^1T_2$ , which are typically found in the visible region.<sup>[21]</sup> If the compound provides no further sources for color, e.g. charge-transfer, the spin crossover will appear as a color change from or to colorless. Since the  $d-d$  transitions are low in intensity compared to charge-transfer- or  $\pi-\pi$ -transitions, they might not be visible in systems where the latter ones are found as well.

#### 1.1.4. Cooperative Effects

The previous sections have shown that spin crossover is subject to a very subtle equilibrium. Even what seems to be a small disturbances can lead to the loss, intensification or variation of the spin transition properties. Hence, rather little effects have to be accounted for as well. During a change of the spin-state, the compound experiences a first order phase transition.<sup>[23]</sup> This conversion, which origins from the change in bond lengths, is transmitted throughout the bulk material via contacts between neighboring complexes and, if present, counter ions and solvent molecules. Such interactions are mediated by classical or non-classical hydrogen bonds or  $\pi-\pi$ -stacking. It is obvious, that the absence of contacts leads to a hindered propagation of the spin transition. If the

complexes are connected directly or else bridged by solvent molecules or counter ions, the spin-state change of one metal is relayed to its attached neighbors. Accordingly, the larger the cooperativity in a given system is, the more abrupt is the spin crossover.<sup>[24,25]</sup> A reliable method to investigate the cooperative effects in the solid state is to compare the spin crossover behavior of a crystalline compound with its behavior in solution.<sup>[26]</sup> By detaching the complexes from one another and their peripheral network, the complexes act as isolated molecules and their spin transition behavior can be altered. Alternatively, it is possible to dope a system showing very abrupt spin transition due to large cooperativity with a non-spin crossover active metal.<sup>[27]</sup> Thus, the intermolecular connections are still available but any phase transition is buffered by the foreign atoms and is not further transmitted. As a consequence, with a growing percentage of doped metal, the spin crossover becomes less abrupt.

### 1.1.5. Solvent and Anion Effects

Next to connections between complexes, the influence of the interactions between anions or solvent molecules and the complex via direct coordination or classical and non-classical hydrogen bonds on the properties of a spin crossover compound shall be discussed in more detail. To modify the SCO properties in a very direct way, coordinating counter ions can be used. They directly affect the ligand field splitting, because they provide some of the donor atoms. Since the critical temperature  $T_{1/2}$  is dependent on the LFS, the effect of remotely different coordinating counter ions onto an otherwise similar system can be monitored by magnetic measurements.<sup>[28]</sup> It has been shown, that a change of the coordinating counter ions can result in a large shift of the transition temperature by 93 K.<sup>[29]</sup>

This is of course only possible when a ligand is used, that does not occupy every coordination site a metal offers. However, there are also ways to modify the crystal field splitting, and hence the transition temperature, with ligands which enclose a metal ion entirely. In the previously described approach, the electron density at the coordinating N-donor atoms was shifted by different substituents to obtain a different LFS. A more subtle course to achieve the desired electron density shift is the use of hydrogen bonds between solvent molecules or counter ions to amine-protons which are bound to the



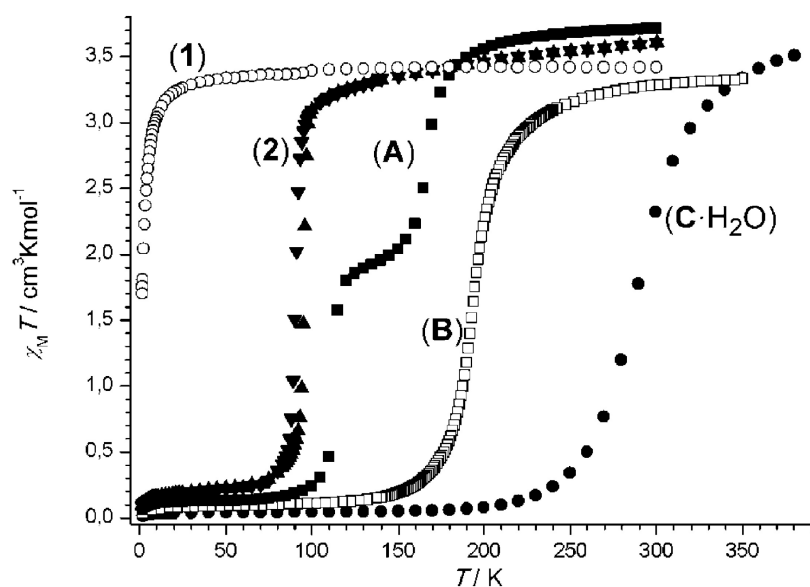


Figure 1.6.:  $[\text{Fe}(\text{L})_2(\text{NCX})_2]$  represents a good example of the effect counter ions and hetero atom substitution have on spin crossover properties: **(1)** L = oxadiazole and X =  $\text{NCS}^-$ , **(2)** L = Selenodiazole and X =  $\text{NCS}^-$ , **(A)** L = thiadiazole with X =  $\text{NCS}^-$ , **(B)** L = thiadiazole with X =  $\text{NCSe}^-$  and **(C)** L = thiadiazole with X =  $\text{NCBH}_3^-$ .<sup>[29]</sup>

nitrogen-donor atoms.<sup>[30]</sup> This more indirect method is better suited for a fine tuning of the transition temperature.

While counter ions are rigidly anchored in a crystal structure, solvent molecules may be removed from it under reduced pressure. In some cases, it is additionally possible to reintroduce the solvents to a complex afterwards. If these molecules additionally affect the spin transition behavior in the way mentioned above, it is possible to trigger a SCO with their removal or reintroduction. This gives rise to new applications for spin crossover compounds. The reversible introduction and extraction of guest molecules enforcing a switch of the spin-state qualifies them as ideal chemosensors for solvents. And due to the many changes a SCO occurs with and the vast possibilities to detect or monitor the ST, evaluation will be simple as well.

It is obvious, that not only the nature of contacts is important but also the number. A larger number of contacts in the solid state results in a higher magnitude of the cooperativity and hence a more pronounced spin crossover behavior. In section 1.1.4, the importance of cooperativity within the solid state has already been mentioned. Solvents and counter ions were identified as possible transmitter for intermolecular long

range interactions. When an influence of the electron-density of the donor atoms by these molecules is given as well, the intermolecular contacts become a powerful tool to control the spin crossover behavior entirely regarding the shape, hysteresis and occurrence itself.

### 1.1.6. Occurrence of Spin Transition

The nature of a spin transition is not always the same. In fact, there are five categories in which most of the transitions can be divided (see figure 1.7). In a) a gradual SCO is shown, which is often observed if there are no or only weak cooperative effects. In case of strong cooperativity, an abrupt transition is found instead, as depicted in b). Of course, there is no clear borderline between a) and b). This can be different when the cooperativity is very high because it promotes the appearance of a hysteresis, as shown in c). This property gives the class of spin crossover compounds a new and technically promising feature.<sup>[31]</sup> It has been shown, that the size of the hysteresis depends not only on the cooperative effects, but also on the applied scan rate and other factors.<sup>[32,33]</sup>

It is also possible to have a stepwise SCO as depicted in d). This originates either from

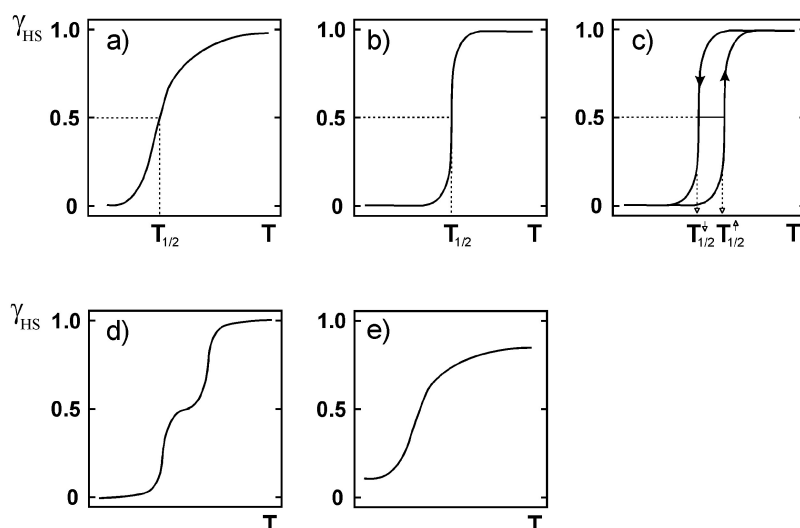


Figure 1.7.: Scheme of the five main categories of spin transition: a) gradual; b) abrupt; c) with hysteresis; d) two-step; e) incomplete.<sup>[15]</sup>

a mononuclear complex that shows intermolecular cooperativity or phase transition, or else from a multi-nuclear compound with intramolecular interactions.<sup>[34,35]</sup> The simplest model systems for the latter cases are dinuclear complexes. It is possible that two metal ions do not switch simultaneously even though they are in a chemically identical environment. Instead they convert separately at different temperatures. The step in the diagram can be the result. It represents a mixed  $[HS-LS]$ -state, where one of the two metal centers has already switched its state while the second one still stabilizes its original state. This differentiated behavior is attributed to strong intramolecular interactions: by changing from one state to another, the switching metal influences changes the LFS of the second metal center. The new situation disfavors a second transition and can even suppress it. The picture of e) gives an example for an incomplete spin transition. This should not be confused with the situation in d). It can occur, for instance, when a sample is cooled too fast. A part of it will be frozen in the  $HS$ -state and the transition to the  $LS$ -state is kinetically hindered.<sup>[36]</sup>

### 1.1.7. Structural Considerations

The change of bond lengths during the spin-state switching directly affects the geometry of the complex leading to a more distorted octahedral sphere in the *high-spin*-state. The *cis*- and *trans*-bond angles  $\phi$  and  $\psi$  between the donor atoms of the ligand and the metal center are deformed. In an ideal octahedron these are  $90^\circ$  and  $180^\circ$ , respectively. The octahedral distortion parameter  $\Sigma_{ODP}$  gives the deviation of the experimental *cis*-angles from the ideal ones, and describes hence the distortion of the coordination environment.

$$\Sigma_{ODP} = \sum_{i=1}^{12} (|90^\circ - \phi_i|) \quad (1.3)$$

Typical values for  $\Sigma_{ODP}$  in the  $HS$ -state are above  $100^\circ$ .<sup>[37]</sup> The geometry is more ordered in the *low-spin*-state, where  $\Sigma_{ODP}$  shows values below  $80^\circ$  and the octahedral coordination sphere is closer to the ideal geometry. The ligand can be accounted for the distortion as well. This is the case if the used ligand is multidentate and occupies more than one coordination site of the metal. Due to the rigidity of the ligand backbone and the longer distance the system deforms.

## 1.2. Detection of Spin Crossover

The schematic representation of a SCO from an iron(II)-center in figure 1.2 illustrates the transition itself and as well the changes that accompanies the event. The *HS*- and *LS*-species differ essentially from each other, which yields to many options for their differentiation and characterization. In the following, the most common and applied methods will be discussed to give a proper overview of the detection of spin crossover.

### 1.2.1. Magnetic Measurements

Switching from *high-spin* to *low-spin* results in a different number of unpaired electrons which influences the magnetic properties. The magnetic moment of the *LS*-state has always less paramagnetic character than the *HS*-state, but in case of iron(II) the *LS*-state even becomes diamagnetic. Such a drastic alteration can easily be detected via magnetic measurements using a SQUID (*S*uperconducting *Q*uantum *I*nterference *D*evice) magnetometer. It records the temperature dependent change of the magnetic molar susceptibility  $\chi_m$  of a sample at various temperatures. With the collected data and the knowledge of the expected susceptibilities before and after a spin transition it is possible to calculate the mole fractions  $\gamma_{HS}$  and  $\gamma_{LS}$  according to the formula:

$$\chi(T) = \gamma_{HS}(T)\chi_{HS} + (1 - \gamma_{HS}(T))\chi_{LS} \quad (1.4)$$

at any temperature. With these data, a plot of  $\gamma_{HS}$  vs.  $T$  can be illustrated for a graphical representation of the spin transition as seen in figure 1.7. The shape of the curve itself contain a lot of information about the system. A common variation is a plot of  $\chi T$  vs.  $T$ . An advantage is the possibility of comparing the actual values with the expected, allowing a quantitative analysis of the sample. With the suiting equipment it is also possible to carry out measurements with the simulation of external perturbations, such as the irradiation with light, the application of pressure (see section 1.1.2).<sup>[38–42]</sup>

### 1.2.2. Single Crystal X-Ray Diffraction

Due to the population or depopulation of the antibonding  $e_g$ -orbitals, the donor atom to metal bond lengths for the different states are not equal. As a rule of thumb, the average distances are between 1.9 Å and 2.0 Å for the *low-spin*-state and 2.1 Å to 2.2 Å for the *high-spin*-state, which is about 3-4% change in cell volume.<sup>[43]</sup> The bond angles are affected as well, as pointed out in section 1.1.7. Such experimental values can only be observed with single crystal X-ray diffraction (XRD). It is additionally the only possibility to determine connections and contacts within a structure. Intermolecular interactions, such as hydrogen bonds and  $\pi$ - $\pi$ -stacking, can be examined to evaluate their influence on the spin crossover properties. It is possible to monitor the contraction or enlargement of the molecule with XRD. This is of course only possible, if the integrity of the crystal is not lost due to crackling or pulverization during the cooling or heating process. The bond lengths shift can have enormous effects on the crystal: from a simple expansion or contraction of the system, a feature that earned this class of compounds the name "breathing crystals", to a space group change and up to the destruction of the crystal.<sup>[44]</sup> Dinuclear compounds with symmetry elements such as centers of inversion or mirror planes are of special interest in that context. In some cases, the asymmetric unit comprises only one metal center whereas the second one is generated by that symmetry element. Subsequent to a mixed [*HS-LS*]-state forming partial spin crossover, the iron centers are not equivalent anymore, which results in a change of the space group.<sup>[45]</sup>

### 1.2.3. Mössbauer-Spectroscopy

One of the most established methods to detect spin crossover in iron compounds is Mössbauer-spectroscopy.<sup>[46]</sup> It was first used by König *et al.* in order to proof the influence of the temperature onto the spin-state switching.<sup>[47]</sup> It uses the large differences of the quadrupole splitting  $\Delta E_Q$  and the isomer shift  $\delta$  to distinguish between the *HS*- and the *LS*-state of both iron(II) and iron(III).<sup>[49]</sup> This is demonstrated in figure 1.8. The temperature dependence onto the spin-state and therefore  $\Delta E_Q$  and  $\delta$  is clearly visible in the picture. In a plot of the transmission in percentage versus the velocity of the source,

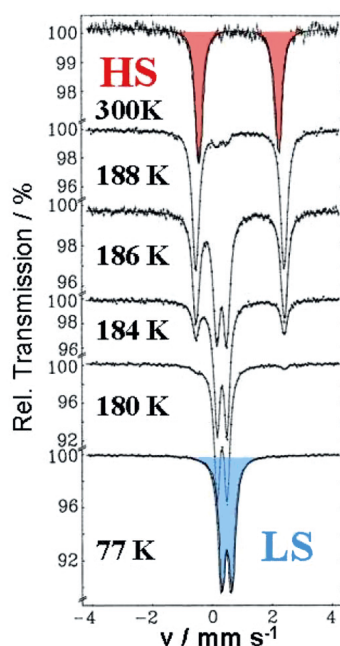


Figure 1.8.: Variable temperature measurement of a sample of [Fe(phen)<sub>2</sub>(NCS)<sub>2</sub>] using Mössbauer-spectroscopy.<sup>[48]</sup>

the area beneath the signal of a *HS* or *LS*-species is proportional to its abundance in the sample. With the help of special developed programs for Mössbauer data fitting, the nature of the experimental data is fitted and can be assigned afterwards to the appropriate spin-state.<sup>[15]</sup> This feature makes the method very valuable for the determination of the absolute ratio between the *high-spin*- and *low-spin*-fraction at different temperatures in a sample.

#### 1.2.4. Other Methods

One of the probably most convenient changes are the optical transitions. As stated before, iron(II) is colorless in the *HS*-state, whereas it shows strong colors in the *LS*-state. If there is no color originating from e.g. charge-transfer or the ligand itself, the spin transition can be followed by the naked eye.<sup>[50,51]</sup> Even though further measurements are needed to confirm that such an effect is actually a result of a spin transition, it is a fast method for a prescreening. Additionally, UV/Vis-spectra can be recorded. Both spin-states show characteristic absorption bands. In case of the *HS*-species, the

${}^5T_2 \rightarrow {}^5E$  transition appears in the near infrared, whereas the two transitions  ${}^1A_1 \rightarrow {}^1T_1$  and  ${}^1A_1 \rightarrow {}^1T_2$  of the *LS*-state appear in the visible region. If the measurements are carried out under different temperatures, the SCO can be monitored upon vanishing and appearance of the according absorption bands.

A reliable method for the detection of a phase transition is the measurement of the heat capacity with differential scanning calorimetry (DSC).<sup>[52]</sup> Because of the deformation of the geometry prior to the spin transition, a SCO itself can be considered as a phase transition.<sup>[40]</sup> The change in entropy, which is in the order of 50 to 80 J mol<sup>-1</sup> K<sup>-1</sup>, is the driving force for the spin crossover. The determination of the entropy is possible with a DSC measurement, thus this is a useful tool for the characterization of SCO.<sup>[43]</sup>

### 1.3. Ligand Considerations

Most important for the appearance of SCO is a ligand field splitting appropriate in energy to the used metal ion. Since every metal ion in a specific oxidation state comes with an individual natural splitting of the d-orbitals, there is only little tolerance in the choice of the donor atoms.<sup>[53]</sup> Over the last decades it has been shown, that the most fitting environment for iron(II) SCO compounds is of an FeN<sub>6</sub>-type, followed by N<sub>4</sub>O<sub>2</sub> and some rare cases of N<sub>4</sub>C<sub>2</sub>.<sup>[54–57]</sup> The work at hand will further on focus on the FeN<sub>6</sub> coordination environment.

There are several approaches to form an octahedral coordination sphere with N-donor atoms. An approved method is the use of ligands where the N-donor atoms are part of an aromatic system.<sup>[4]</sup> An established system showing very diverse spin transition behavior was introduced by the group of Sally Brooker<sup>[45]</sup>. It is a bis-tridentate ligand with a symmetric disubstituted triazole as a central motive, which forms a dinuclear complex by coordinating two iron(II) centers with two ligand molecules. Every ligand provides two amine-bound protons which are able to build classical or non-classical hydrogen bonds. Moreover, the triazole offers a non-coordinating nitrogen that can be substituted.

Taking this compound as a model system, there are two general approaches to modify

the ligand in order to change the SCO properties: first, the ligand field splitting can be altered. This is possible by introducing a hetero atom into either the pyridine rings or the five membered central motive, which shifts the electron density at the N-donor atoms. Alternatively, the amine-bound protons can be substituted. Since they are directly connected to the N-donor atom, it will change the electron density and therefore the LFS as well.

The second option is to add steric hindrance to the system. When bulky groups are introduced to the periphery, the repulsion between neighboring molecules becomes larger, which distorts the geometry and favors the *HS*-state. With this course the transition temperature can be lowered. A complex which was in the *low-spin*-state is going to be in the *high-spin*-state.<sup>[58]</sup>

Another aspect that should be considered is the usage of coordinating counter ions. Their influence has been discussed in section 1.1.5. The tremendous effect they have upon a SCO is well documented in the literature.<sup>[28,29]</sup> The use of two bidentate ligands such as phenanthroline and bipyridine can provide the necessary coordination environment.<sup>[59]</sup> The counter ions can be chosen depending on the used ligand and, most important, exchanged by more suitable ones. This is one of the large advantages of this kind of system. The spin transition properties can be fine tuned by using appropriate counter ions like  $\text{XCN}^-$  (X being N, Se or  $\text{H}_3\text{B}$ ),  $\text{OCN}^-$  or  $\text{CN}^-$ , without a modification of the ligand itself.<sup>[28,60–62]</sup>

### 1.4. Mono-, Di- and Polynuclear Compounds

The first compounds exhibiting spin transition properties, discovered in 1931 by Cambi *et al.*, were mononuclear thiocarbamate complexes.<sup>[1]</sup> Since then, the focus of the research has shifted towards iron(II). Reasons for that are the more pronounced transition between the *HS*- and *LS*-states, the better resolution of measurements and the larger occurrence of effects such as LIESST or thermochromism compared to iron(III) or Co(II).<sup>[38,39,63–65]</sup>

Many phenomena that occur in spin crossover materials can be explained with the help of mononuclear complexes. The general concept of the ligand field splitting influenc-



ing the transition temperature  $T_{1/2}$  can be proven by using coordinating counter ions with different ligand strength (see figure 1.6).<sup>[29]</sup> However, cooperative effects in such compounds are of intermolecular nature and restricted to those.<sup>[66,67]</sup> An advantage of multinuclear compounds is the possibility to exhibit intramolecular interactions as well.<sup>[46,68][69]</sup> Besides the two states a single iron(II)-center can adopt, larger systems might also show several configurations depending on the number of metal ions.

The most straight forward arrangement to investigate intramolecular interactions are dinuclear complexes. Furthermore, they are able to stabilize a  $[HS-LS]$ -state. With temperature dependent measurements of the magnetic susceptibility, Real *et al.* observed this state as a stepwise the decrement of  $\chi T$  in the compound  $[\text{Fe}(\text{bt})(\text{NCS})_2]_2$ .<sup>[35]</sup> However, it is not possible to unambiguously allocate the first transition to a specific metal center. The first crystallographic prove of a distinct  $[HS-LS]$ -state was reported more than a decade later for the compound  $[\text{Fe}(\text{II})_2(\text{PMAT})_2](\text{BF}_4)_4 \cdot \text{DMF}$  by the group of Brooker *et al.* <sup>[45]</sup>. The different bond lengths and angles for the two iron(II)-centers confirmed their different spin-states. Another method which is suitable to detect a mixed  $[HS-LS]$ -species is Mössbauer-spectroscopy. The appearance of characteristic patterns from the occurring spin-states can be distinguished if an external magnetic field is applied. The requirement for a  $[HS-LS]$ -state are strong intramolecular interactions between the metal centers. If the intermolecular interaction dominate the intramolecular interactions, such a mixed state will not occur. Instead, every other iron(II) complex will switch to the  $[LS-LS]$ -state, while the other complexes remain in the  $[HS-HS]$ -state.<sup>[35,45,46,70,71]</sup>

## 2. Objective and Aims

In chapter 1 has been pointed out, that there are two very important aspects which influence the ligand field splitting and have to be considered therefore as well in order to fully understand the occurrence of spin crossover. On the one hand, the geometry can be used to provoke a distortion of the coordination sphere. Since there is a direct correlation of the bond lengths and angles to the occupation of the antibonding  $e_g$ -orbitals, the transition properties can be altered by the geometry. On the other hand, the complex cations can be connected via intermolecular hydrogen bonds. This kind of cooperativity can affect the whole system, because a structural alteration accompanying a spin transition is mediated along the cationic connections. Additionally, the electron density at the donor atoms and hence the ligand field splitting can be influenced by such hydrogen bonds. Both, intermolecular connections and structural aspects, are of great value for the fine tuning of the spin crossover properties.

The main purpose of this work was the synthesis of dinuclear iron(II) compounds using an oxadiazole based ligand analog to the PMAT-system by Brooker *et al.* and the investigation of the influence of the hetero atom onto the resulting complexes. Furthermore, the effects of several counter ions onto the cooperativity regarding the spin crossover properties were to be studied as well.

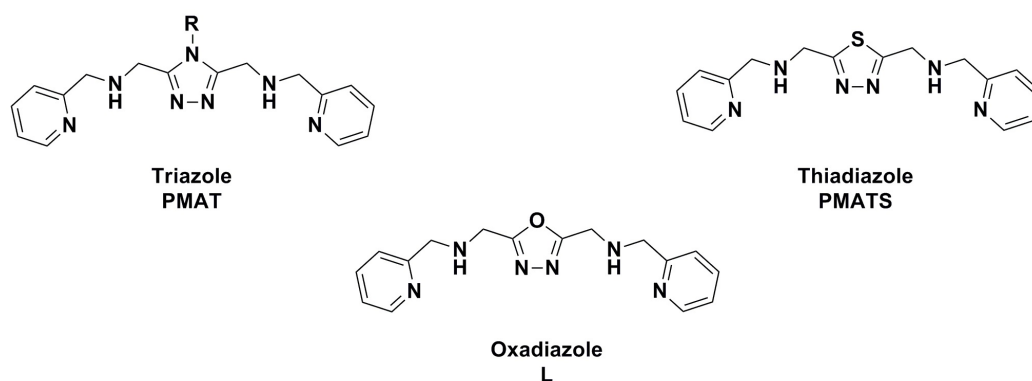


Figure 2.1.: Top left: triazole-based ligand PMAT by Brooker *et al.*<sup>[72]</sup>; top right: thiadiazole based ligand PMATS by our group<sup>[73]</sup>; middle: oxadiazole based ligand used for this work.

Previous work in our group has shown, that a substitution of the triazole system within the PMAT ligand by Brooker *et al.* (see figure 2.1, left) by a thiadiazole unit leads to a novel ligand PMATS (see figure 2.1, right), which can be employed for the preparation of dinuclear iron(II) compounds. Regarding their structure, they are very similar to the complexes which were reported using the PMAT system. (figure figure 2.2)

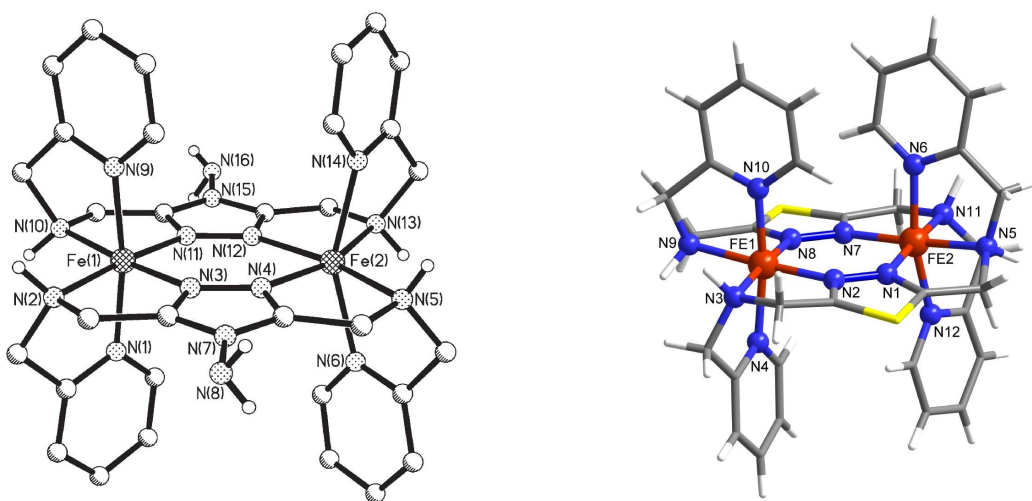


Figure 2.2.: Left: crystal structure of the dinuclear iron(II) complex  $[\text{Fe}_2(\text{PMAT})_2]$  based on the PMAT ligand.<sup>[45]</sup> Right: crystal structure of the dinuclear iron(II) complex  $[\text{Fe}_2(\text{PMATS})_2]$  based on the thiadiazole analogue by our group.<sup>[73]</sup>

Interestingly, the substitution of the hetero atom had tremendous effects onto the spin-state around room temperature. In figure 2.3, magnetic measurements of the triazole compound (left) and the thiadiazole compound (right) are compared. For the triazole system by Brooker *et al.*, a  $[\text{HS-HS}]$ -state is observed around room temperature. In contrast, for the novel compound of our group a  $[\text{LS-LS}]$ -state is found over almost the whole temperature range.

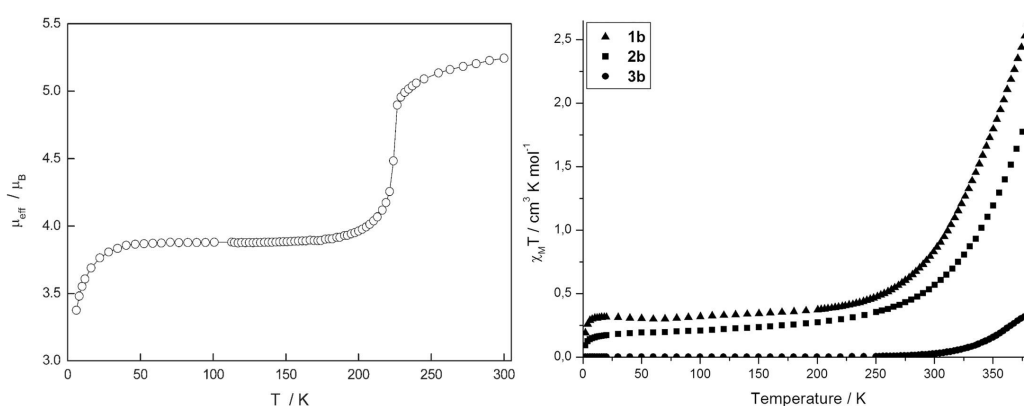


Figure 2.3.: Left: magnetic moment vs. temperature of the  $[\text{Fe}_2(\text{PMAT})_2]$  compound.<sup>[45]</sup> Right: magnetic moment in  $\chi_M T$  of the  $[\text{Fe}_2(\text{PMATS})_2]$  compound.<sup>[73]</sup>

Inspired by these fascinating results, we were interested in the effect, which a replacement of the thiadiazole backbone by an oxadiazole would bear. The smaller ionic radius of the formal  $\text{O}^{2-}$ -ion compared to the  $\text{S}^{2-}$ -ion should shorten the angle between the oxygen and carbon atom in the five membered ring and the carbon atom of the methylene group in two and five position. The consequence would be a larger distance between the opposing N-donor atoms belonging to the methylamine groups of two separate ligands and therefore a larger distortion, which would favor the *HS*-state. Moreover, oxygen has a larger negative inductive effect. This reduces the electron density of the N-donor atoms in the ring, lowering the ligand field splitting.

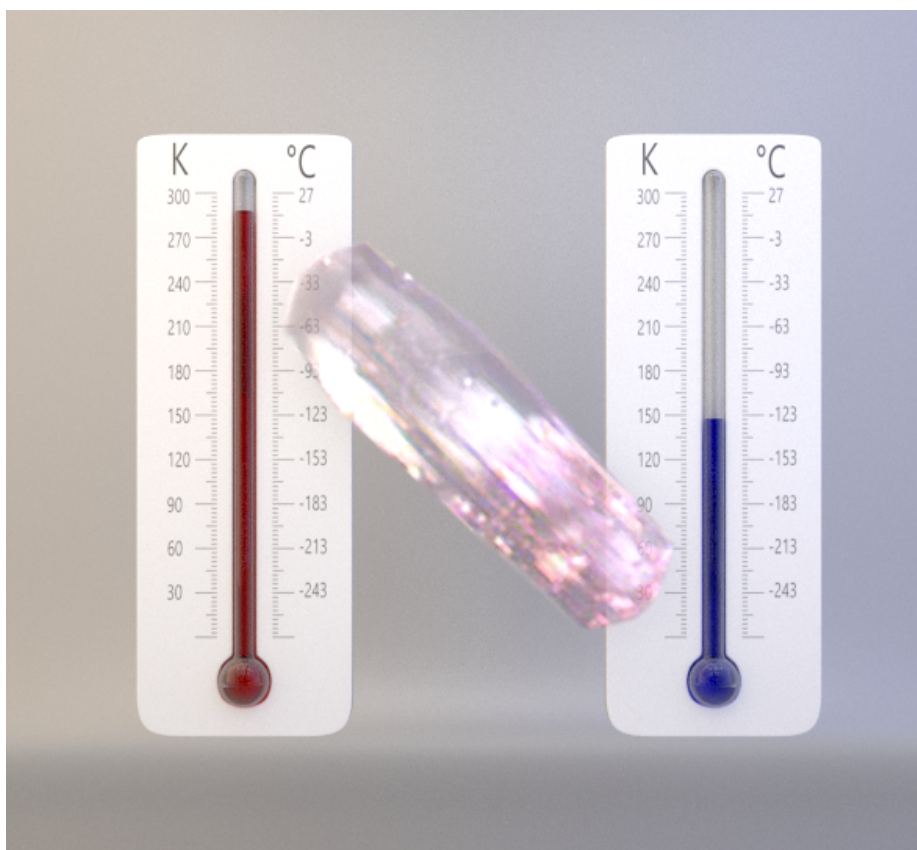
A second aspect was the usage of different counter ions. Even though their effect onto the system is known, it is still nearly impossible to predict the synthetic outcome of a complexation concerning the intermolecular contacts and a rational design for the connectivity. An introduction of several distinct anions into the structure should deepen the understanding for cooperative effects, which leads to diverse spin transition behavior, and how the formation of contacts between complex cations and anions or solvents can be rationalized.

### 3. The First 1,3,4-Oxadiazole Based Dinuclear Iron(II) Complexes Showing Spin Crossover Behavior With Hysteresis

#### 3.1. Introduction

After the successful synthesis of the oxadiazole based ligand 2,5-bis([(2-pyridylmethyl)amino]methyl)-1,3,4-oxadiazole (see figure 2.1), which is analog to the thiadiazole ligand by our group and the triazole ligand by Brooker *et al.*, it was possible to synthesize three iron(II) complexes. Key feature of the new system is the oxadiazole as the ligand backbone. Even though, in the context of spin crossover, some ligands with the same central unit are found, so far to the best of our knowledge there are no reports of an oxadiazole based compound which actually shows spin transition.<sup>[29,45,73,74]</sup> By mixing solutions of the ligand and an iron(II) salt in acetonitrile, single crystals suitable for X-ray diffraction experiments have been obtained. The structures incorporate two iron(II)-centers coordinated by two ligand molecules, giving a  $[\text{Fe}_2(\mu\text{-L})_2]^{4+}$  cation as a central motive. The fourfold positive charge was compensated by four different counterions, depending on the used metal salts. The number of solvent molecules differed between two and four. The structure determination was performed at 193 K, except for the perchlorate compound, which was additionally investigated by XRD at 100 K. Furthermore, variable temperature magnetic measurements were carried out with an applied field of 1 kOe to determine the molar susceptibility  $\chi_M$  in a temperature range from 10 K to 300 K. Mössbauer-measurements were conducted at room temperature and at 85 K to confirm the presence of iron(II) in different spin state.

## 'The First 1,3,4-Oxadiazole Based Dinuclear Iron(II) Complexes Showing Spin Crossover Behavior With Hysteresis'



**Christian Köhler** and Eva Rentschler

*Eur. J. Inorg. Chem.* **2016**, 13-14, 1955-1960.

## 3.2. Abstract

Three new dinuclear complexes  $[\text{Fe}(\text{II})_2(\mu\text{-L})_2]\text{X}_4$  (**L** is the bis-tridentate ligand 2,5-bis[(2-pyridylmethyl)amino]methyl-1,3,4-oxadiazole and  $\text{X} = \text{ClO}_4^-$ ,  $\text{BF}_4^-$  and  $\text{CF}_3\text{SO}_3^-$ ) have been synthesized and fully characterized by single-crystal X-ray diffraction, Mössbauer-spectroscopy and magnetic susceptibility measurements. Upon cooling, a trapped [*high-spin low-spin*]-state of the iron(II) centres is detected. Depending on the counterion, a pronounced thermal hysteresis is found. In one case, it was possible to observe a space group change that accompanies the spin transition. This is the first system showing spin crossover based on an oxadiazoles ligand.

## 3.3. Introduction

Whether a spin state of an octahedral 3d transition metal complex with the electronic configuration  $d^4$  to  $d^7$  shows high spin *HS* or low spin *LS*, strongly depends on the ligand field strength of the coordinating ligand.<sup>[1]</sup> At the threshold of the ligand field splitting, a transition between the two spin states can be induced by a change in temperature, pressure or the irradiation with light (LIESST).<sup>[2]</sup> This effect is called spin crossover (SCO). It is an extensively studied field due to the large potential in electronic applications.<sup>[3,4]</sup> One of the most investigated metal ions showing this phenomenon is iron(II).<sup>[5]</sup> Here, a key feature is the drastic change of the magnetic properties from a diamagnetic to a paramagnetic state, which is easily detected. Additionally, a change in color (thermochromism) is giving an easy way to observe the transition.<sup>[6]</sup>

In the solid state the SCO strongly depends on the cooperative interactions between the metal centers by intermolecular contacts between the complexes. This is mostly achieved by hydrogen bonds or  $\pi$ - $\pi$  interactions between aromatic moieties of the ligand system.<sup>[7]</sup> A more pronounced communication of the metal centers leads to a more abrupt transition and, eventually, to a hysteresis.<sup>[8]</sup> However, mononuclear compounds are limited to these intermolecular interactions. In comparison, the intramolecular metal-metal interaction in polynuclear compounds is more easily controllable due to close proximity to one another.<sup>[9]</sup> In dinuclear complexes a mixed [*HS-LS*]-spin-state

can occur additionally as a third state to the diamagnetic [*LS-LS*] and the paramagnetic [*HS-HS*]-state. A prominent example is the dinuclear iron(II) PMAT complex by the group of Brooker.<sup>[10]</sup> This is the first system where a mixed [*HS-LS*]-state has been confirmed by X-ray diffraction. Inspired by this work, our group explored the behavior of the analogous thiadiazole. While in the former example the dinuclear compounds remain in the [*HS-LS*]-state and do not switch to the fully diamagnetic [*LS-LS*]-state, we recently reported the synthesis and characterization of a 1,3,4-thiadiazole based dinuclear iron(II) [*LS-LS*] complex showing incomplete SCO around room temperature.<sup>[11]</sup> This and the work of other groups demonstrated the large influence of the heteroatom in the backbone of the structure.<sup>[12]</sup> We consequently investigated the effect of an oxadiazole backbone regarding the spin transition properties.

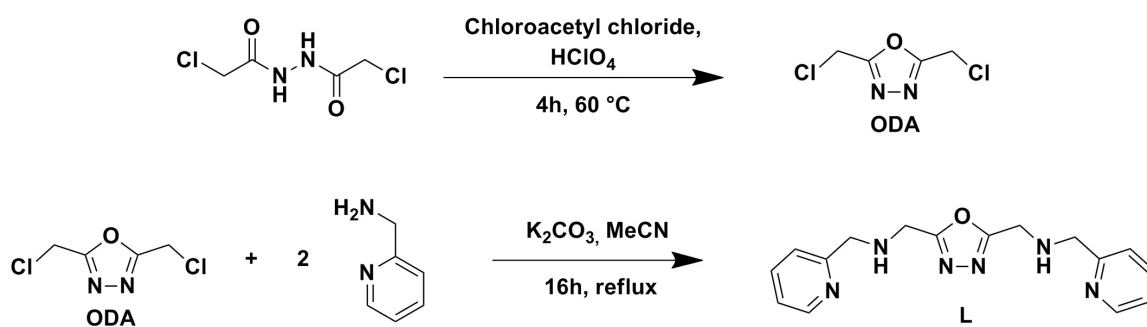
In the present study we now report the first set of novel oxadiazole based dinuclear iron(II) compounds showing spin crossover. Via magnetic susceptibility measurements and Mössbauer-spectroscopy an abrupt spin transition around 150 K is observed. Using single crystal X-ray diffraction at various temperatures a mixed [*HS-LS*]-state below 150 K is confirmed. Additionally, we observe large differences in the connectivity between the counterions and the cations, leading to a hysteresis of 26 K for one of the compounds.

## 3.4. Results and Discussion

### 3.4.1. Syntheses

Scheme 1 shows the synthesis of the ligand system 2,5-bis([(2-pyridylmethyl)amino]-methyl)-1,3,4-oxadiazole (**L**). The precursor 2,5-bis(chloromethyl)-1,3,4-oxadiazole is prepared by an intramolecular condensation reaction of 1,2-bis(chloroacetyl)hydrazide.<sup>[13]</sup> By reacting the product with 2-(aminomethyl)pyridine in a nucleophilic substitution, the desired ligand **L** is synthesized.<sup>[14]</sup>





**Scheme 1.** Synthesis of **L** and the ODA precursor.

Depending on the counteranion, various techniques were used to obtain dinuclear complexes. In case of perchlorate, single crystals of  $[\text{Fe}(\text{II})_2\text{L}_2](\text{ClO}_4)_4 \cdot 4\text{MeCN}$  (**1**) formed after mixing solutions of ligand and metal salt in acetonitrile. For other counteranions vapor diffusion with diethyl ether and THF was used to obtain single crystals of  $[\text{Fe}(\text{II})_2\text{L}_2](\text{BF}_4)_4 \cdot 2\text{MeCN}$  (**2**) and  $[\text{Fe}(\text{II})_2\text{L}_2](\text{CF}_3\text{SO}_3)_4 \cdot 2\text{MeCN}$  (**3**), respectively.

### 3.4.2. Crystal Structures

X-ray diffraction was performed for compounds **1** and **3** at 193 K, for compound **2** at 173 K. For crystallographic data in more detail, see SI. **1** crystallizes in the monoclinic space group  $I2/a$ , **2** and **3** in the triclinic group  $P\bar{1}$ . The cations of all three structures contain two Fe(II) atoms which are doubly  $\mu_2$ -bridged by the 1,3,4-oxadiazole backbone of the two chelating ligands L. They are arranged in a way that both pyridyl groups of one ligand are directed either up or down. This gives in all three cases a distorted octahedral N6 coordination sphere for both of the metal centers. In addition, there are four non-coordinating counteranions (**1**:  $\text{ClO}_4^-$ ; **2**:  $\text{BF}_4^-$ ; **3**:  $\text{CF}_3\text{SO}_3^-$ ) as well as four solvent molecules in the perchlorate structure **1** and two solvent molecules in **2** and **3**. As expected for iron(II) in HS, the average Fe-N bond lengths in **1**, **2**, and **3** are 2.180 Å, 2.1976 Å and 2.190 Å, respectively. More detailed Fe-N bond lengths are summarized in section 3.4.2.

**Table 1.** Selected bond lengths in [Å], bond angles of N-Fe-N in [°] and the octahedral distortion parameter  $\Sigma$  in [°] for compounds **1**, **2** and **3**. For compound **1**, the values from the measurements at both temperatures are included.

	1 (@ 100 K)		1 (@ 193 K)	2 (@ 173 K)	3 (@ 193 K)
	Fe1 <i>HS</i> /Å	Fe2 <i>LS</i> /Å	Fe/Å	Fe/Å	Fe/Å
N1-Fe/N6-Fe	2.145(8)/2.120(8)	2.010(9)/2.017(8)	2.140(4)/2.136(4)	2.132(2)/2.154(2)	2.139(2)/2.139(2)
N2-Fe/N4-Fe	2.291(8)/2.148(9)	2.102(8)/1.943(9)	2.275(4)/2.130(4)	2.328(2)/2.137(2)	2.291(2)/2.127(2)
N3-Fe/N5-Fe	2.177(8)/2.345(8)	1.969(8)/2.107(8)	2.113(3)/2.284(4)	2.132(2)/2.302(2)	2.132(2)/2.313(2)
N-Fe <i>Average</i>	2.204	2.0248	2.180	2.198	2.190
<i>cis</i> -N-Fe-N <i>Average</i>	91.2	90.1	90.7	90.7	90.7
<i>trans</i> -N-Fe-N <i>Average</i>	158.0	172.1	162.6	162.3	162.6
$\Sigma$ [a]	136.7	70.2	121.0	126.1	125.5

[a] The octahedral distortion parameter  $\Sigma$  adds up the absolute differences of the ideal octahedral *cis*-angle from the actual *cis*-N-Fe-N angles of the compound.

The N-Fe-N *cis*-angles show an average of 90.7° for all compounds, even though they actually range from 74.6° to 119.9°. The average *trans*-angles are 162.5°, which is far from the ideal angle of 180°. The so called octahedral distortion parameter  $\Sigma$  adds up the absolute differences of the ideal octahedral *cis*-angle of 90° from the actual *cis*-N-Fe-N angles of the compound. It gives values of 121.0° for **1**, 126.1° for **2** and 125.5° for **3**. This difference from to an ideal octahedral geometry also shows the *HS* nature of the metal centers.<sup>[15]</sup> An important aspect to be considered is the introduction of an oxygen atom in the heterocyclic ring of the ligand. This has two effects: on the one side, it changes the electronic structure in the heterocycle. As a more electronegative atom it decreases the electron density at the nitrogen donor atoms. This results in a smaller ligand field splitting  $\Delta$ , making the *HS*-state more favorable. Additionally, the angle between the two nitrogen donor atoms in the oxadiazole and the amine nitrogen donor atom changes. In the analogous thiadiazole complex recently published by our group, this angle is nearly linear. This gives the system a larger flexibility compared to that of triazole. Here, the smaller radius of the heteroatom reduces that angle to an average of 168.0°, making the structure of the ligand more rigid. A large deviation of the octahedral geometry is therefore expected.

For **1** X-ray diffraction was performed, additional to 193 K, at 100 K (section 3.4.2). Due to a pulverization of crystals in the process of cooling, no diffraction experiment for both of the other compounds could be run at 100 K. Upon cooling compound **1**, a change of the space group to *Ia* is observed, cancelling the center of inversion relating the metal centers in the molecule at high temperature. After the phase transition, the two iron(II) atoms clearly can be distinguished. While the average bond length for Fe1-N is 2.204 Å and therefore only slightly larger than the value at 193 K, the Fe2-N bond length is with 2.025 Å much shorter than before. This is attributed to the depopulation of the  $e_g$ -orbitals.<sup>[16]</sup> The shrinking of the bonds by 7.1 % is in good agreement with the reported values for a spin crossover. Interestingly, the contraction of the N6 coordination sphere of Fe2 has another effect: for the second metal center, all bond lengths are elongated. As discussed above, the backbone of the ligand system is quite rigid. This influence comes to light once more: by switching one center into the *LS*-state, the second one gets even more distorted. This interplay is reflected by the change of the octahedral distortion parameters ( $\Sigma(\text{Fe1},HS) = 136.7^\circ$ ,  $\Sigma(\text{Fe2},LS) = 70.16^\circ$ ). While the average

*cis*-angle remains nearly constant ( $\Delta(\text{Fe1}) = 0.4^\circ$ ;  $\Delta(\text{Fe2}) = 0.6^\circ$ ), the *trans*-angles change more drastically by  $4.6^\circ$  to  $158.0^\circ$  for the *HS* center and  $9.5^\circ$  to  $172.1^\circ$  for the *LS* center. Being in that constrained geometry dictated by the rigidity of the oxadiazole, it is very unlikely for the iron(II) center in the *HS*-state to undergo a spin transition as well.

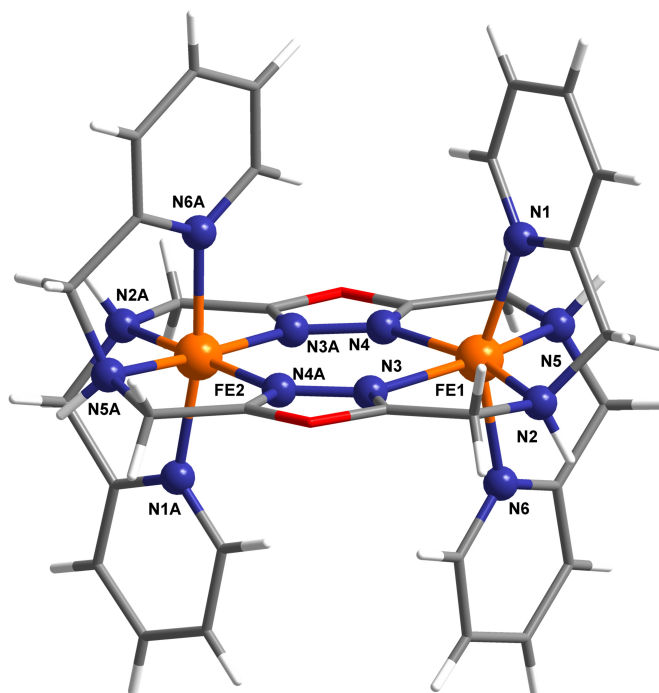


**Figure 1.** Crystal structure of  $[1]^{4+}$  measured at 100 K. Solvent molecules and counteranions have been omitted for clarity. Nitrogen and iron atoms have been highlighted and labelled. Colour code: iron is orange, nitrogen blue, oxygen red, carbon grey and hydrogen white.

In figure 2, a cutout of the molecular packing in compound **3** is shown. A very important role is attributed to the intermolecular interaction between the complexes. Here the counteranions and solvent molecules can become crucial, because they are linking the cations via hydrogen bonds. The cooperativity, which is introduced this way has enormous effects on the resulting spin crossover properties, such as  $T_{1/2}$ , sharpness of a transition and the occurrence of a hysteresis. <sup>[14]</sup>

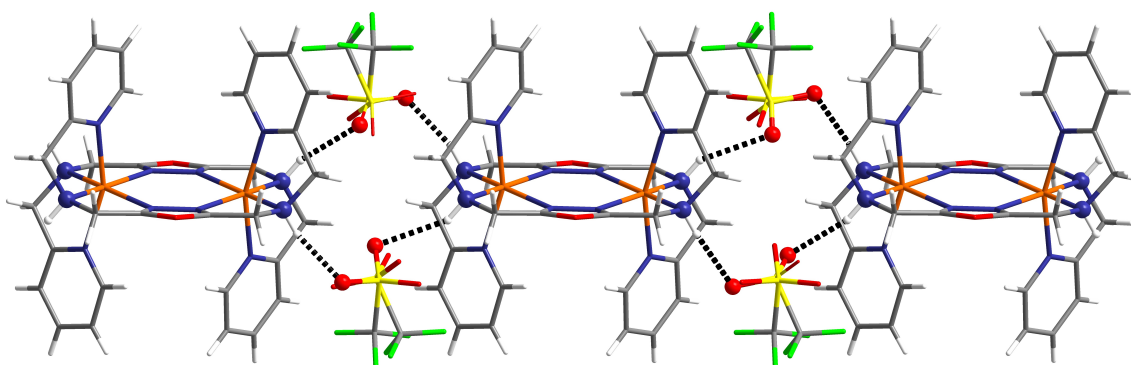


**Figure 2.** Representation of the hydrogen bonds in compound **3** (black dashed lines). Solvent molecules and some counteranions have been omitted for clarity. Selected atoms have been highlighted. The disorder of the counterions occurs alternating. Hydrogen bonds are shown as dashed lines for only one of the disordered position each.

It is straight forward that the intermolecular interaction has the largest influence when it is mediated directly to the transition active centers. An ideal position in our system is the amine proton at the nitrogen donor atom. It is the most direct way to shift the electron density at the metal center.

In all three compounds, the solvent molecules do not form any hydrogen bonds that affect the amine group. However, they are necessary for the integrity of the crystal structure and loss of solvent molecules results in the absence of spin crossover.

More important in the present compounds is to discuss the role of the counteranions. Close examination of compound **2** shows four  $\text{BF}_4^-$  anions enclosing the cation. However, no  $\text{NH}-\mu_2-\text{BF}_4^--\text{NH}$  connections are observed. All bonds from amine protons to counterions tend to form a bridge between the NH group and an aromatic or else an aliphatic proton. The picture is different in compound **1**. Here, every cation is twisted to its next neighbor. The square planes of two molecules, each generated by the four oxadiazole nitrogen and the four amine nitrogen, show a dihedral angle of  $81.3^\circ$ . One of the amine protons and its symmetry equivalent build a hydrogen bond towards an oxygen of the  $\text{ClO}_4^-$  anion. The same oxygen binds to the other amine proton in the next cation, which is orientated the other way. In this manner a twisted grid is formed where all of the amine protons are  $\mu_2$ -bridged to one another by the same oxygen atom from one of the counteranions. In compound **3** the cations form a linear chain. They are

bridged by hydrogen bonds mediated through the counteranions. Two opposing amine protons are connected to an oxygen atom from two  $\text{CF}_3\text{SO}_3^-$ . A second oxygen from the same anion builds hydrogen bonds to the NH group from the neighboring cation. This arrangement shows the largest cooperativity. Every disturbance of the ligand field of any iron(II) center is transmitted directly to the next molecule, where it has the same effect due to the similar order of the cations.

### 3.4.3. Magnetic Measurement and Mössbauer-spectroscopy

Variable-temperature magnetic measurements were carried out on freshly prepared crystalline samples of **1**, **2** and **3** with an external magnetic field of 1 kOe in a temperature range from 10 K to 300 K. For compound **1** and **2**, a sweep mode was used with a scan rate of 5 K/min in the temperature range from 10 K to 100 K and 200 K to 300 K. In between 100 K and 200 K, the sweep velocity was 1 K/min. For the measurement of compound **3**, a settle mode was used with a scan rate of 1 K/min, except in the ranges, where the spin transition occurs. Here, the scan rate was 0.5 K/min (158 K to 149 K and from 170 K to 180 K).

At 300 K compound **1** shows a value for  $\chi_M T$  of  $7.14 \text{ cm}^3 \text{ K mol}^{-1}$ . Upon cooling the susceptibility decreases slightly to  $6.55 \text{ cm}^3 \text{ K mol}^{-1}$  until it reaches 170 K. At this point, a rapid decline is observed which comes to a halt at 126 K, where  $\chi_M T$  settles at  $3.80 \text{ cm}^3 \text{ K mol}^{-1}$ . Further lowering the temperature has no effect on the magnetic susceptibility in a range from 100 K to 50 K. Only below 50 K  $\chi_M T$  starts to decrease slightly again to reach  $3.29 \text{ cm}^3 \text{ K mol}^{-1}$  at 10 K. This lowering of the  $\chi_M T$  value at low temperature probably arises from intermolecular interactions, saturation and contributions from zero-field splitting. Increasing temperature leads again to the same plateau value for the magnetic moment of  $3.80 \text{ cm}^3 \text{ K mol}^{-1}$ . Once again a rapid increment of the susceptibility is monitored with the same shape as in the cooling process. Upon reaching a temperature of 170 K, the slope shows again a very small gradient. The magnetic moment is with  $6.58 \text{ cm}^3 \text{ K mol}^{-1}$  slightly higher compared to the values during cooling. Raising the temperature again to 300 K leaves the sample with a value of  $7.18 \text{ cm}^3 \text{ K mol}^{-1}$ .

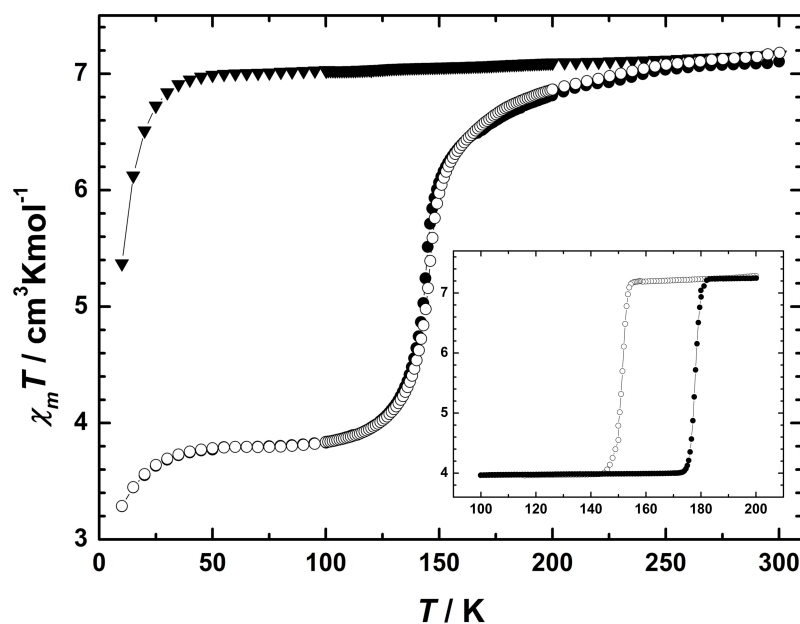


**Figure 3.**  $\chi_M T$  versus T data for compound **1** (solid circles: cooling, open circles: heating) and **2** (triangles) and compound **3** (small picture). The data is per dinuclear complex molecule.

For compound **2**, the variable temperature magnetic data revealed no spin transition. At 300 K, the value for  $\chi_M T$  of  $7.14 \text{ cm}^3 \text{ K mol}^{-1}$  is similar to the value of compound **1**. Decreasing the temperature has no effect on the magnetic susceptibility until 50 K is reached, where  $\chi_M T$  declines to a final value of  $5.37 \text{ cm}^3 \text{ K mol}^{-1}$  at 10 K. This behavior is proof for us, that the change of  $\chi_M T$  at a temperature below 50 K here and as well as in compound **1** is not caused by a spin transition of the second iron(II). In contrast to the curve of compound **1**, the magnetic moment vs. temperature for compound **3** has a much more abrupt shape. The value of  $7.24 \text{ cm}^3 \text{ K mol}^{-1}$  observed at 200 K remains almost constant with decreasing temperature. At 154 K the value for  $\chi_M T$  shows a steep descent until the temperature reaches 149 K where it settles immediately to  $3.97 \text{ cm}^3 \text{ K mol}^{-1}$ . Upon further cooling the magnetic moment remains constant until 100 K. While increasing the temperature again, it attracted our attention that the magnetic moment did not rise when 149 K was reached. Instead it lasted until 174 K. At that point, a steep increase in  $\chi_M T$  is found, which stopped at 182 K reaching finally the same value of  $7.24 \text{ cm}^3 \text{ K mol}^{-1}$ . The divergence in the steep decrease or increase of the magnetic moment upon cooling and heating reveals a hysteresis loop

with a noticeable width of 26 K. The origin of this hysteresis is probably caused by cooperative effects that arise from intermolecular hydrogen bonds as discussed above. It is expected to find this pronounced behavior only for compound 3, as in here a distortion of the ligand field at one metal has the largest influence on the rest of the iron(II) centers.

Mössbauer-spectroscopy was performed on a freshly prepared crystalline sample of **1** to gain insight in the nature of the local spin-states of the single iron in the dimer complex. Spectra were recorded at 293 K and at 100 K.

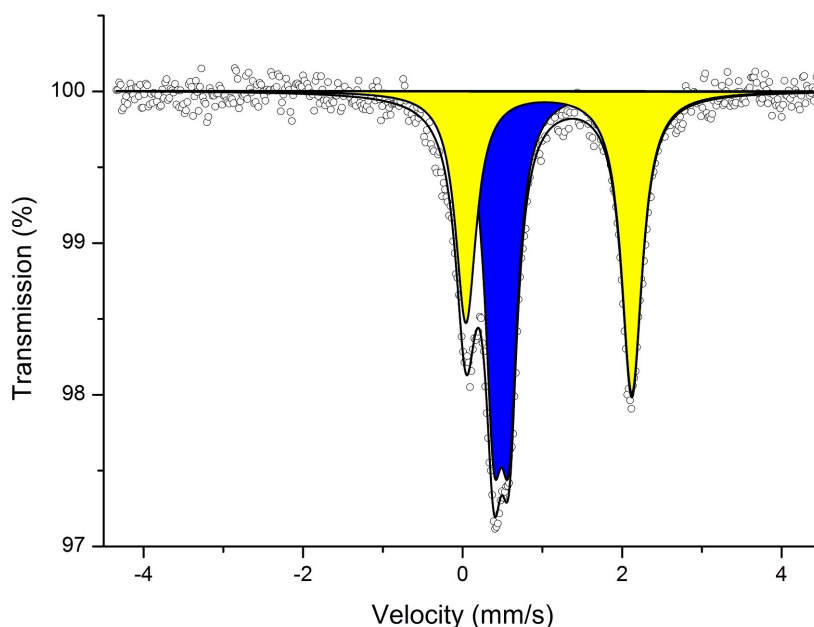


**Figure 4.** Mössbauer spectra of compound **1** at 100 K. The open circles are the experimental data, the black solid line shows the fit, the blue area is *LS* fraction, the yellow the *HS* fraction.

At high temperature, only a single doublet with an isomer shift (IS) of  $0.9393(58) \text{ mm s}^{-1}$  and a quadrupole splitting  $\Delta$  (QS) of  $2.128(12) \text{ mm s}^{-1}$  is found (see SI). This indicates that both Fe(II)-ions are in the *HS*-state. The crystallinity of the sample causes small texture effects which leads to an asymmetry of the doublet. The spectrum at 100 K differs significantly (figure 4). Again a doublet refers to the *HS*-state (IS =



1.0811(55) mm s<sup>-1</sup>,  $QS = 2.080(11)$  mm s<sup>-1</sup>). Additionally, however, a second signal with an  $IS$  of 0.4862(52) mm s<sup>-1</sup> and a small  $QS = 0.1907(86)$  mm s<sup>-1</sup> is present which clearly can be assigned to an Fe(II) *LS* species. Relative areas of the signals reveal a ratio of 48.7 % *LS* to 51.3 % *HS*. This proves that the decrement of the magnetic susceptibility is caused from a spin transition. Looking at the crystal structure at 100 K, it is clear that this ratio is a result of a molecule incorporating the *HS* and the *LS*-state rather than a 1:1 mixture of [*HS-HS*] and [*LS-LS*] molecules. The comparable values for **3** are found to be  $IS = 1.0834(49)$  mm s<sup>-1</sup>,  $QS = 2.4904(98)$  mm s<sup>-1</sup> for Fe(II) *HS* site and  $IS = 0.4957(88)$  mm s<sup>-1</sup> and  $QS = 0.229(11)$  mm s<sup>-1</sup> for the Fe(II) *LS* site at 100 K.

### 3.5. Conclusion

We prepared and characterized the novel bis-tridentate oxadiazole bridging ligand **L** and used it for reaction with different iron(II) salts. At room temperature, iron(II) centers of three dinuclear compounds are in the *HS*-state, demonstrated by the magnetic susceptibility, Mössbauer-spectroscopy, single crystal X-ray diffraction and the absence of color of the crystal.

With lowering the temperature, two out of three iron(II)-oxadiazole based complexes show SCO. The color change upon cooling was the first indication for SCO. Magnetic susceptibility studies revealed a magnetic moment that originates from a mixture of an iron(II) *HS* and *LS* species at low temperature. Mössbauer-spectroscopy confirmed the presence of both states. Finally, X-ray diffraction ruled out a statistical iron(II) [*HS-HS*] and [*LS-LS*] mixture, but proves a distinct [*HS-LS*]-state due to the clear differences in bond lengths, angles and octahedral distortion parameters. Furthermore, one of the compounds show a sharp hysteresis of 26 K, which is explained by the intermolecular hydrogen bonds that leads to a large cooperativity.

### 3.6. Experimental Section

**General Methods and Materials:** All chemicals were purchased from Alfa Aesar, Deutero, Fisher Chemicals, Sigma-Aldrich and Acros Organics and used without further purification. The NMR spectra were recorded at room temperature by using a Bruker DRX 400 spectrometer and analysed with the program MestReNova.<sup>[17]</sup> Magnetic susceptibility data was collected with a Quantum Design SQUID magnetometer MPMSXL in a temperature range of 10-300 K with an applied field of 10 kOe. <sup>57</sup>Fe-Mössbauer spectra were recorded at the Johannes Gutenberg University Mainz by Dr. Vadim Ksenofontov and Sergii Shylin. ESI mass spectra, FD mass spectra and elemental analyses (C, H, N and S) were measured at the microanalytical laboratories of the Johannes Gutenberg University Mainz. X-ray diffraction data were collected at 100 K and 193 K with a Bruker SMART diffractometer and a STOE IPDS 2T at the Johannes Gutenberg University Mainz. The structures were solved with ShelXT and refined with ShelXL 2013 with the program Olex2.<sup>[18]</sup> CCDC 1434701 (for **1**·4MeCN, 100 K), 1434702 (for **1**·4MeCN, 193 K), 1434703 (for **2**·2MeCN, 100 K) and 1434704 (for **3**·2MeCN, 193 K) contain the supplementary crystallographic data for this paper. These data can be obtained free of charge from The Cambridge Crystallographic Data Centre via [www.ccdc.cam.ac.uk/datarequest/cif](http://www.ccdc.cam.ac.uk/datarequest/cif). **Caution!** The prepared perchlorate complexes are potentially explosive. Even though no explosions occurred, only small amounts should be prepared and handled with care.

**Ligand Synthesis:** 1,2-Bis(chloroacetyl)hydrazine and 2,5-bis(chloromethyl)-1,3,4-oxadiazole were prepared as described in the literature,<sup>[13]</sup> 2,5-bis-[(2-pyridylmethyl)-amino]-methyl-1,3,4-oxadiazole was synthesized by a modified version of the analogous 1,3,4-thiadiazole ligand.<sup>[11]</sup>

**2,5-Bis-[(2-pyridylmethyl)amino]methyl-1,3,4-oxadiazole (L):** 2-(Aminomethyl)pyridine (3.244 g, 30.00 mmol) and potassium carbonate (6.910 g, 50.00 mmol) were suspended in acetonitrile (600 mL) and heated to 70 °C. A solution of 2,5-bis(chloromethyl)-1,3,4-oxadiazole (1.670 g, 10.00 mmol) in acetonitrile (100 mL) was added dropwise over a period of 30 min. After complete addition, the suspension was stirred and re-

fluxed for additional 16 h. After cooling to room temperature, the white precipitate was filtered and the solvent removed under reduced pressure. The resulting brown oil was purified by column chromatography (aluminium oxide; chloroform/methanol, 9:1) to give the pure product as orange oil. Yield: 1.831 g (5.9 mmol, 59 %)  $^1\text{H}$  NMR (400 MHz,  $\text{CDCl}_3$ , 25 °C):  $\delta$  = 8.54 [2H, d,  $J$  = 4.1 Hz,  $H5\text{Py}$ ], 7.63 [2H, td,  $J$  = 7.7, 1.7 Hz,  $H4\text{Py}$ ], 7.28 [2H, d,  $J$  = 7.8 Hz,  $H2\text{Py}$ ], 7.16 [2H, dd,  $J$  = 6.5, 5.1 Hz,  $H3\text{Py}$ ], 4.06 [4H, s, ODA- $\text{CH}_2$ ], 3.97 [4H, s,  $\text{CH}_2$ -Py], 2.50 [2H, s, NH] ppm.  $^{13}\text{C}$  NMR (400 MHz,  $\text{CDCl}_3$ ):  $\delta$  = 165.73 (C, ODA), 158.55 (C1-Py), 149.55 (C5-Py), 136.71 (C4-Py), 122.57 (C2-Py), 122.37 (C3-Py), 54.20 (Py- $\text{CH}_2$ ), 43.37 ( $\text{CH}_2$ -ODA) ppm. FD-MS ( $\text{CHCl}_3$ ):  $m$  (%) = 309.25 (11.13) [ $\text{L} - \text{H}^+$ ], 310.26 (17.71) [ $\text{L}$ ], 311.26 (100) [ $\text{L} + \text{H}^+$ ], 312.23 (16.73) [ $\text{L} + 2 \text{H}^+$ ].

**$[\text{Fe}_2(\mu\text{-L})_2](\text{ClO}_4)_4 \cdot 4\text{MeCN}$  (1):** A solution of **L** (0.10 mmol, 31 mg) in acetonitrile (4 mL) was added to a solution of  $\text{Fe}(\text{ClO}_4)_2 \cdot x\text{H}_2\text{O}$  (0.10 mmol, 25 mg) in acetonitrile (3 mL). An immediate color change from yellow to brown was observed. After a few hours single crystals suitable for single crystal X-ray diffraction could be obtained. Yield: 45 mg (0.034 mmol, 34 %).  $\text{C}_{32}\text{H}_{38}\text{Cl}_4\text{Fe}_2\text{N}_{12}\text{O}_{19}$  [ $[\text{Fe}_2(\mu\text{-L})_2](\text{ClO}_4)_4 \cdot \text{H}_2$  (1145,98): calc. C 33.47, H 3.34, N 16.64; found C 33.22, H 3.00, N 14.72.

**$[\text{Fe}_2(\mu\text{-L})_2](\text{BF}_4)_4 \cdot 2\text{MeCN}$  (2):** A solution of **L** (0.10 mmol, 31 mg) in acetonitrile (4 mL) was added to a solution of  $\text{Fe}(\text{BF}_4)_2 \cdot 6\text{H}_2\text{O}$  (0.10 mmol, 34 mg) in acetonitrile (3 mL). An immediate color change from yellow to brown was observed. Using vapor diffusion with ether, crystals suitable for single crystal X-ray diffraction could be obtained after 24 hours. Yield: 19 mg (0.016 mmol, 17 %).  $\text{C}_{35}\text{H}_{40.5}\text{B}_4\text{F}_{16}\text{Fe}_2\text{N}_{13.5}\text{O}_2$  [ $[\text{Fe}_2(\mu\text{-L})_2](\text{BF}_4)_4 \cdot 1.5\text{MeCN}$ ] (1141.19): calcd. C 36.84, H 3.58, N 16.57; found C 36.80, H 3.64, N 16.86.

**$[\text{Fe}_2(\mu\text{-L})_2](\text{CF}_3\text{SO}_3)_4 \cdot 2\text{MeCN}$  (3):** A solution of **L** (0.20 mmol, 62 mg) in acetonitrile (4 mL) was added to a solution of  $\text{Fe}(\text{CF}_3\text{SO}_3)_2$  (0.20 mmol, 71 mg) in acetonitrile (5 mL). An immediate color change from yellow to brown was observed. After adding 4 mL tetrahydrofuran, crystals suitable for single crystal X-ray diffraction could be obtained after several hours. Yield: 41 mg (0.029 mmol, 14.5 %).  $\text{C}_{40}\text{H}_{42}\text{F}_{12}\text{Fe}_2\text{N}_{14}\text{O}_{14}\text{S}_4$

$[\text{Fe}_2(\mu\text{-L})_2](\text{CF}_3\text{SO}_3)_4 \cdot 2\text{MeCN}$  (1410.78): calcd. C 34.06, H 3.00, N 13.90, S 9.09; found C 33.91, H 3.17, N 14.09, S 9.16.

### 3.7. Acknowledgements

Dr. Vadim Ksenofontov and Sergii Shylin are kindly acknowledged for collecting the Mössbauer data of compound **1** and **3** at 100 K and 293 K. Dr. Dieter Schollmeyer is thanked for the XRD measurement of compound **1** at 100 K.

Keywords: Spin Crossover·Molecular Magnetism·1,3,4 Oxadiazole·Hysteresis·Iron(II)

### 3.8. References

- [1] P. Gütllich, A. B. Gaspar, Y. Garcia, *Beilstein Journal of Organic Chemistry*, **2013**, 9, 342-391.
- [2] S. Brooker, J. A. Kitchen, *Dalton Trans.*, **2009**, 7331-7340.
- [3] O. Kahn, *Science*, **1998**, 279, 44-48.
- [4] M. A. Halcrow, *Chem. Soc. Rev.*, **2011**, 40, 4119-4142.
- [5] P. Gütllich, *Eur. J. Inorg. Chem.*, **2013**, 581-591.
- [6] P. Gütllich, H. A. Goodwin, in *Spin Crossover in Transition Metal Compounds I*, (Eds.: P. Gütllich, H. A. Goodwin), Springer Berlin Heidelberg, **2004**, pp. 1-47.
- [7] L. A. Barrios, E. Peyrecave-Lleixà, G. A. Craig, O. Roubeau, S. J. Teat, G. Aromí, *Eur. J. Inorg. Chem.*, **2014**, 6013-6021.
- [8] B. Weber, W. Bauer, J. Obel, *Angew. Chem. Int. Ed.*, **2008**, 47, 10098-10101.
- [9] V. Niel, J. M. Martinez-Agudo, M. C. Muñoz, A. B. Gaspar, J. A. Real, *Inorg. Chem.*, **2001**, 40, 3838-3839.
- [10] M. H. Klingele, B. Moubarak, J. D. Cashion, K. S. Murray, S. Brooker, *Chem. Commun.*, **2005**, 987-989.
- [11] C. F. Herold, L. M. Carrella, E. Rentschler, *Eur. J. Inorg. Chem.*, **2015**, 3632-3636.

- [12] J. Klingele, D. Kaase, M. Schmucker, Y. Lan, G. Chastanet, J.-F. Létard, *Inorg. Chem.*, **2013**, 52, 6000-6010.
- [13] R. Zhang, R. Jordan, O. Nuyken, *Macromol. Rapid Commun.*, **2003**, 24, 246-250.
- [14] J. A. Kitchen, N. G. White, G. N. L. Jameson, J. L. Tallon, S. Brooker, *Inorg. Chem.*, **2011**, 50, 4586-4597.
- [15] P. Guionneau, M. Marchivie, G. Bravic, J.-F. Létard, D. Chasseau, in *Spin Crossover in Transition Metal Compounds I*, Vol. 234, Springer Berlin Heidelberg, **2004**, pp. 97-128.
- [16] J. A. Kitchen, N. G. White, V. A. Milway, G. N. Jameson, J. L. Tallon, S. Brooker, *Inorg. Chem.*, **2013**, 52, 11185-11199.
- [17] J. C. Cobas, F. J. Sardina, *Concepts in Magnetic Resonance*, **2003**, 19A, 80-96.
- [18] O. V. Dolomanov, L. J. Bourhis, R. J. Gildea, J. A. K. Howard, H. Puschmann, *Journal of Applied Crystallography*, **2009**, 42, 339-341.

### 3.9. Supporting Information

*Eur. J. Inorg. Chem.* **2016**, 13-14, 1955-1960.

#### **SUPPORTING INFORMATION**

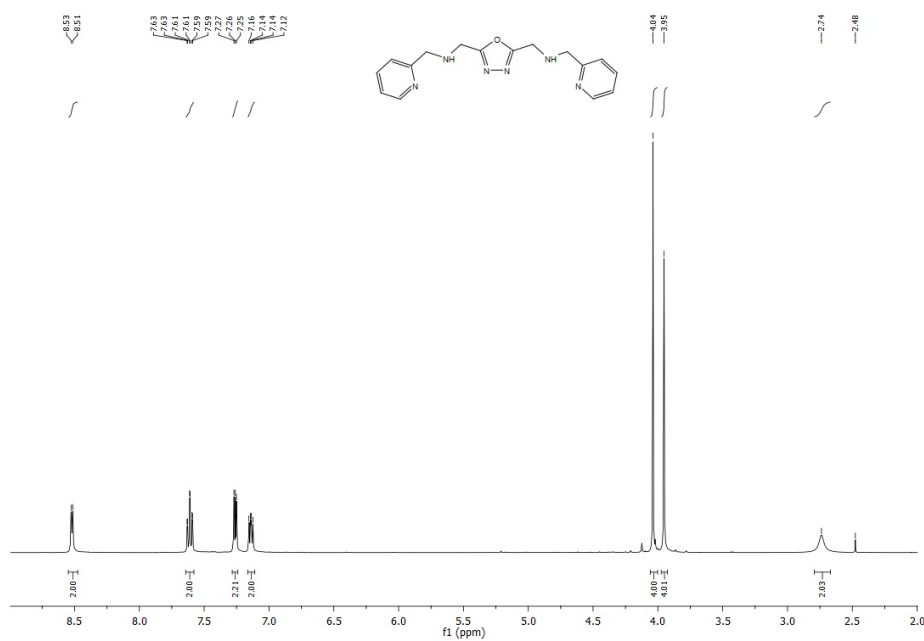
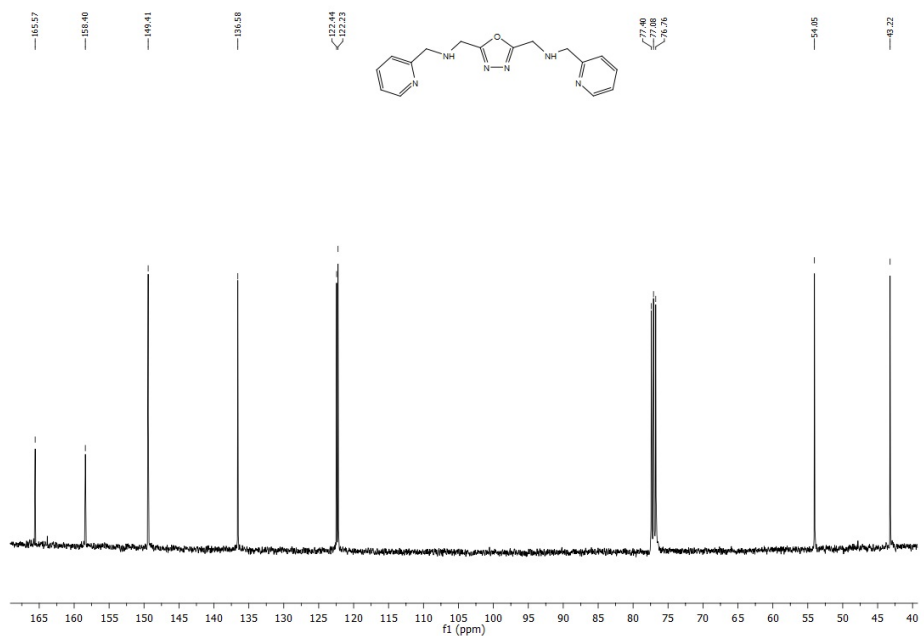
**DOI:** 10.1002/ejic.201501278

**Title:** The First 1,3,4-Oxadiazole Based Dinuclear Iron(II) Complexes Showing Spin Crossover Behavior with Hysteresis

**Author(s):** Christian Köhler, Eva Rentschler\*

NMR spectroscopy  
X-ray Diffraction  
Mössbauer Spectroscopy  
Miscellaneous Pictures

## NMR-Spectroscopy

Figure 3.1.:  $^1\text{H-NMR}$  spectrum of 2,5-bis([(2-pyridylmethyl)amino]methyl)-1,3,4-oxadiazole (L)Figure 3.2.:  $^{13}\text{C-NMR}$  spectrum of 2,5-bis([(2-pyridylmethyl)amino]methyl)-1,3,4-oxadiazole (L)

## X-Ray Diffraction

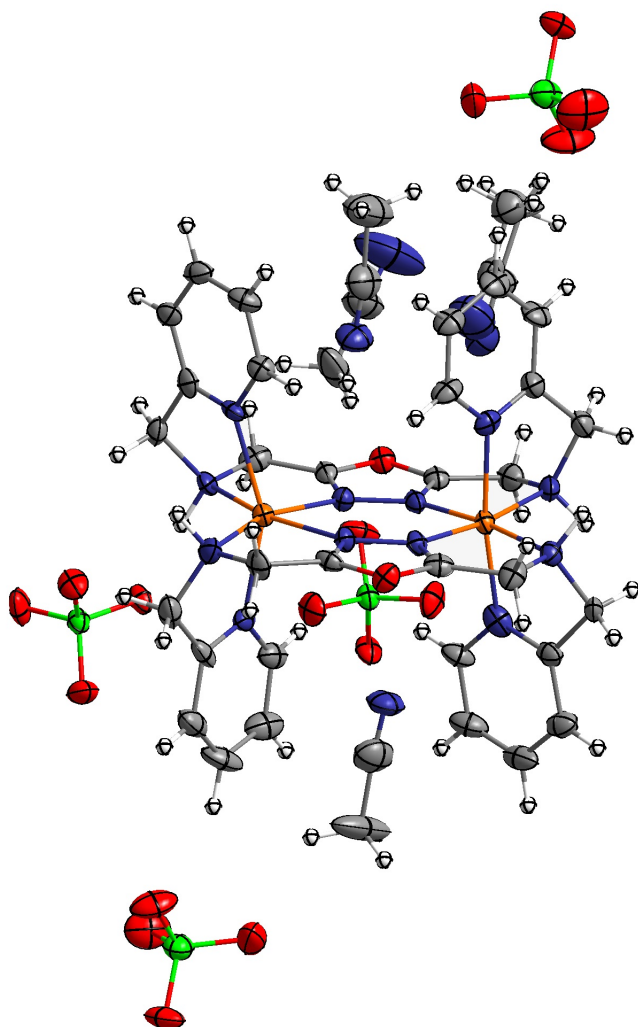
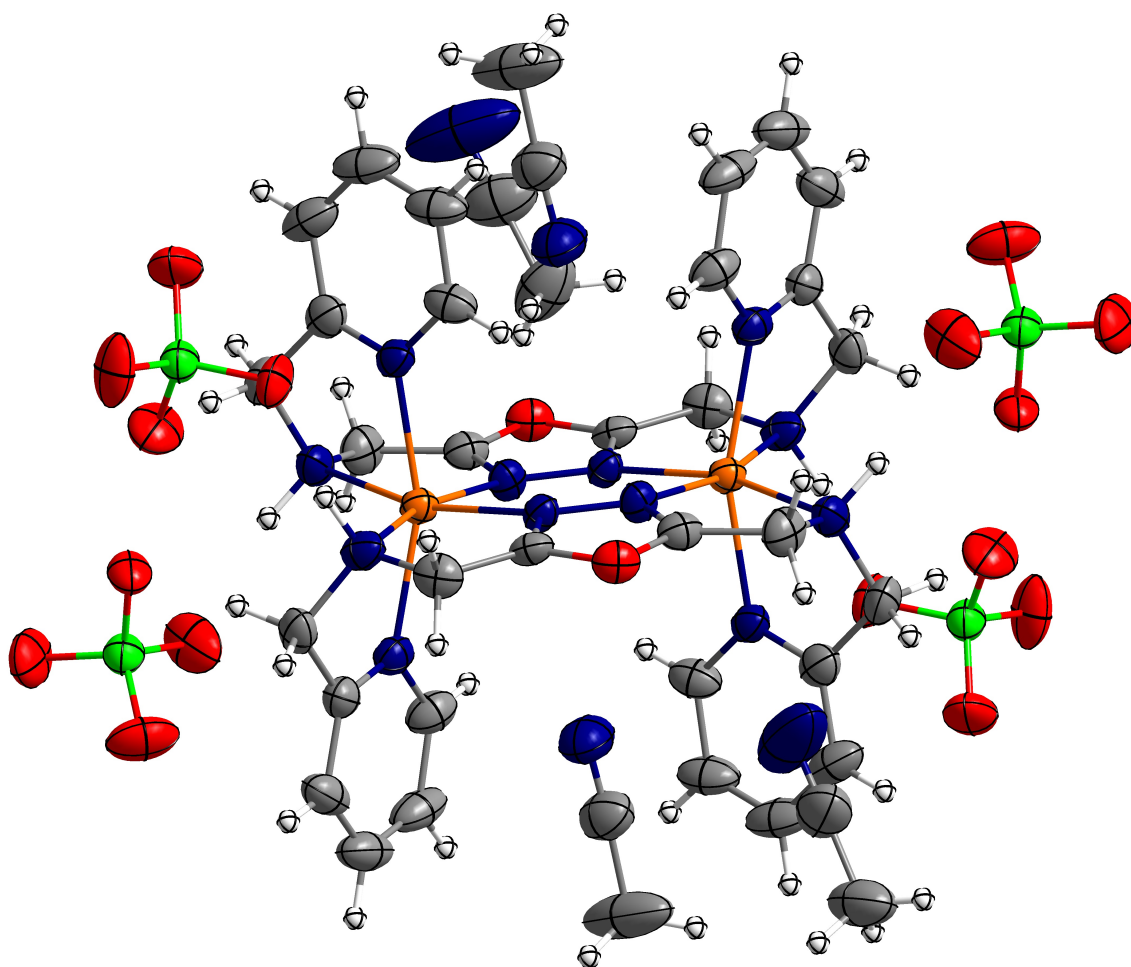


Figure S3: Molecular structure of **1·4MeCN** ( $[[\text{Fe}(\text{II})_2\text{L}_2](\text{ClO}_4)_4 \cdot 4\text{MeCN}]$ ) at 100 K with thermal ellipsoids. Colour scheme: orange - Fe(II), red - O, blue - N, grey - C, white - H, green - Cl





Molecular structure of **1**·4MeCN ( $[[\text{Fe}(\text{II})_2\text{L}_2](\text{ClO}_4)_4 \cdot 4\text{MeCN}]$ ) at 193 K with thermal ellipsoids. Colour scheme: orange - Fe(II), red - O, blue - N, grey - C, white - H, green - Cl

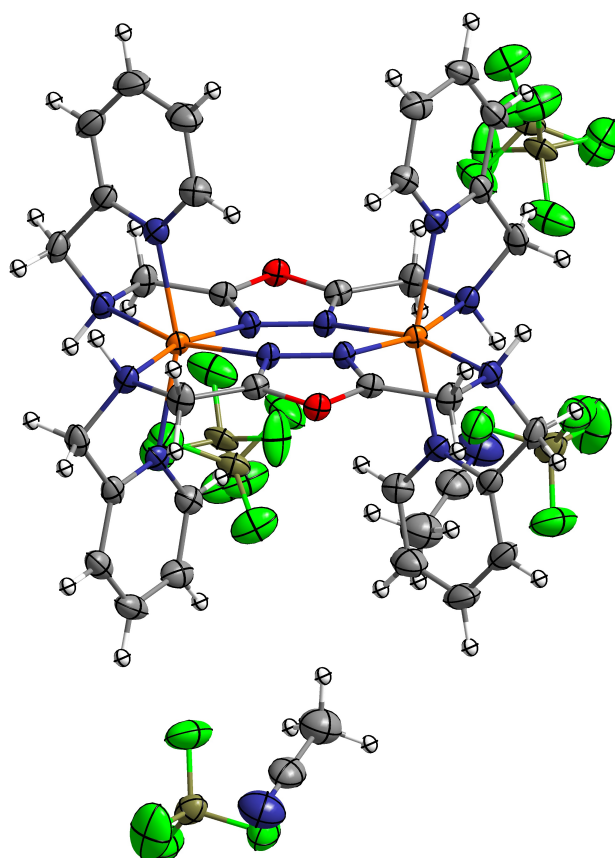


Figure 3.3.: Figure S4: Molecular structure of **2·2MeCN** ( $[[\text{Fe}(\text{II})_2\text{L}_2](\text{BF}_4)_4 \cdot 2\text{MeCN}]$ ) at 173 K with thermal ellipsoids. Colour scheme: orange - Fe(II), red - O, blue - N, grey - C, white - H, light green - F, dark green - B

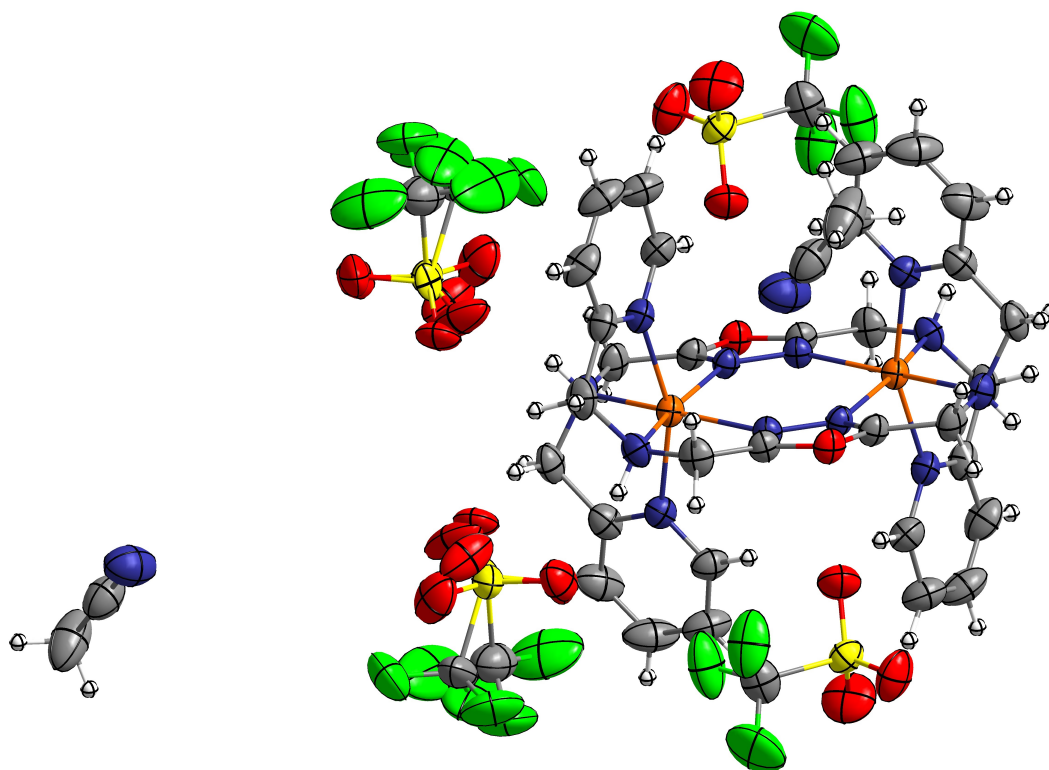


Figure S5: Molecular structure of **3**·2MeCN ( $[[\text{Fe}(\text{II})_2\text{L}_2](\text{CF}_3\text{SO}_3)_4 \cdot 2\text{MeCN}]$ ) at 193 K with thermal ellipsoids. Colour scheme: orange - Fe(II), red - O, blue - N, grey - C, white - H, light green - Cl, yellow - S

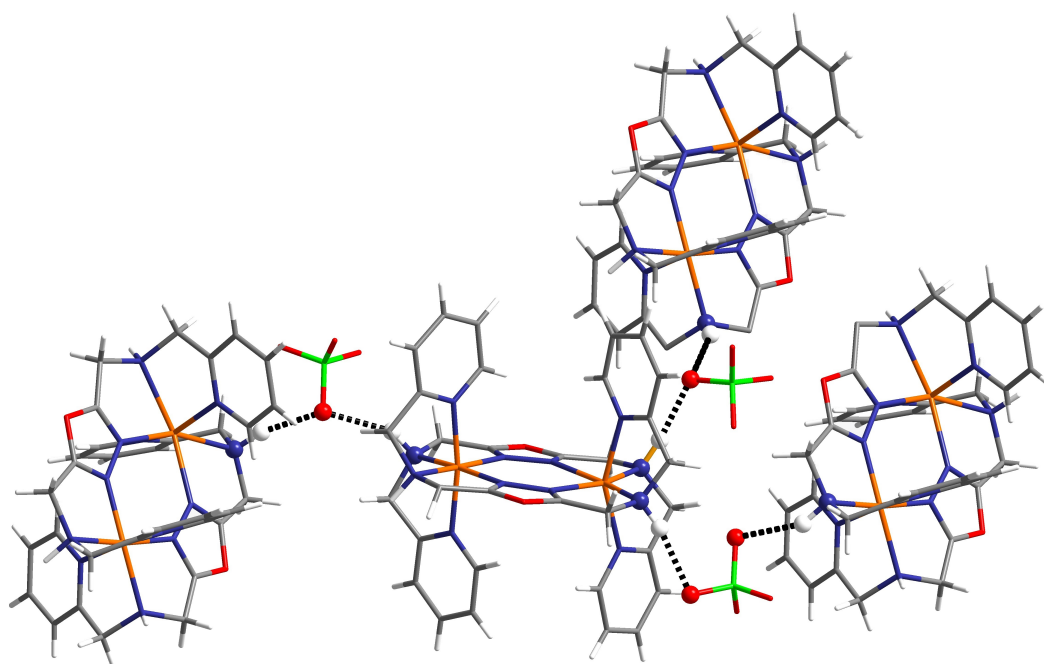


Figure S6: Hydrogen bonds in **1**·4MeCN ( $[[\text{Fe}(\text{II})_2\text{L}_2](\text{ClO}_4)_4 \cdot 4\text{MeCN}]$ ) at 193 K with thermal ellipsoids. Colour scheme: orange - Fe(II), red - O, blue - N, grey - C, white - H, light green - Cl, yellow - S. Selected atoms have been highlighted. Hydrogen bonds are shown as black, dashed lines.

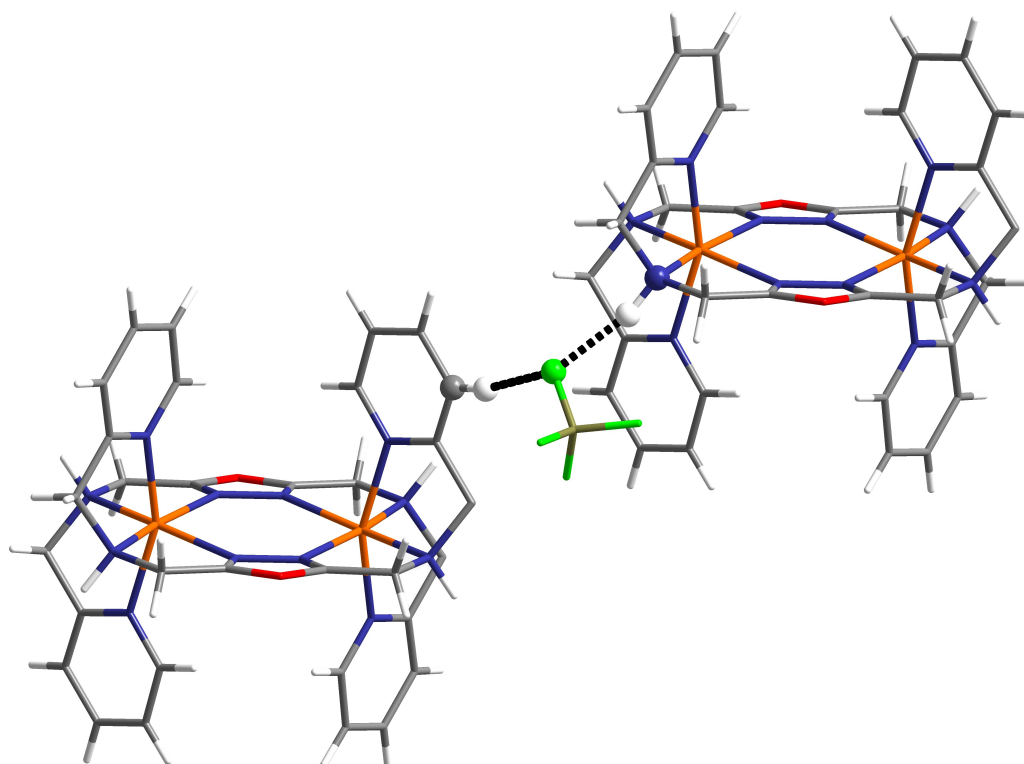


Figure S7: Hydrogen bonds in **2**·2MeCN ( $[[\text{Fe}(\text{II})_2\text{L}_2](\text{BF}_4)_4 \cdot 2\text{MeCN}]$ ) at 173 K with thermal ellipsoids. Colour scheme: orange - Fe(II), red - O, blue - N, grey - C, white - H, light green - Cl, dark green B. Selected atoms have been highlighted. Hydrogen bonds are shown as black, dashed lines.

Table 3.1.: Crystallographic parameters for compounds **1**, **2** and **3**

	1·4MeCN (100 K)	1·4MeCN (193 K)	2·2MeCN	3·2MeCN
Formula	C <sub>40</sub> H <sub>48</sub> Cl <sub>4</sub> Fe <sub>2</sub> N <sub>16</sub> O <sub>18</sub>	C <sub>40</sub> H <sub>48</sub> Cl <sub>4</sub> Fe <sub>2</sub> N <sub>16</sub> O <sub>18</sub>	C <sub>36</sub> H <sub>42</sub> B <sub>4</sub> F <sub>16</sub> Fe <sub>2</sub> N <sub>14</sub> O <sub>2</sub>	C <sub>40</sub> H <sub>42</sub> F <sub>12</sub> Fe <sub>2</sub> N <sub>14</sub> O <sub>14</sub> S <sub>4</sub>
Formula weight	1294.44	1294.44	1161.77	1410.81
Crystal system	monoclinic	monoclinic	triclinic	triclinic
space group	<i>Ia</i>	<i>I2/a</i>	<i>P</i> <sup>-</sup> <sub>1</sub>	<i>P</i> <sup>-</sup> <sub>1</sub>
<i>a</i> /Å	19.656(8)	19.8102(12)	10.411(5)	10.7467(4)
<i>b</i> /Å	10.534(5)	10.3740(4)	10.658(5)	12.3747(5)
<i>c</i> /Å	25.305(17)	25.8968(16)	) 12.712(5)	13.3181(5)
<i>α</i> /°	90	90	114.092(5)	63.307(3)
<i>β</i> /°	95.555(10)	95.771(5)	101.008(5)	89.653(3)
<i>γ</i> /°	90	90	102.816(5)	66.053(3)
<i>V</i> /Å <sup>3</sup>	5215(5)	5295.1(5)	1191.1(9)	1412.07(10)
<i>Z</i>	4	4	1	1
<i>T</i> /K	100.15	193.15	173.15	193.15
<i>ρ</i> /cm <sup>3</sup>	1.649	1.624	1.620	1.659
<i>μ</i> /mm <sup>-1</sup>	0.850	7.012	0.723	0.775
<i>R</i> ( <i>int</i> )	0.0577	0.0501	0.0605	0.0541
<i>S</i>	0.976	1.026	1.017	1.043
<i>R</i> 1 ( <i>I</i> > 2σ( <i>I</i> ))	0.0571	0.0500	0.0367	0.0424
<i>wR</i> 2	0.1166	0.1278	0.0886	0.1093

## Mössbauer Measurement

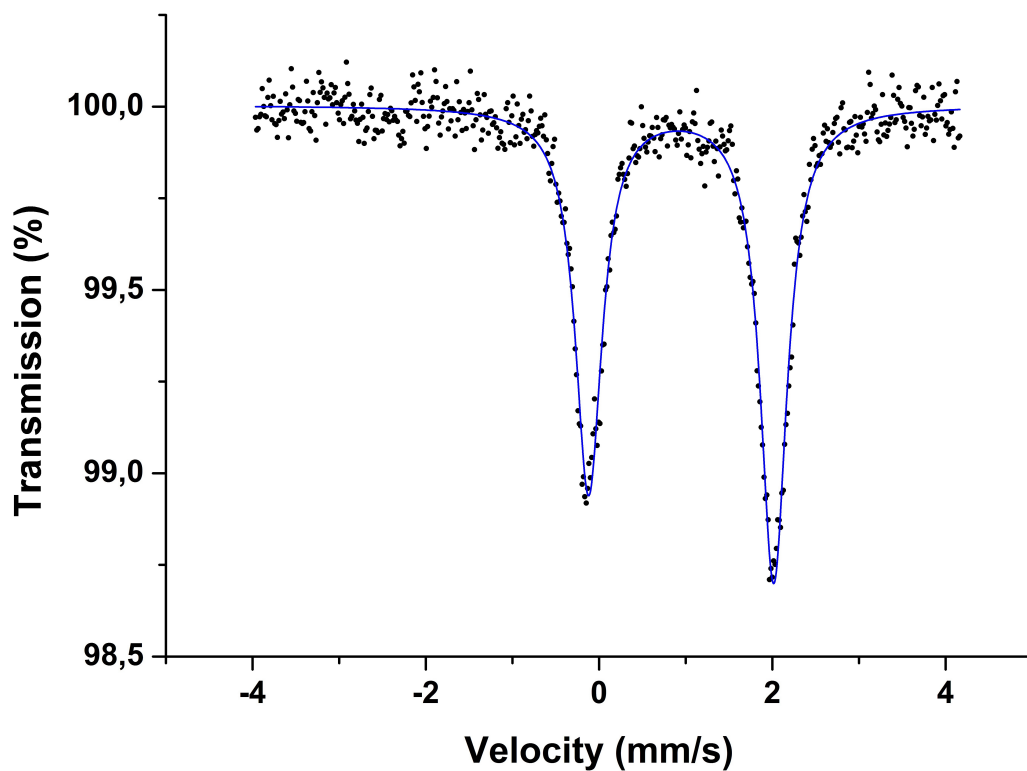
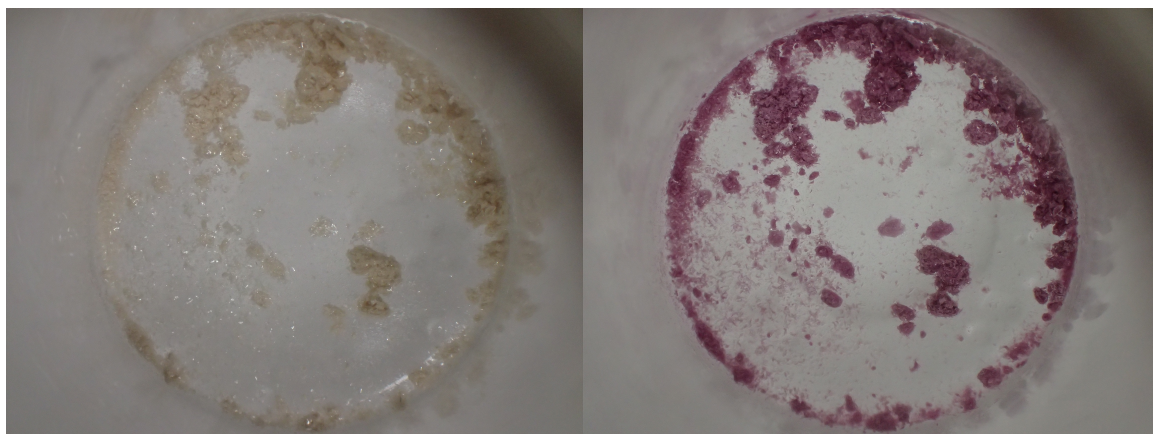
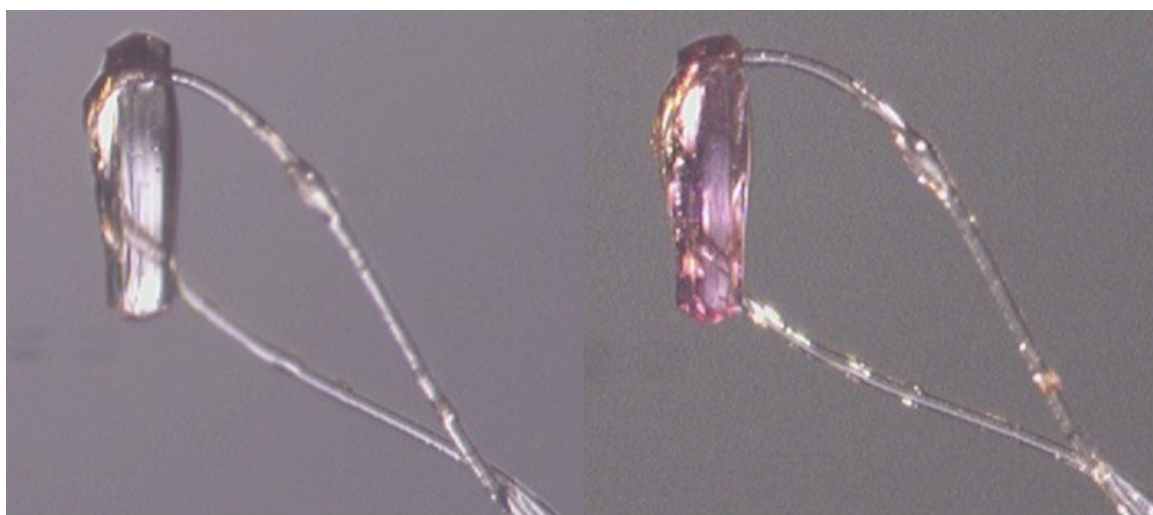


Figure S8: Mössbauer spectrum of **1** at 293 K. The dots show the experimental data, the blue line is the fit showing Fe(II) in *HS* site. Isomer Shift = 0.9303(58) mm s<sup>-1</sup>, quadrupole splitting = 2.128(12) mm s<sup>-1</sup> and site population: 100 %.

## Miscellaneous Pictures



Picture S1: Left: polycrystalline sample of 1 at room temperature. Right: sample after cooling with liquid nitrogen.



Picture S2: Left: single crystal used for X-ray crystallography at 170 K. Right: single crystal after cooling to 100 K.



### 3.10. Summary

We were successful in synthesizing compounds **1**, **2** and **3** with the composition  $[\text{Fe}_2\text{L}_2]\text{X}_4$  (X: **1** =  $\text{BF}_4^-$ , **2** =  $\text{ClO}_4^-$  and **3** =  $\text{CF}_3\text{SO}_3^-$ ). Using single crystal XRD, the structures were solved in the space group  $P\bar{1}$  for **2** and **3**, whereas **1** crystallizes in the space group  $I2/a$ . In all three compounds, the bond lengths between the N-donor atoms and the iron(II)-centers are comparable and indicate a  $[\text{HS-HS}]$ -state at 193 K and, in extension, at room temperature. The recorded Mössbauer spectra of **2** confirmed the  $[\text{HS-HS}]$ -state at room temperature. Lowering the temperature to 85 K results in a mixture of 51.3% *HS* and 48.7% *LS* revealing a ratio of 1:1 within the error.

This data was verified by magnetic measurements. Lowering the temperature of a sample of compound **1** from 300 K,  $\chi_M T$  decreases abruptly from an initial value of  $7.14 \text{ cm}^3 \text{ K mol}^{-1}$  at approximately 170 K to  $3.80 \text{ cm}^3 \text{ K mol}^{-1}$  at 126 K and remains constant until 50 K. The plateau region, which occurs below 120 K, emerges from a mixture of *high-spin* and *low-spin*. Further cooling results in a spin crossover independent decrement of  $\chi_M T$  which probably arises from small zero field contribution. The XRD measurement at 100 K revealed, that the space group is changing from  $I2/a$  to  $Ia$  during the transition, which is attributed to a sudden loss of the inversion center. Closer examination of the structure shows, that after the transformation the iron centers are not any longer equivalent. The average Fe-N bond lengths for Fe1 is  $2.204 \text{ \AA}$  whereas for Fe2 it is  $2.025 \text{ \AA}$ , which makes it possible to assign the metal centers two different spin states and proves the occurrence a mixed  $[\text{HS-LS}]$ -state.

Surprisingly, the magnetic data of **2** and **3** differ significantly from the data of **1**. For **2**,  $\chi_M T$  is with  $7.14 \text{ cm}^3 \text{ K mol}^{-1}$  constant from 300 K until 50 K, where the value drops to  $5.37 \text{ cm}^3 \text{ K mol}^{-1}$  due to zero field splitting comparable to **1**. Compound **3** shows again a spin transition, but here, it is a very abrupt and sharp one, starting at 154 K until 149 K. Upon reheating the sample up to 300 K, the  $\chi_M T$  value increases not as expected at around 150 K, which would indicate a stabilization of the  $[\text{HS-HS}]$ -state, but remains at  $3.97 \text{ cm}^3 \text{ K mol}^{-1}$  until 174 K. Only at this temperature  $\chi_M T$  reaches its initial value again, giving a pronounced thermal hysteresis of 26 K.

The origin of this behavior is found in the crystal structure. In **1** and **3**, hydrogen bonds from the amine bound proton are formed towards oxygen atoms from the counterions,

whereas in **2** the hydrogen bonds acceptors are fluorine ions. The withdrawal of electron density mediated via the proton at the N-donor atom by the fluorine reduces the LFS, and the *LS*-state cannot be stabilized anymore.

The different appearance of the spin transition in compound **1** and **3** is owed to the different number of intermolecular contacts. In **1**, every complex cation is connected via a counter ion to four other cations. If one of them undergoes a spin crossover, its neighbor will only be affected in a small way. In compound **3**, a cation is connected to its direct neighbors by two hydrogen bonds, which increases the impact of a spin transition on the neighbors compared to the interactions in compound **1**, leading to the appearance of a hysteresis. This shows once again the importance of counterions and intermolecular interactions. Their exchange resulted in three different forms of spin crossover: a complete absence, a gradual transition and a very abrupt transition with the occurrence of a hysteresis. Furthermore were the interactions in **3** so strong, that a spin state switching involved a pulverization of the crystal. Only in compound **1**, they were not too stressing for the crystal, that XRD measurements could be conducted, but on the other hand strong enough to show a complete spin crossover and a distinct [*HS-LS*]-state could be detected.

## 4. Further Investigations

The work in chapter 3 has shown, that the oxadiazole is indeed suited for the use as backbone in spin crossover compounds. The complexes showed a large diversity and highly interesting magnetic behavior, which gave rise to several modifications of the system. They were all targeting on the improvement of the transition properties using various effects illustrated in the introduction.

### 4.1. Modifications: Incorporation of Cobalt(II)

Crystallization experiments with cobalt(II) were carried out in order to explore the influence of this exchange onto the magnetic behavior for this compound as well.

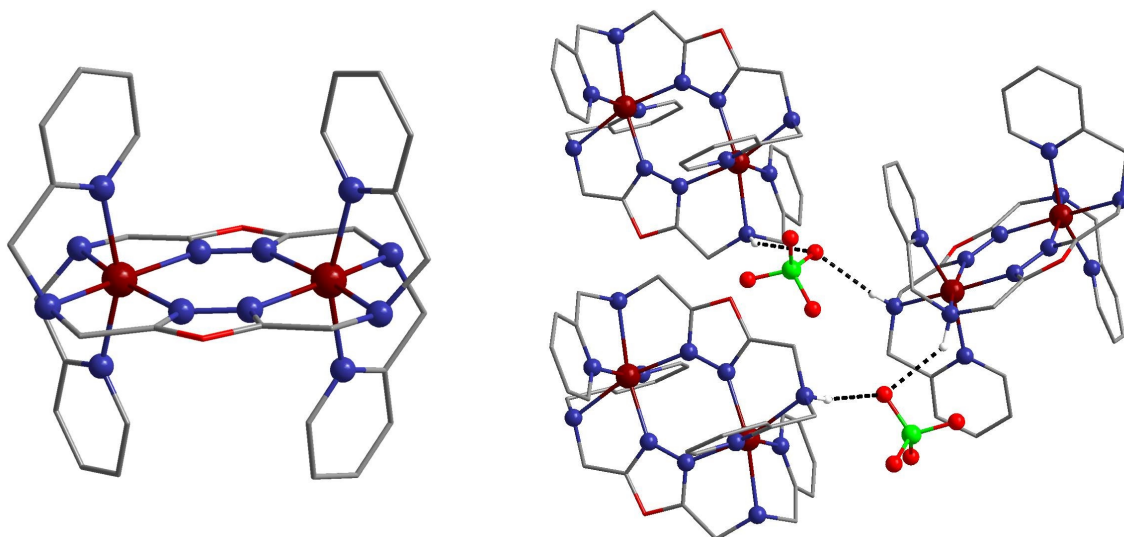


Figure 4.1.: Crystal structure of compound 4. Left: only cationic central motive  $[\text{Co}_2\text{L}_2]^{4+}$ ; right: visualization of hydrogen bonds between the cations and the counter ions. Other hydrogen atoms are omitted for clarity. Color code: dark red - Co, light green - Cl, red - oxygen, deep blue - nitrogen, grey - carbon.

It was prepared in the same manner as compound **1**: by mixing solutions of the ligand **L** and cobalt perchlorate solved in acetonitrile compound **4** was isolated as small light pink single crystals with the composition  $[\text{Co}_2(\mu_2\text{-L})_2](\text{ClO}_4)_4 \cdot 4\text{MeCN}$ . They were characterized by single crystal XRD experiments. The structure can be solved in the space group  $C2/c$ . This is essentially the same group as  $I2/a$  since they both belong to space group number 15, which was used to solve the iron(II) analog compound **1**.<sup>[75]</sup> The cation is isostructural to **1**, and the counter ions are arranged in the same way in both structures, only the positions of the solvent molecules are mirrored. Besides the structural differences resulting from the metals, they are almost similar. The average bond distances are 2.106 Å for  $\text{N}_{\text{Py}}\text{-Co}$ , 2.092 Å for  $\text{N}_{\text{ODA}}\text{-Co}$  and 2.260 Å for  $\text{N}_{\text{amine}}\text{-Co}$ . The *cis*- and *trans*-N-Co-N-bond angles are ranging from 76.13° to 118.06° and 159.22° to 165.55°, respectively, and the octahedral distortion parameter  $\Sigma_{\text{ODA}}$  sums up to 114.03°. Comparing these values to the literature, the dinuclear complexes are in the  $[\text{HS-HS}]$ -state.<sup>[76]</sup>

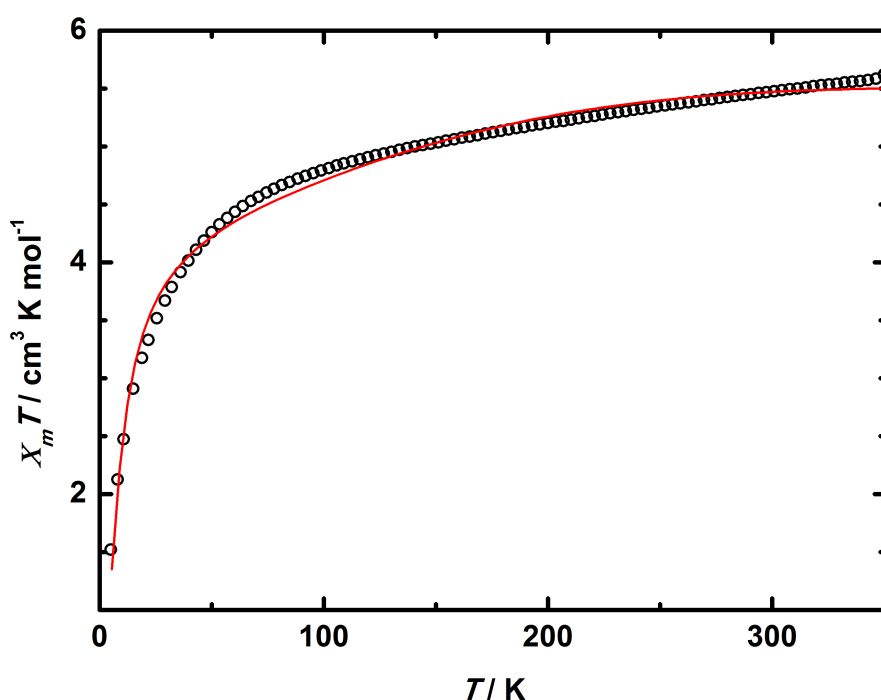


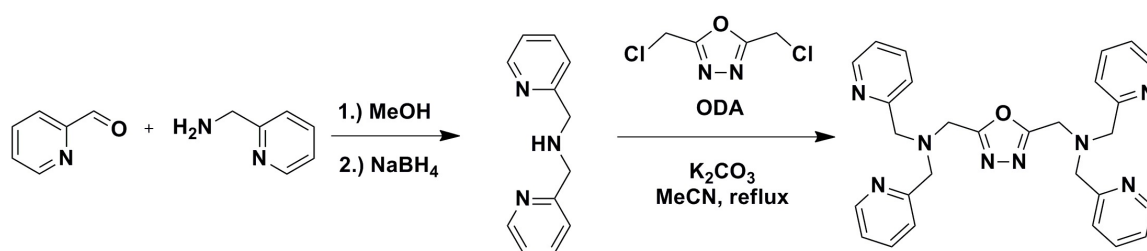
Figure 4.2.:  $\chi_M T$  vs.  $T$  plot for compound **4**. Black circles represent the experimental data, the fit is presented as a red line. Data per Co(II)-complex.

Magnetic measurement in a temperature range between 350 K and 5 K with a scan rate of 5 K/min were conducted to identify the spin-state of the system. At 350 K, the magnetic susceptibility has a value of  $5.61 \text{ cm}^3 \text{ K mol}^{-1}$  and descends slowly to  $4.60 \text{ cm}^3 \text{ K mol}^{-1}$  until 75 K. At lower temperatures  $\chi_M T$  decreases rapidly to a minimum of  $1.52 \text{ cm}^3 \text{ K mol}^{-1}$  at 5 K, which is attributed to an antiferromagnetic coupling between the metal centers. A simulation using the parameters  $g = 2.044$ ,  $J = -1.537 \text{ cm}^{-1}$ ,  $|D| = 3.223 \text{ cm}^{-1}$  and a temperature independent paramagnetism ( $\text{TIP} = 4 \cdot 10^{-4} \text{ cm}^3 \text{ mol}^{-1}$ ) is in good agreement with the experimental data. The measurement confirms the stabilization of the *high-spin*-state at room temperature. A spin crossover was not observed at any temperature.

As expected, it is not possible for the ligand to stabilize the *low-spin*-state. The reason for that is probably the rigid backbone of the ligand. The occupation of the energetically degenerated  $e_g$ -orbitals by only one electron enforces a Jahn-Teller distortion. To stabilize the *LS*-state in Co(II) compounds, the system must be able to follow that change of geometry.<sup>[77]</sup> The results match the statement from section 1.1.2, that every metal ion needs a unique coordination environment in order to show spin crossover. Since iron(II) complexes with the ligand **L** showed astonishing results, it was not surprising that a substitution of the metal lead not to any valuable results. There were no further experiments with Co(II) after these findings.

## 4.2. Modifications: Coordinating Counterions

A series of modified ligands were designed to improve further on the spin transition properties. The first ligand was drafted to gain from the benefits of coordinating anions, which were intensively discussed in section 1.1.5. For that matter, 2-(aminomethyl)pyridine was replaced during the synthesis by bis(2-pyridylmethyl)amine, leading to the desired ligand **L2** 2,5-bis([N,N'-(dipyridin-2-ylmethyl)amino]methyl)-1,3,4-oxadiazole. The precursor bis(2-pyridylmethyl)amine was synthesized according to the literature.<sup>[78]</sup> In comparison to **L**, the ligand **L2** represents a bis-tetradentate system. Therefore, one ligand should be sufficient to coordinate two metals, while the remaining four coordination sites will be occupied by coordinating counter ions. Using several different

Figure 4.3.: Synthesis of the ligand system **L2**.

methods, which have proven themselves being promising by giving compounds **1-3**, the ligand was used for the complexation of different iron(II) salts containing coordinating and non-coordinating counter ions. Unfortunately, none of the attempts yielded the desired complexes. Instead, a seven-coordinated sodium species forming, a one-dimensional chainlike structure (compound **5**), was isolated and characterized by single crystal XRD.

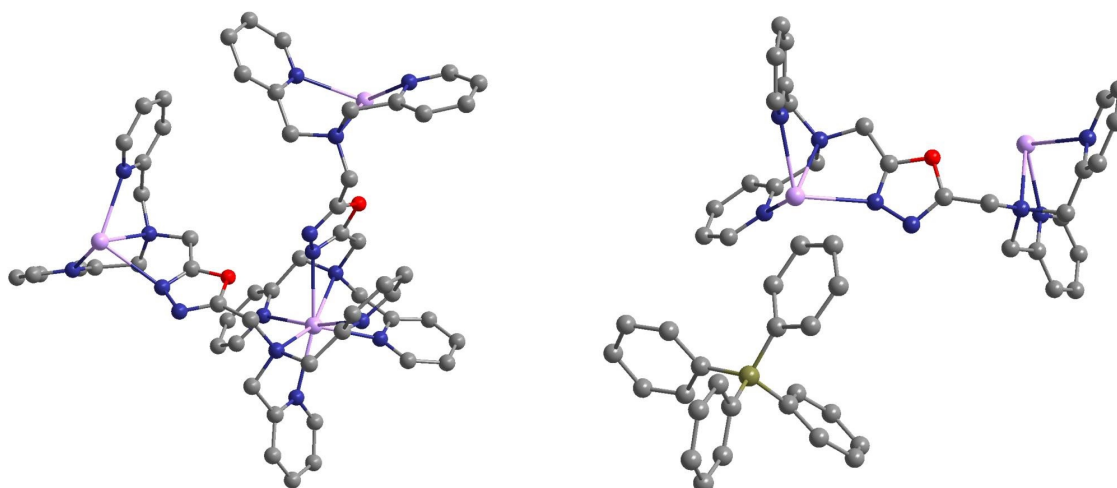


Figure 4.4.: Left: cutout of the chainlike structure of compound **5**; right: one ligand coordinated to sodium. Hydrogen atoms are omitted for clarity. Color code: purple - sodium, red - oxygen, deep blue - nitrogen, grey - carbon, dark yellow - boron.

The asymmetric unit comprises one ligand molecule, one sodium ion and a quarter of a water molecule. The charge is balanced by a tetraphenylborate counter ion, which is connected to the complex by  $\pi$ - $\pi$  stacking. Every ligand is bridging two sodium ions. Interestingly, the coordination is not symmetrically: one side of the ligand uses addition-

ally to the N-donor atoms of both pyridine substituents and the secondary amine one of the oxadiazole N-donor atoms, while in the other half of the ligand the second nitrogen in the oxadiazole backbone is not used for coordination. This way every sodium ion is in a capped trigonal prismatic coordination geometry.

Due to the different coordination number it is difficult to compare the structure with the prior ones. A closer examination of the angles in the fourfold coordinating half of the ligand (left half in the right picture in figure 4.4) shows, that they are far from the ideal octahedron angle of  $90^\circ$ . An octahedral coordination geometry can probably not be realized with this ligand. This is probably the reason for the unusual coordination number seven of the metal.<sup>[9]</sup>

Even though the structure is not as expected, it gives a lot of useful information about the ligand itself. If an iron ion would be coordinated in the same manner as the sodium is in the left half of the right picture with two additional coordinating counter ions, the resulting octahedral geometry would probably be too distorted to stabilize anything but the  $[HS-HS]$ -state. As a consequence, there were no further experiments conducted with this ligand. .

### 4.3. Ligand Modifications: Blocking of H-Bonds

Another approach to investigate the influence on the properties regarding spin transition would be a substitution of the amine bound protons. Even though this would block the formation of hydrogen bonds, it seems like a worthwhile alternative, because the intermolecular contacts were not only leading to spin crossover and hysteresis, but also to an absence of any transition at all. A suppression of the rather arbitrary forming and hardly controllable interactions makes a more rational design possible.

The evaluation of the data of compound **1-3** gives rise to the assumption, that they should show spin crossover even without forming hydrogen bonds to the counter ions. This is based on the observation, that the most electron withdrawing anion  $\text{BF}_4^-$  prevents a stabilization of the *low-spin*-state. Therefore, the substitution of the proton by a benzyl group should be beneficial for two reasons: first, the group has a positive inductive effect, increasing the electron density at the N-donor atom, thus raising the

transition temperature.

To pursue this approach, the ligand **L3** 2,5-bis([(N-benzyl-N'-pyridin-2-ylmethyl)-amino]methyl)-1,3,4-oxadiazole was synthesized by a reaction of 2,5-dichloromethyl-1,3,4-oxadiazole (ODA) and the precursor (N-benzyl-N'-pyridin-2-ylmethyl)amin, which was synthesized according to the literature:<sup>[79]</sup>

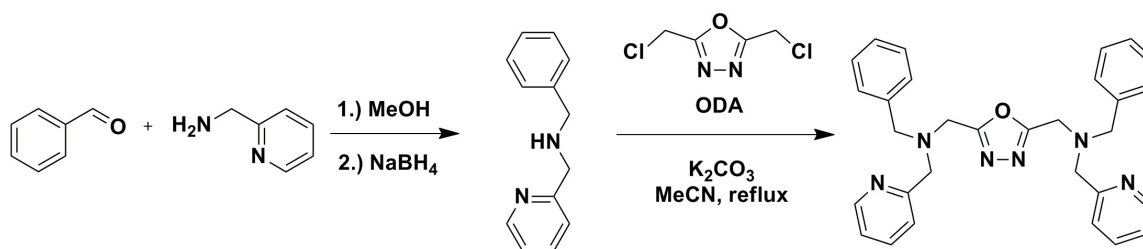


Figure 4.5.: Synthesis of the ligand **L3**.

In the next step, the ligand was used for the complexation of various iron(II) salts. The same crystallization methods were used as for compounds **1-4**. Unfortunately, an isolation of complexes as single crystals was not successful.



## 5. Summary and Outlook

The main objective of this work was the preparation of dinuclear iron(II) compounds by employing the ligand system **L** = 2,5-bis([(2-pyridylmethyl)amino]-methyl)-1,3,4-oxadiazole. Key feature of the ligand was the incorporation of an oxadiazole as central unit into a bis-tridentate ligand following the ligand-motive of Brooker *et al.* For the complex synthesis, three iron(II) salts bearing different counterions were used. The novel compounds were investigated in regard of their spin crossover properties. So far, there is no reported oxadiazole based system that shows spin transition behavior.

There are two major differences between the oxadiazole motive and the respective triazole or thiadiazole: first, the hetero atoms have a different influence on the electron density of the N-donor atoms in the respective ring system. In theory, the electronegativity increases from the sulfur ion to the oxygen ion and reduces the electron density in the ring system. Therefore, a stabilization of the *HS*-state is most likely for an oxadiazole based ligand, whereas it has been shown by our group that a sulfur based ligand favors the *LS*-state.

The second difference is the size of the hetero atom. The effect of the geometry onto the spin crossover properties were discussed in chapter 1. The ionic radius of a formal  $O^{2-}$  is much smaller than the radius of a formal  $S^{2-}$ . This affects the angles between the substituents at the position two and five and the ring, and leads to a larger distance between the opposing N-donor atoms of the amine group in the square plane. As a result, the system is supposed to be more rigid and tensed, which leads to a population of the *HS*-state. Furthermore, the coordination geometry should be more distorted. These assumptions are in good agreement with the reported systems by Klingele *et al.* which use oxadiazole based ligands. They stabilize exclusively the *HS*-state, whereas analog thiadiazoles, selenodiazoles or triazoles show spin crossover.

The successful synthesis of the ligand **L** (**L** being 2,5-bis([(2-pyridylmethyl)amino]-methyl)-1,3,4-oxadiazole) and its use for the reaction with several iron(II) salts yielded

the first oxadiazole based system with spin crossover properties. In the three novel compounds **1-3**, with the composition  $[\text{Fe}_2(\mu_2\text{-L})_2]\text{X}_4$  ( $\text{X} = \text{ClO}_4^-$  for **1**,  $\text{BF}_4^-$  for **2** and  $\text{CF}_3\text{SO}_3^-$  for **3**), different counter ions are used to compensate the positive charge of their isostructural cation. The variation of the counter ions leads to a diverse transition behavior ranging from none at all to gradual transition and up to the occurrence of hysteresis. With our new system we are able to stabilize the  $[\text{HS-HS}]$ -state at room temperature and induce in two out of three complexes a thermal spin transition to a mixed  $[\text{HS-LS}]$ -state with a transition temperature of  $T_{1/2} = 145$  K for **1** and  $T_{1/2} = 152$  K for **3**. It should be mentioned, that, even though the first crystal structure with a distinct  $[\text{HS-LS}]$ -state was reported in 2005 for the compound  $[\text{Fe}_2(\text{PMAT})_2](\text{BF}_4)_4 \cdot \text{DMF}$  by Brooker *et al.* (see chapter 2), a monitoring of the spin transition via XRD measurement in this manner is still rather rare. Additionally, **3** shows a 26 K wide hysteresis. Unfortunately, further cooling below 50 K does not lead to a stabilization of the fully diamagnetic  $[\text{LS-LS}]$ -state. This is probably because the transition of one metal center distorts the coordination geometry of the second metal center. As a result, the Fe-N bond lengths become even longer and the value of the octahedral distortion parameter increases, which disfavors a transition of the second metal center.

The different nature of the spin crossover originates from the differing number of contacts between the complex cations and anions as well as the different elements to which hydrogen bonds are formed. **2** displays non-classical hydrogen bonds towards the fluorine atom of neighboring counter ions, whereas in **1** and **3** the hydrogen bonds are towards oxygen atoms of the anions. The resulting disparate shift of electron density in **1** and **3** compared to **2** explains the absence of spin crossover properties in the latter one. Additionally, the close transition temperatures of **1** and **3** are a result of both hydrogen bonds formed to an oxygen atom. Taking a look at the long range intermolecular interactions, one finds that in **1** every cation is surrounded by four other cations and a connection to each of them is formed via hydrogen bonds that are mediated by one counter ion. In **3**, every cation is neighbored by two other cations. Again they are connected by hydrogen bonds mediated by a counter ion, but here, two cations are connected by two of those contacts. This leads to a larger cooperativity and the appearance of the hysteresis. Even though the importance of cooperativity is well established,

such a differentiated behavior, which is only achieved by the exchange of counter ions, is rather rare.

The successful functionalization of an oxadiazole in the way described above is a breakthrough in the challenging task of finding novel systems that are suitable for the application in spin crossover compounds. Future work should focus on the extend of the spin transition so that all three states  $[HS-HS]$ ,  $[HS-LS]$  and  $[LS-LS]$  can be stabilized. An approach to do so would be the design of a ligand, which is more flexible and is able to follow the first spin transition:

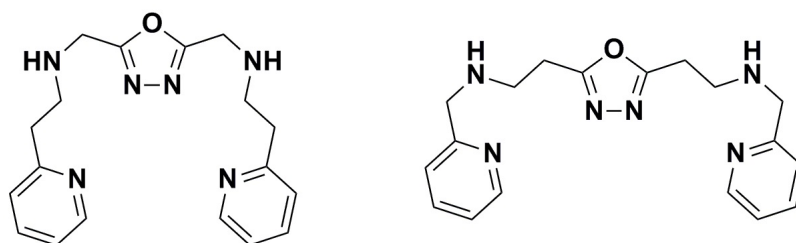


Figure 5.1.: Possible ligand designs to improve the spin crossover properties.

The main problem of a spin transition of the second metal is the distortion of its coordination geometry by the first spin crossover. The replacement of the methylene group by an ethylene group between the amine and either the pyridine ring (left picture in figure 5.1) or the oxadiazole (right picture in figure 5.1) should provide the ligand with the ability to compensate the geometry change which originates from the spin state switching of the first iron(II) center.

It is also important to be able to control the transition temperature which is directly dependent on the electronic environment of the N-donor atoms. For a rational optimization, hardly controllable influences such as hydrogen bonds should be avoided. A promising route would therefore be the substitution of the amine bound protons. The successive exchange of protons by methyl groups should increase the + I effect and change therefore the LFS. Additional to the elimination of these intermolecular interactions, the electron density at the N-donor atom can be controlled by the inductive effect of the substituent. First attempts in this direction were the synthesis of **L3**. A simpler system which is more rationally extendable is shown in figure 5.2:

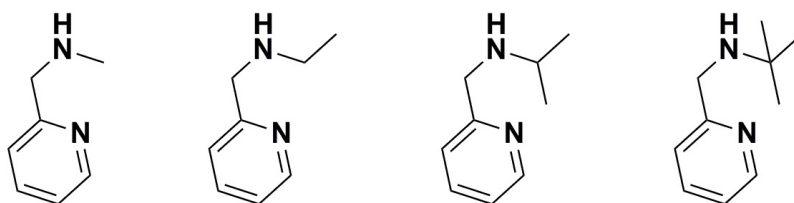


Figure 5.2.: A series of secondary amines which could be used as precursors to investigate systematically the inductive effect of various substituents.

Finally, the effects of other solvents and counter ions onto the cooperativity should be investigated since they have an enormous influence onto the resulting properties, as demonstrated in this work. Unfortunately, it is very difficult to estimate the influence of newly incorporated components onto the structural arrangement, especially when they are not part of the ligand system. For an exploration of this behavior, a series of crystallization experiments must be conducted where the composition of solvents and counterions is varied. The resulting compounds should be examined for any structural patterns, which would allow a rationalization of the coordination process. Additionally, different crystallization methods should be applied, to investigate the possibility of isolating different phases from the same compound.

---

**Part II.**

**Functionalized Phosphonates as Bridging  
Ligands in Inorganic-Organic Hybrid-Materials**



---

## Kurzzusammenfassung

Die Verwendung von magnetischen Materialien ist zu einem festen Bestandteil der heutigen Materialwissenschaften geworden. Ein Großteil von Anwendungen basiert auf dem einzigartigen, magnetischen Verhalten, dass ungepaarte Elektronen mit sich bringen. Die wichtigste und einflussreichste Anwendung stellt die Adressierbarkeit von ferromagnetischen Materialien dar, die das Speichern von Daten in der Informationstechnik revolutionierte. Und obwohl die verwendeten Verbindungen und Methoden in den letzten Jahrzehnten drastisch verbessert wurden, so ist das grundlegende Prinzip bis heute das Standardverfahren in der modernen Datenspeicherung.

Unter den magnetischen Eigenschaften ist die Adressierbarkeit von ferromagnetischen Verbindungen nur eine von vielen, die großes Potential in der Entwicklung neuer und wegweisender Technologien zeigt. Voraussetzung für diese Eigenschaften ist das Vorhandensein ungepaarter Elektronen. Besonders die 3d und 4f Metallionen erfüllen diese Bedingungen. Verbindungen, die Metallionen beider Gruppen vereinen, können entsprechend von den speziellen Vorteilen beider Gruppen profitieren.

In diesem Teil der vorliegenden Arbeit wird die Verwendung von Multi-funktionellen Liganden zur Herstellung neuer hetero-metallischen Koordinationsverbindungen und deren Verhalten ausgedehnte Netzwerke zu bilden untersucht. Da Phosphonate eine große Vielfalt an Koordinationsmodi bieten und gleichzeitig bereitwillig viele verschiedene Metalle zu koordinieren vermögen, sind sie in den synthetisierten Liganden das zentrale Leitmotiv. Um die Bildung hetero-metallischer Verbindungen zu begünstigen, wird eine zweite Funktionalität, die eine andere Koordinationsumgebung bietet, in den Liganden integriert.

Die Umsetzung mit verschiedenen Metallsalzen führte zu mehreren homo-, und hetero-metallischen Verbindungen, deren ausgedehnte Netzwerke sowohl 3d als auch 4f Metalle enthielten. Durch die Verwendung diverser Kristallisationstechniken und die Veränderung des pH-Wertes konnten die durch Röntgenspektroskopie an Einkristallen bestimmten Strukturen der Produkte beeinflusst werden. Zur Untersuchung der magnetischen Eigenschaften wurden Messungen der magnetischen molaren Suszeptibilität und der Magnetisierung bei verschiedenen Temperaturen durchgeführt.

---

## Abstract

The utilization of magnetic materials has become an essential task in modern materials science. A great deal of applications is based on the unique properties which come along with unpaired electrons. The most relevant application, and probably one of the most influential discoveries during the last century, is the addressability of ferromagnetic materials, which enabled the storage of data in the information technology. Even though the employed materials and methods have experienced a massive improvement during the last decades, the basic concept is to date the standard in regard of data storage.

Among magnetic materials, the addressability of ferromagnetic compounds is only one of many properties, which hold the potential for new groundbreaking applications. The requirement to observe such phenomena is the presence of unpaired electrons. Especially the 3d transition metal ions and the 4f rare earth metal ions satisfy these requirements. Compounds, which incorporate several different or both types of elements, can consequently benefit from both advantages they bear: large spin ground states and magnetic anisotropy of the 4f metal ions and strong magnetic coupling of the 3d transition metal ions.

In this part of the work at hand, the preparation of novel heterometallic coordination complexes based on multi functionalized ligands forming extended more-dimensional networks is investigated. Offering a high diversity in coordination modes and a broad spectrum of metal ions which can be coordinated, the phosphonate group is the central motive in all presented ligand system. In order to increase the probability of the formation of heterometallic compounds, a second functionality is part of the ligand as well, which provides a different coordinative environment.

Using these ligands in combination with various metal salts, several homometallic and heterometallic extended networks incorporating 3d transition metal ions as well as 4f rare earth elements could be obtained. The reactions outcomes were controllable by the employment of various crystallization techniques and the utilization of the pH value. The complexes were structurally characterized by single crystal X-ray diffraction. To investigate their magnetic properties, temperature dependent measurements of the magnetic molar susceptibility and the magnetization were conducted.



## 6. Introduction

### 6.1. Inorganic-Organic Hybrid-Materials

The fusion of inorganic compounds with organic linkers has produced a vast variety of materials, which show an astonishing diversity in their compositions, structures and properties.<sup>[80–83]</sup> Over the years, a larger number of subclasses evolved from this approach, which makes a classification rather hard.<sup>[84]</sup> Fortunately, many of these subclasses can be condensed and divided in two major categories: extended inorganic hybrids and coordination polymers (CP), also known as metal organic frameworks (MOF).<sup>[85]</sup> The key feature of both groups is the formation of a network in one, two or three dimensions by the connection between metal ions and organic ligands. A third category is given by molecular systems including both, inorganic and organic components. However, these zero-dimensional structures will not be discussed in the work at hand.

Coordination polymers and extended inorganic hybrids require the same essential building units: an inorganic component, which can be in its simplest form any metal ion from the periodic table, and an organic ligand, which must be able to coordinate to the respective metal ion.<sup>[86]</sup> Both classes are very similar and in order to separate them, a close examination of the connectivity between the inorganic part and the organic linker is necessary. For coordination polymers, the metal ions are linked by a bi-functional ligand, leading to an  $[M-L-M-L]_n$  pattern with M being the metal and L the bridging ligand. In other words, the structure is equivalent to an alternating copolymer. In contrast, extended inorganic hybrids connect two or more metal ions via the same donor atom or coordinating group belonging to one ligand, giving an  $[M-D-M]_n$  array, with D being a donor atom or coordinating group such as Cl, S, O, phosphate or sulfate.<sup>[87]</sup> Due to its large terrestrial abundance and its high reactivity, the donor atom is in most of the cases oxygen.<sup>[88][89]</sup> This means, that the rest of the ligand must not have any bridging character. A graphical representation of the two coordination modes can be found in figure 6.1.

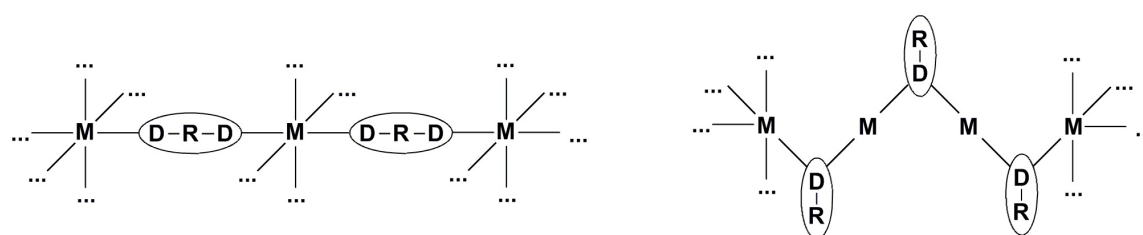


Figure 6.1.: Schematic representation of MOFs or CPs (left) versus extended inorganic frameworks (right). D represents the donor atoms, R the organic residues and M the metal ions. D-R-D- and D-R-arrays are ligands

With this differentiation it is possible to define a metal-organic-metal connectivity  $O^n$  and an inorganic connectivity  $I^n$ , where  $n$  is the number of dimensions to which the bonds are extended. Every metal-non-metal contact can then be assigned to either of them. Of course it is possible to have both types of connections in the same compound. This allows a mixture within the two types of bridging modes and leads to several subclasses. The possible combinations are classified in table 6.1.

Table 6.1.: Categorization of the different bridging modes from hybrid materials by the use of the inorganic connectivity  $I^n$  and the metal-organic-metal connectivity  $O^n$  according to<sup>[85]</sup>.  $n$  is the number dimensions in which a network expands. By adding up the values of  $n$ , the overall dimensionality can be determined. Table is adapted from<sup>[90]</sup>.

$O^n I^n$	$I^0 O^n$	$I^1 O^n$	$I^2 O^n$	$I^3 O^n$
$I^n O^0$	Molecular complexes	Hybrid inorganic chains	Hybrid inorganic layers	3-D inorganic hybrids
$I^n O^1$	Chain coordination polymers	Mixed inorganic organic layers	Mixed inorganic organic frameworks	/
$I^n O^2$	Layered coordination polymers	mixed inorganic organic frameworks	/	/
$I^n O^3$	3-D coordination polymers	/	/	/

Additional to CPs and hybrid inorganic structures, which both can occur either as chains ( $I^1$  or  $O^1$ ), layers ( $I^2$  or  $O^2$ ) or 3-D compounds ( $I^3$  or  $O^3$ ), mixed inorganic organic layers ( $I^1O^1$ ) and mixed inorganic organic frameworks ( $I^2O^1$  or  $I^1O^2$ ) are defined. In the following, the different classes will be discussed in more detail.

The chemical and physical properties of all mentioned compounds are very dependent on the incorporated metal ions and the ligand design. A careful choice of the metal ion can lead to a variety of highly interesting features such as spin crossover properties, ferromagnetic and antiferromagnetic interactions, single chain magnetism (SCM), a large magnetocaloric effect, luminescence or the slow relaxation of the magnetization.<sup>[91–95]</sup> As mentioned above, the ligand design can influence the properties of a compound as well. For example, the lengths of a bridging ligand can be changed: by exchanging pyrazine by 4,4'-bipyridine, the distance between metal ions can be varied.<sup>[96]</sup> In the field of MOFs, this way the size of pores or channels can be controlled. Of course, the choice of donor atoms can be of large relevance, too. The compound  $[\text{Fe}(\text{Rtrz})_3]\text{A}_2 \cdot n\text{H}_2\text{O}$  shows highly interesting spin crossover behavior due to the formation of one-dimensional  $I^1O^0$  chains, where one iron center is coordinated in an octahedral geometry by six N-donor atoms.<sup>[97]</sup> The importance of the coordination environment in order to observe spin crossover was intensively discussed in part I.

## 6.2. Coordination Polymers

Compounds with the connectivity  $I^0O^1$  to  $I^0O^3$  are called coordination polymers, although  $I^0O^3$  like structures are more commonly referred to as MOFs. The requirements for the construction of a CPs is a metal and an appropriate ligand which has to be at least bi-functional to link two metal centers. In order to obtain linear  $I^0O^1$  chains, ligands must be used where the donor atoms and the organic tether form a linear arrangement, such as isonicotinoate<sup>-</sup> or oxalate<sup>2-</sup>. The more critical factor is the metal center, which basically determines the dimensionality by its preferred coordination number. For a chain like structure,  $\text{Ag}^+$  or  $\text{Au}^+$  ions with a coordination number of two can be used.<sup>[98]</sup> There are two approaches to extend a linear chain to an  $I^0O^2$  layer: first, the metal center can be substituted by a central ion which favors a square planar coordination

geometry, such as nickel(II) and platinum(II).<sup>[99]</sup> The second approach uses unsymmetrically substituted ligands to extend to another dimension, for example benzene-1,3-dicarboxylate<sup>2-</sup>.<sup>[100]</sup> This route is in practice not as straightforward as the first one, because there are several possible arrangements of the ligand around the metal center, which would lead to a different outcome. The aspect of self assembly in this context will be discussed in a following section.

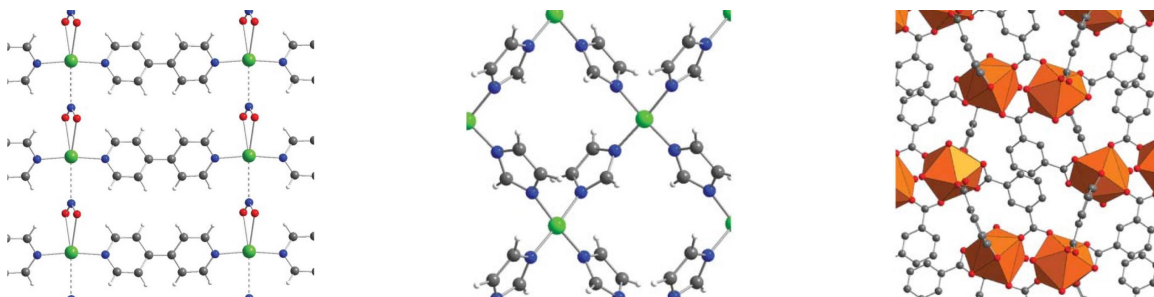


Figure 6.2.: Left: one-dimensional  $I^0O^1$  chain; middle: two-dimensional  $I^0O^2$  layer with a square planar geometry at the metal ion; right: two-dimensional  $I^0O^2$  layer with an unsymmetrically substituted ligand.<sup>[85,98–100]</sup>

Moving on from two-dimensional compounds to MOFs, the general synthetic approach does not differ very much. Already three decades ago, 3-D metal organic frameworks were the result of crystal engineering: suitable metal ions and rigid linkers were combined to form a  $[\text{CuPt}(\text{CN})_4]_n^-$  network.<sup>[101]</sup> The reason for the formation of this structure is the distinct affection of the two metal ions for different coordination environments: platinum favors the "carbon-end" of the cyanide, whereas copper prefers an  $N_4$ -coordination sphere. The square planar coordinated platinum ions generate a two-dimensional network, which is extended by the tetrahedral coordination geometry of the copper ions to the third dimension. It is obvious, that the geometry plays a key role in the formation of MOFs. The octahedral coordination sphere is due to its three dimensional form suitable as well.<sup>[102]</sup>

Alternatively, the use of so-called secondary building units (SBUs) has proven itself to be very potent for the design of metal organic frameworks.<sup>[103]</sup> Preformed complexes of molecular nature based on carboxylates are used in order form extended three-dimensional networks. In other words, complexes are used as ligands, a strategy which

was first applied by Kahn *et al.*<sup>[104]</sup> Examples for this kind of compounds are the basic zinc acetate or the dimeric paddle-wheel complexes.<sup>[105]</sup> The reason for their excellent applicability is the rigid coordination bond of the carboxylate, locking a metal ion in position. This leads to stable structures which withstand the exchange of guest ions as well.

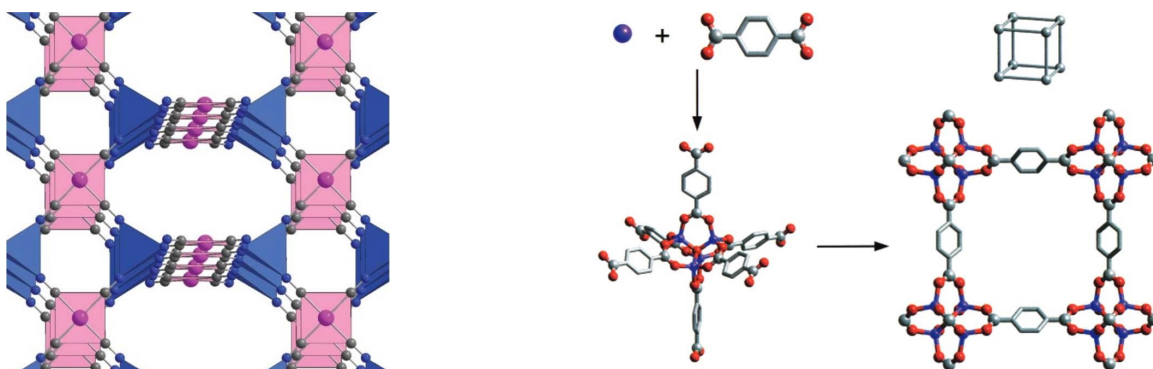


Figure 6.3.: Left: the use of a suitable combination of metal ions and ligands lead to the formation of a metal organic framework.<sup>[101]</sup> Right: utilization of secondary building units.<sup>[103]</sup>

### 6.3. Extended Inorganic Hybrids

Besides the linkage of two or more metal ions by different donor atoms from one ligand molecule it is as well possible, that the same donor atom of a ligand connects several metal ions. More-dimensional structures containing such contacts are terminological separated from pure coordination polymers, because their bridging mode is observed generally in inorganic compounds.<sup>[87]</sup> However, they are of great value to the class of inorganic-organic hybrid-materials. This is not only because of the extremely large number of possible structural permutations, which are accessible by this approach, but also because of the introduction of the highly interesting properties evoked by metal oxides.

Common groups, which are forming  $M^nO^0$  connections, are for example carboxylates, phosphates and phosphonates or sulfates. As these are the bridging units, their choice and hence their properties have a large impact on the resulting structure. The coordi-

nation ability of all above mentioned groups is dependent on the pH value. The work of Bein and Stock showed the influence of protonation and deprotonation on the structure and properties of systems containing pH-sensitive groups: by increasing the pH value, the deprotonation grade of the acidic groups rises as well leading to a higher dimensionality.<sup>[106]</sup> The reason is quite obvious: the removal of a proton, for example at a phosphonate group, results in a negative charge, which is spread across the group, excluding the still protonated OH-group. This  $\text{R-PO}_3\text{H}^-$  ion provides a perfect coordination environment for a metal ion. Upon a second deprotonation, the remaining  $\text{R-PO}_3^{2-}$  group is even more willing to coordinate to several metal ions due to its high charge. This way, the dimensionality of the resulting complex can be altered specifically by a proper adjustment of the pH value.

The use of hydrothermal conditions for the synthesis of zeolites is well documented and also applied for the preparation of other inorganic hybrids.<sup>[84]</sup> But the use of temperature as a variable equal to compound ratios or choice of solvent was first investigated in 2004, when five different cobalt succinates were synthesized from a temperature range between 60°C and 250°C under otherwise equal reaction conditions.<sup>[107]</sup> The effect can be explained by a reduction of the waters viscosity under these conditions. As a consequence the diffusion process is augmented, leading to a solvent extraction from any solids and a preferred crystal growth.<sup>[108]</sup>

Nevertheless, the resulting structure of a reaction towards extended inorganic hybrids is dependent on similar factors as it is in the synthesis of coordination polymers. By varying the metal ion, the coordinating group (i.e. the ligand), the solvent and so on, the course of a reaction is strongly influenced. However, the introduction of the pH value and the temperature as a structure directing variable is a highly valuable tool in the rational design of more-dimensional networks.

### 6.4. Mixed Inorganic-Organic Materials

A closer examination of the structures of the two presented categories brings to light, that they demand two different features. As in organic polymers, the coordination polymers need an at least bifunctional ligand or monomer. Instead of linking them via cova-

lent bonds, they are connected by coordinative bonds to the metal centers. There are only little requirements for the donor atoms as long as they are matching the used metal ion. Due to their bridging nature, it is the opposite with inorganic hybrids: the donor atoms i.e. the coordinating groups must be chosen carefully to assure the formation of an extended network, while their number is rather insignificant. Obviously, a ligand that includes two or three functionalities, from which one is suitable for the formation of  $I^n$  connectivity, should allow the preparation of mixed inorganic-organic materials. And indeed, this approach has lead to several  $I^nO^n$  systems with  $n \neq 0$ .<sup>[109,110]</sup>

The introduction of the pH value as a structure directing lever was attributed to a stepwise deprotonation of polyprotic acids and the emerging readiness to form multiple coordination bonds. However, this dependency of certain pH-sensitive groups can be used in quite another way. Acidic functionalities tend to form no coordinative bonds at all, as long as they are fully protonated. But once they are deprotonated they readily coordinate to one or several appropriate metal ions. If two various groups are combined in one multi-functionalized ligand system, they can be deprotonated at different pH values according to their different pKa values.<sup>[106]</sup>

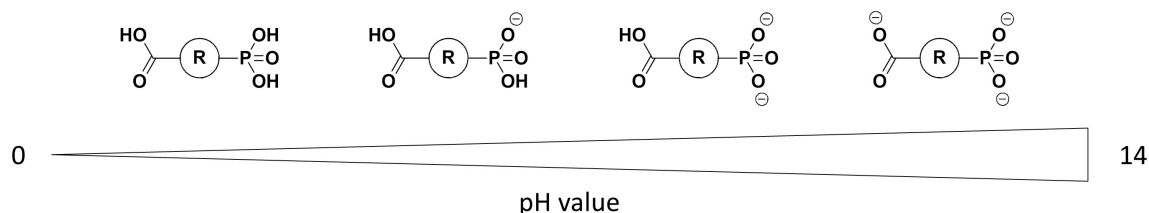


Figure 6.4.: Schematic representation of the stepwise deprotonation of a ligand system with multiple acidic protons dissociating at various pKa values.

The first change in dimensionality at the presented system is caused by an extension from  $I^1O^0$  to  $I^2O^0$  because of the complete deprotonation of the phosphonic acid. Further increment of the pH value results in the formation of an  $I^2O^1$  connectivity by a deprotonation of the carboxylic acid. If the pH value is used in such a way, mixed inorganic organic materials can be prepared from purely extended inorganic hybrids.

## 6.5. Applications of Hybrid-Materials

The combination of extended inorganic hybrids and coordination polymers to mixed inorganic-organic materials not only yields a vast variety of structures, but also holds the potential for new materials with highly interesting properties. In section 6.1 the important interplay of metal ions and ligand design was pointed out by highlighting several features such compounds can possess, if the key components are chosen appropriately. Potential applications for these properties are versatile: large magnetocaloric effects can be used for magnetic refrigerating, SMMs are considered as a possible application in ultra dense storage devices, and long-range magnetic ordering is essential in frontiers of molecular magnetism.<sup>[111–115]</sup>

One of the most utilized characteristic of hybrid-materials is the possibility to build stable 3-D frameworks with controllable pore size and their enormous large surface. If adjusted properly, they qualify as catalysts, for the storage of gases such as hydrogen, or in the separation of gases.<sup>[80,81,116,117]</sup> Hybrid-materials show potential regarding their optical properties as well. There are a lot complexes including rare-earth metal ions, which tend to show phosphorescence or fluorescence. Additionally it is possible to introduce chromophors into the organic ligand to adjust the optical properties of the hybrid-material for special applications.<sup>[100,118,119]</sup>

## 6.6. Phosphonates in Hybrid-Materials

The phosphonate group belongs to one of the most versatile coordinating groups in coordination chemistry.<sup>[83,84]</sup> The phosphorous atom is bound to a carbon atom, which connects it to the organic part of a ligand system, and three oxygen atoms, which can act as donor atoms. Two of the oxygen atoms can be protonated to give the free phosphonic acid. Alkylphosphonic acids can be synthesized using the Michaelis-Arbuzov reaction, where a trialkyl phosphite is reacted with an alkyl halide. For the preparation of arylphosphonic acids, a catalyst must be present and the reaction conditions have to be adjusted.<sup>[120–122]</sup> The resulting compounds show unique coordination properties because of the phosphonates highly diverse coordination modes, which are dependent



on the grade of deprotonation.<sup>[123]</sup> Considering the large number of donor atoms and especially the high charge, it is not surprising that the completely deprotonated group (left picture in figure 6.5) tends to form systems with higher dimensionality. If this is not desired, one way to avoid the formation of extended networks is the protonation of one of the oxygens (right picture in figure 6.5). This way, the connectivity can be reduced. Another way to avoid an expansion to all dimensions is the use of co-ligands. They are able to block coordination sites at the metal, thus preventing the formation of too many phosphonate-metal bonds. By an adequate use of one or both of this methods, the dimensionality can be controlled up to a certain degree.<sup>[124]</sup>

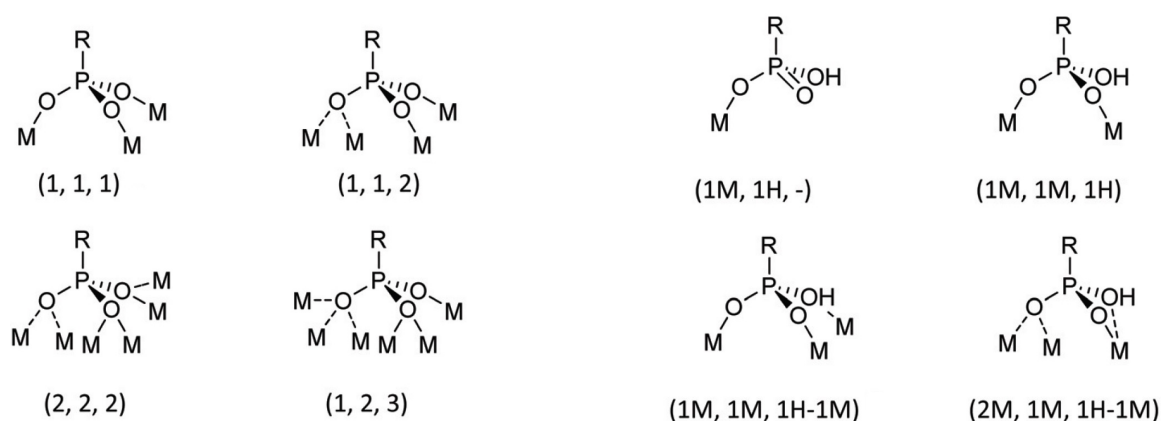


Figure 6.5.: Left: coordination modes of a twofold deprotonated phosphonate. Right: coordination modes of a single deprotonated phosphonate.<sup>[123]</sup>

One of the key features of the phosphonate group is the ability to form compounds by self assembly. This means, that the motive of a structure is not directed by external influences, but that it is rather determined due to local interactions originating from the components themselves.

### 6.6.1. Hydrothermal Synthesis

The first compounds containing phosphonate groups were prepared by Alberti in 1977 from the reaction of benzene phosphonic acid or hydroxymethanephosphonic acid with zirconium.<sup>[86]</sup> Even then, the reactions were carried out under elevated temperatures

(60°C). This is pointed out because the usual approach, which is used in order to obtain metal-phosphonates or hybrid-materials in general, is hydrothermal synthesis.<sup>[96]</sup> This method was already established in solid state chemistry several decades ago.<sup>[125]</sup> One of its major advantages are the relatively low temperatures between 100°C and 250°C which are used in comparison to other methods in solid state chemistry, where temperatures around and above 1000°C are commonly used.<sup>[126][127]</sup> Of course, such conditions are not applicable if organic components are part of the reaction. This made hydrothermal synthesis superior to other methods and opened the field to the preparation of inorganic-organic hybrid-materials.

### 6.6.2. Evolution of Phosphonate Compounds

After the discovery of the zirconium phosphonates in 1978, the field of phosphonate chemistry rapidly grew to become a permanent element in coordination chemistry. This was not only but also because of the tendency of phosphonate to form microporous materials under certain conditions, and their usage for gas storage.<sup>[81,88]</sup> Besides the more-dimensional extended systems, phosphonate based compounds also developed towards molecular structures, i.e.  $1^0O^0$ , which show fascinating magnetic properties such as single-molecule magnetism. However, this work will not comprise a discussion about low dimensional phosphonates. They are merely mentioned to emphasize the large diversity of this particular group.<sup>[128-134]</sup>

The donor atoms of the phosphonate group are oxygen atoms and previous work has shown, that it possesses excellent premises for the coordination of several transition metal ions. Additionally, phosphonates qualify as coordinating group for lanthanides due to the oxophilicity of rare earth elements.<sup>[135]</sup> Furthermore, they do not have any restrictions regarding the size of the metal centers they are coordinating. This ability to provide a coordination environment for both, 3d transition metal ions and lanthanides, led to the first heterometallic three dimensional 3d-4f phosphonate in 2007 by Ma *et al.*<sup>[136]</sup>

The highly diverse coordination modes enable the deposition of phosphonates on surfaces where they form self assembled monolayers by reacting with metal oxides such as  $HfO_x$  and  $AlO_x$ .<sup>[137]</sup> This property is highly valuable for the attachment of organic

compounds onto surfaces and led to the development of several techniques for the anchoring of phosphonates onto surfaces.<sup>[138,139]</sup>

## 6.7. Recent Progress

The field of inorganic-organic hybrid-materials is still growing fast. During the last decade, a countless number of new homometallic molecular, chainlike, layered and three-dimensional structures were published. Accordingly, the number of potential applications rises steadily and they are additionally driven towards organic electronic devices such as organic thin-film transistors, organic light emitting diodes or hybrid photovoltaic cells.<sup>[123,137,140,141]</sup> There are also many reports regarding heterometallic system, even though most of them are of molecular nature.<sup>[91,95,142–144]</sup> The synthetic approach which is used in general was introduced by Kahn *et al.* Here, a metal complex is synthesized and used as a precursor. Subsequently, it is reacted with the second metal to yield heterometallic and more-dimensional compounds.<sup>[104]</sup> Nevertheless, heterometallic compounds based on phosphonates with a dimensionality other than zero are still rare. The reason is found in the synthetic approach, which is usually employed in the preparation of phosphonate-based compounds. The outcome of solvothermal or hydrothermal techniques is rather serendipitously and it is not guaranteed, that all metal ions from the reaction mixture will be incorporated in the resulting complex.<sup>[91]</sup> However, it was this technique which led to the first heterometallic phosphonate. A reason for the success was the use of a bi-functional ligand which led due to the second coordination site to a heterometallic compound.<sup>[136]</sup>

## 7. Objectives and Aims

The previous chapters have emphasized the enormous variety in properties phosphonate based hybrid materials can bear, making them extremely valuable for potential applications such as hydrogen storage, catalysis, or photoluminescent devices. The formation of phosphonic acid self assembly monolayers on  $\text{AlO}_x$  or  $\text{HfO}_x$  surfaces, for example, led to the development of ultrathin phosphonate based organic thin-film transistors. In regard of molecular magnetism, especially heterometallic systems are of great interest because, if carefully designed, they are able to incorporate 3d transition metal ions as well as 4f elements. Compounds which contain these metal ions are known for their unique magnetic properties: 3d ions tend to show strong magnetic coupling, which can result in a large spin ground state. Rare earth elements have a large spin ground state themselves and exhibit additionally large magnetic anisotropy. There is a great deal of highly relevant heterometallic complexes, which strongly influence the fields of single molecule magnetism, magnetic refrigerating or systems with a large spin ground state.<sup>[145]</sup>

The road to heterometallic compounds is the employment of bi- or multi functional ligands. The phosphonate group is able to coordinate transition metal ions as well as rare earth elements. This ability to coordinate such distinct metal ions is attributed to the many possible coordination modes of this particular group (see figure 6.5) and the large number of oxygen atoms it carries. The usual approach to realize phosphonate metal bonds is hydrothermal synthesis. The special reaction conditions lead in most cases to a crystallization instead of a precipitation. However, the combination of hydrothermal synthesis and self assembly with this many coordination modes at hand can cause a certain inaccuracy regarding the prediction of the reactions outcome. One way to improve on this disadvantage is the introduction of a second functionality, which is able to precoordinate a metal and hence direct the reaction towards a desired product. Ideally, such a group brings auxiliary features as well and provides, for example, a different coordinative environment, which is favored above the phosphonate ones by specific metal ions.

The aim of this work was the preparation and characterization of heterometallic and more-dimensional extended networks, which are able to form both inorganic  $I^n$  and organic  $O^n$  connections mediated by phosphonate based multi-functional ligands. To ensure a coordination of at least two different metal ions, the ligand had to provide at least two functionalities which offer different coordination environments.

In the scope of this work, a phosphonate based ligand was synthesized: it holds two phosphonate groups and a bipyridine unit as third functionality ( $H_4L$ ). The various groups are linked by an aromatic system which is able to mediate magnetic interaction.

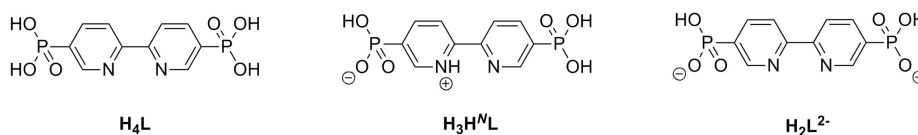


Figure 7.1.: Ligand  $H_4L$  (2,2'-bipyridinyl-5,5'-diphosphonic acid, left) incorporates two phosphonate groups which are attached at the 5,5'-position of a 2,2'-bipyridine backbone. The ligand crystallizes in the form  $H_3H^+L$  (middle). The most often observed protonation grade of the ligand is displayed in the right.

The ligand was studied regarding its coordinative behavior towards several 3d and 4f ions. For that matter, various crystallization methods were employed, including hydrothermal synthesis. As one of the critical components, the pH value was utilized to influence the outcome of the reactions. The goal was the preparation of single crystalline compounds, which satisfy the requirements for a structural characterization by the means of single crystal XRD. The obtained compounds were to be magnetically characterized via temperature dependent measurements of the magnetic molar susceptibility and the magnetization in order to investigate their magnetic properties.

## 8. More-Dimensional Inorganic-Organic Hybrid-Materials Based on Phosphonates

### 8.1. Introduction

Previous studies showed the large potential of 4,4'-biphenyldiphosphonic acid for the synthesis of multidimensional homo- and heterometallic hybrid-materials.<sup>[146,147]</sup> In all cases the phosphonate group acted as a linker between at least two metal centers by either  $I^1$  or else  $O^1$  connections. Comparing the results, the dimensional restrictions, which can be forced upon a compound due to the use of a low pH value and co-ligands were demonstrated in an impressive way. Unfortunately, the only way to yield heterometallic compounds was the introduction of metal-oxides. A bypass to that problem is the replacement of the biphenyle-system by a 2,2'-bipyridine backbone, because of the well documented readiness of transition metal ions to form bipyridine based complexes.<sup>[9,148]</sup> The resulting ligand is depicted in figure figure 8.1. In order to distinguish between protons bound to different groups, they will be labeled either  $H_x$  for protons bound to the oxygen atoms of the phosphonate group with x being their number, or else  $H_y^N$  for protons bound to nitrogen atoms with x being their number.

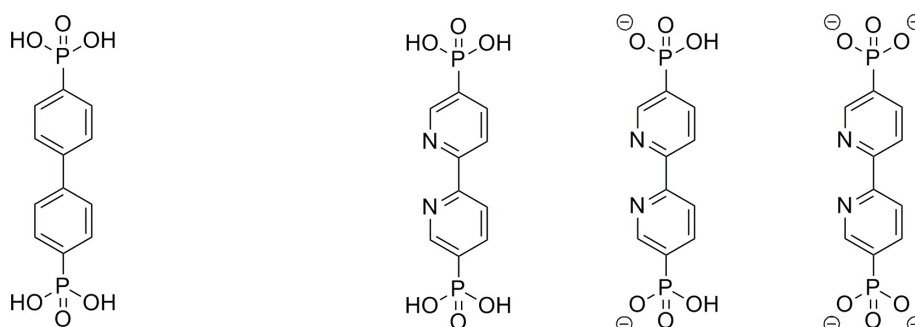


Figure 8.1.: On the left side, the 4,4'-biphenyldiphosphonic acid prototype ligand is depicted.<sup>[146]</sup> Next to it, the ligand system  $H_4L$ ,  $H_2L$  and  $H_0L$  (from left to right) shown with different grades of deprotonation.

The respective ligand (figure 8.1 right) was already discovered in 1998<sup>[122]</sup>, but there are only a few Ru(II) and Zr(IV) complexes in which the ligand was used.<sup>[149–151]</sup> However, the phosphonate had no active part in these compounds but was merely used for the study of the inductive effect of various anchoring groups. To the best of our knowledge, there are no reports of this ligand with the phosphonate groups coordinating at all.

Since 3d-metal-phosphonate bonds are formed in general under hydrothermal conditions, it is, in terms of coordination abilities, inferior compared to the bipyridine functionality. Either prior or else after the addition of a transition metal ion, a lanthanide ion can be introduced, which will on the other hand prefer the phosphonate group as coordination environment due to the oxophilicity of rare-earth elements and its large ionic radius. Avoiding hydrothermal synthesis should aid the realization of a rational design for heterometallic compounds. Instead, two different approaches are combined, which lead to success with non-phosphonate containing ligands: the 'ligand-as-a-complex'-approach by Kahn *et al.* and the use of self assembling materials containing structure directing elements.

By this means, we were able to synthesize several new compounds of homo- and heterometallic nature using Ni(II), Co(II), Co(III), Gd(III), Tb(III) Dy(III) and La(III). Additionally to some molecular structures, several extended one-dimensional chains, two-dimensional layers and three-dimensional frameworks were prepared as intended. All compounds were obtained as single crystals and their structures were determined using single crystal XRD.

# 'Functionalized phosphonates as building units for multi-dimensional homo- and heterometallic 3d-4f inorganic-organic hybrid-materials and their magnetic characterization'

**Christian Köhler** and Eva Rentschler

*Dalton Trans.* (Submitted)

## 8.2. Abstract

Using the multifunctional ligand  $\mathbf{H}_3\mathbf{H}'\mathbf{L}$  (2,2'-bipyridinyl-5,5'-diphosphonic acid), a new family of inorganic-organic hybrid-materials was prepared. The ligand shows a very high flexibility regarding the coordination mode, which lead to a large structural diversity. The compounds **1a**, **1b** ( $[\mathbf{M}(\mathbf{H}_2\mathbf{L})(\mathbf{H}_2\mathbf{O})_4]\cdot 2.5\mathbf{H}_2\mathbf{O}$ ;  $\mathbf{M} = \text{Co}^{2+}$  (a), =  $\text{Ni}^{2+}$  (b)), **2** ( $[\text{Gd}_2(\mathbf{H}_2\mathbf{H}'\mathbf{L})_2(\mathbf{H}_2\mathbf{H}'_2\mathbf{L})(\mathbf{H}_2\mathbf{O})_6]\text{Cl}_4\cdot 14\mathbf{H}_2\mathbf{O}$ ), **3a**, **3b**, **3c** ( $[\text{MCo(III)}(\mathbf{H}_2\mathbf{L})_3(\mathbf{H}_2\mathbf{O})_2]\cdot 6.5\mathbf{H}_2\mathbf{O}$ ;  $\mathbf{M} = \text{Gd}^{3+}$  (a),  $\text{Dy}^{3+}$  (b) and  $\text{Tb}^{3+}$  (c)), and **4** ( $[\text{GdNi(II)}(\mathbf{H}_2\mathbf{L})_3(\mathbf{H}_2\mathbf{O})_3]\text{NaCl}\cdot 6\mathbf{H}_2\mathbf{O}$ ) were isolated and characterized with single crystal X-ray diffraction. Depending on the used metal ions and the stoichiometry, either molecular systems (0D), extended 2D layers or extended 3D frameworks were obtained. In contrast to the general approach in phosphonate chemistry, the compounds were prepared without hydrothermal synthesis, but under ambient pressure. Variable temperature magnetic measurements were carried out to determine the magnetic properties.



### 8.3. Introduction

The field of inorganic-organic hybrid-materials <sup>[1,2]</sup> shows an enormous potential in a broad spectrum of applications, such as adsorption/desorption, catalysis, functionalization of surfaces, nanomaterials or photoluminescent devices. <sup>[3–12]</sup> Additionally, the incorporation of open-shell transition metal ions or rare earth elements into these hybrids yielded a large number of magnetic materials, which exhibit several highly relevant properties from the field of molecular magnetism, e.g. long range magnetic ordering, single chain magnetism, large magnetocaloric effect or slow relaxation of magnetisation. <sup>[13–21]</sup> To bring some order to the vast number of compounds, which belong to the class of inorganic-organic hybrid-materials, Janiak distinguished between coordination polymers (CPs) and inorganic hybrid materials. <sup>[22]</sup> Although they look very much alike, a closer examination reveals two different types of connection between metal centres and ligands. <sup>[23]</sup> Cheetham *et al.* proposed a classification based on the different connectivity: purely inorganic connections, where two or more metal ions are connected via the same coordinating group, are classified as  $I^n$ , with  $n$  being the number of dimensions in which the connections are extended. These compounds belong to the inorganic hybrid materials. When the connection between two metal ions is mediated by a ligand with at least two functionalities, they are denoted  $O^n$  and belong to the coordination polymers. Combinations of both connectivities  $I^nO^n$  are possible as well and called mixed inorganic-organic materials. <sup>[24]</sup>

The predominant type of inorganic-organic hybrid-materials is of homo-metallic nature, <sup>[25,26]</sup> even though the first heterometallic systems by Gatteschi *et al.* date back to 1985. <sup>[27]</sup> Due to their smaller number, they are not as extensively studied as homometallic compounds. <sup>[28]</sup> A reason for the lack of such complexes is the much larger effort their synthesis or their ligands synthesis bear. The challenge in the design of heterometallic compounds originates in the competition of different metal ions for the same or similar coordination sites. <sup>[29]</sup> One approach to overcome this problem involves the combination of two strategies, which are commonly used in coordination chemistry: first, the self-assembly of coordination compounds and second, the desire of different sorts of metal ions for different coordination environments. <sup>[30,31]</sup> To ensure that this strategy is applicable, the used linker ideally features at least two different functionali-

ties, which show a certain distinction in their coordination capabilities. We followed this strategy by employing a bipyridine based ligand, which contains additionally two phosphonate functionalities. The phosphonate group is known for its highly diverse modes of coordination, which can be easily fine-tuned, making it very valuable for the task. [32] The second functionality is a bipyridine site, which is an appropriate choice with its well documented readiness for the coordination of transition metal ions. [33]

A ligand system that provides both groups is 2,2'-bipyridinyl-5,5'-diphosphonic acid ( $\text{H}_4\text{L}$  or  $\text{H}_2\text{H}'\text{L}$ , see scheme 1), first synthesized in 1998 by Penicaud *et al.* [34] It offers a bipyridine functionality which is ideal for the coordination of 3d transition metal ions, while the two phosphonate groups in general build transition metal-phosphonate bonds solely when treated under hydrothermal conditions. On the other hand, the phosphonate groups offer perfect coordination conditions for lanthanide ions due to the oxophilicity of rare earth elements. [35–38]

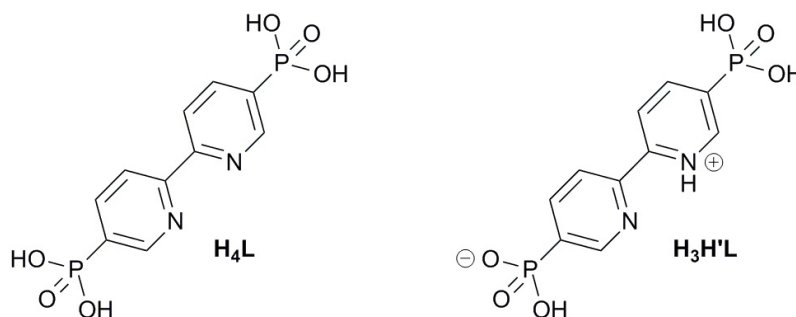
We herein report the synthesis and full characterisation of seven novel compounds incorporating 3d transition metal ions and 4f elements based on a 2,2'-bipyridine-system which was functionalized symmetrically by two phosphonate groups. We were able to prepare 0D and 2D homometallic structures as well as heterometallic 2D and 3D structures with Co, Ni, Gd, Tb and Dy. We investigated the magnetic properties of the compounds with temperature dependent measurements of the molar susceptibility  $\chi_M$  and the field dependent magnetisation  $M$  using a SQUID magnetometer.

## 8.4. Results and Discussion

### 8.4.1. Synthesis

**Ligand considerations.** One approach to overcome the challenges in the design of heterometallic compounds is the use of ligands with different functional groups. That way, different sorts of metal ions do not compete for the same coordination site, but choose the most fitting one. Of course, functionalities which coordinate almost exclusively a specific metal will limit the possible diversity of the systems. But if a group will

coordinate any metal, the selectivity for heterometallic compounds is lost. Therefore, the coordination properties have to be controllable up to a certain degree.



**Scheme 1.** Ligand  $\text{H}_4\text{L}$  and  $\text{H}_3\text{H}'\text{L}$ .

A functional group which can satisfy this requirement is the phosphonate group. It is very versatile in its coordination modes, and its charge can be altered by a change of the pH value. [32,39] A second fitting functionality is a bipyridine unit. It offers, in contrast to the phosphonate, N-donor atoms, is chelating and provides therefore another coordination environment. The coordination behaviour of the two different functionalities allows the synthesis of homometallic and heterometallic complexes with 3d transition metal ions and 4f lanthanide ions. The ligand  $\text{H}_4\text{L}$  (2,2'-bipyridinyl-5,5'-diphosphonic acid, scheme 1) combines those functionalities. It has been used for the preparation of Ru(II) and Zr(IV) complexes, where the metal centres were bound by the bipyridine coordination site. [40–42] However, to the best of our knowledge, there is no report of complexes in which the phosphonate group had an active part regarding coordination chemistry.

**Complex synthesis.** One of the most common and applied methods in phosphonate chemistry is hydrothermal synthesis. [37,43] Unfortunately, the outcome of any reaction is often hard to predict due to the nature of this approach. [44] We decided therefore to employ a different strategy and induced a growth of crystals by either changing the polarity of the solvent or else evaporation of the solvent at elevated temperatures to form the thermodynamically more stable compound. The outcome of the reaction mixture depends on three factors: the ligand/metal ratio, the pH-value and the order of the added metal salts. By varying them, we were able to influence the connectivity and hence the dimensionality of the resulting complex.

### 8.4.2. Crystal Structures

Compound **1a** and **1b** ( $[M(\mathbf{H}_2\mathbf{L})(\text{H}_2\text{O})_4]\cdot 2.5\text{H}_2\text{O}$ ;  $M = \text{Co}^{2+}$  (a),  $\text{Ni}^{2+}$  (b)) are isostructural and comprise one metal centre, one twofold deprotonated ligand  $(\mathbf{H}_2\mathbf{L})^{2-}$  and 6.5 water molecules. The detailed crystal structure can be found in the supporting information. In both cases, the central ion shows an octahedral coordination geometry in which four of the water molecules are included. As expected, the ligand coordinates in an  $\eta_2$ -coordination mode. Despite the large number of possible coordination sites, the complexes are of molecular structure. This emphasizes our earlier statement, that metal-phosphonate bonds are rather formed during hydrothermal synthesis, at least under moderate pH conditions. The nitrogen-metal bond lengths of 2.123 Å and 2.139 Å for **1a** and the oxygen-phosphonate bond lengths within the phosphonates indicate an oxidation state of +2 for the metal ions. <sup>[45]</sup> The positive charge is compensated by the single deprotonated phosphonate groups. Individual complexes are connected via hydrogen bonds mediated by water molecules (see figure S2 in supporting information). Compound **2** ( $[\text{Gd}_2(\mathbf{H}_2\mathbf{H}'\mathbf{L})_2(\mathbf{H}_2\mathbf{H}'_2\mathbf{L})(\text{H}_2\text{O})_6]\text{Cl}_4\cdot 14\text{H}_2\text{O}$ ) forms a two dimensional  $1^1\text{O}^1$  network. The structure was solved in the space group  $P\bar{1}$ . The asymmetric unit contains 1.5 ligand molecules with different grades of protonation, one eightfold coordinated gadolinium(III) ion, ten water molecules from which three are coordinating and two chloride counter ions. A comparison of the oxygen-phosphorus bond lengths reveals that they are either around 1.50 Å or else 1.55 Å. The latter one is the typical bond length for a protonated oxygen atom. Therefore, all phosphonate groups are assumed to be only single deprotonated. Additionally, the nitrogen atoms of the split ligand  $(\mathbf{H}_2\mathbf{H}'_2\mathbf{L})$  are protonated, whereas  $(\mathbf{H}_2\mathbf{H}'\mathbf{L})^-$  shows only one protonated nitrogen, leaving it with a negative charge. Both types of ligands differ as well in their coordination mode. The phosphonate of  $\mathbf{H}_2\mathbf{H}_2'\mathbf{L}$  and the phosphonate of  $(\mathbf{H}_2\mathbf{H}'\mathbf{L})^-$  which is closer to the protonated nitrogen atom are each bridging two lanthanides with two oxygen in a  $\eta_2$ -mode. The remaining phosphonate coordinates to one gadolinium ion via one oxygen atom, which gives in total five metal-phosphonate connections. The remaining three coordination sites of the square antiprismatic sphere are occupied by water molecules. Due to the  $\mu_2$ -bridging mode of the individual phosphonate groups, the central ions show a one dimensional  $1^1$  chainlike structure along the a-axis, as shown

in figure 1 (c), with a mean distance between two lanthanide ions of 5.212 Å. In figure 1 (b), the O<sup>1</sup> connection by the bipyridine acting as a tether along the c-axis is depicted. The spacing between the chains is on average 11.504 Å.

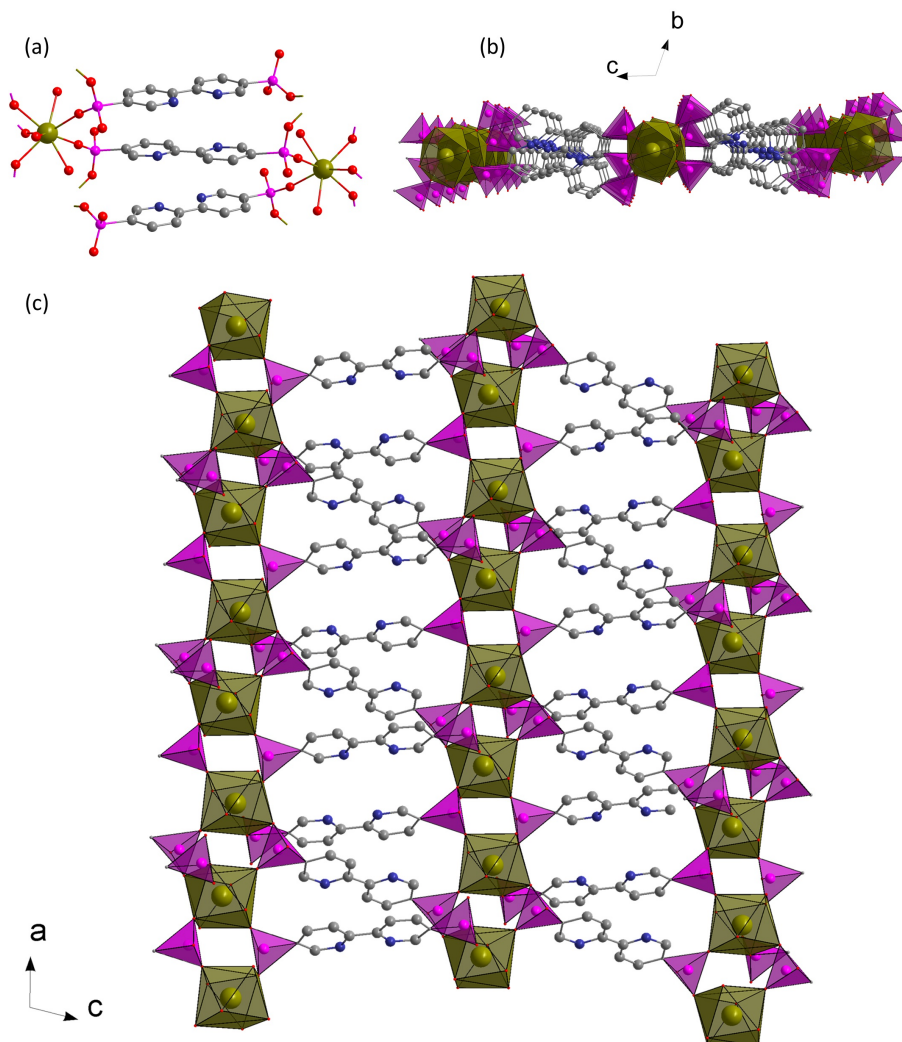


**Figure 1.** (a) Primitive cell of compound **2** with broken off bonds. (b) Top view shows the O<sup>1</sup> tethering of the bipyridine backbone. (c) Graphical representation of the 1<sup>D</sup> gadolinium chains. Colour code: brown - gadolinium, pink - phosphorus, red - oxygen, dark blue - nitrogen, grey - carbon. Hydrogen atoms and solvent molecules have been omitted for clarity.

The layers are connected via hydrogen bonds forming between the counter ions along the b-direction.

Compounds **3a**, **3b**, **3c** ( $[\text{MCo(III)}(\text{H}_2\text{L})_3(\text{H}_2\text{O})_2]\cdot 6.5\text{H}_2\text{O}$ ;  $\text{M} = \text{Gd}^{3+}$  (a),  $\text{Dy}^{3+}$  (b) and  $\text{Tb}^{3+}$  (c), figure 2 (a)) are two-dimensional heterometallic  $\text{I}^0\text{O}^2$  coordination polymers. The structures were solved in the space group  $C2/c$ .

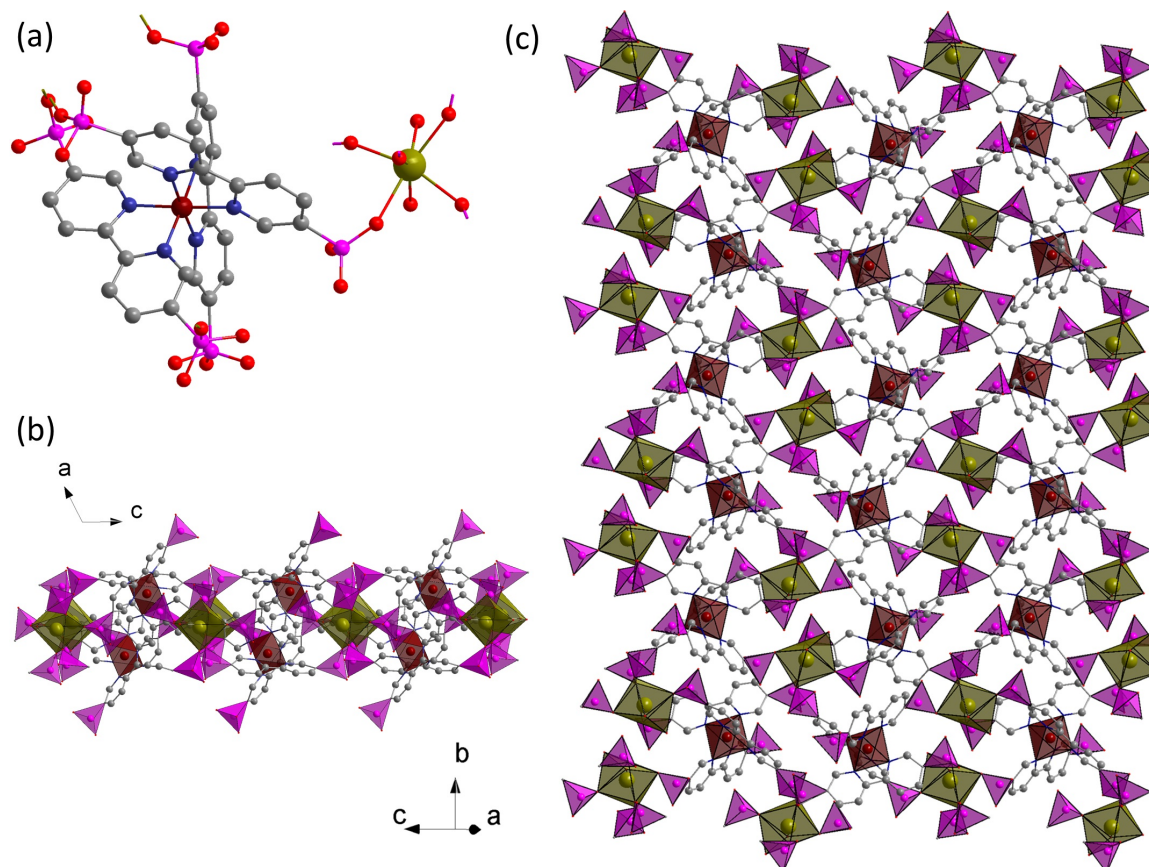


**Figure 2.** (a) Asymmetric unit of compound **3c** with broken off bonds. (b) Side view of a layer illustrating the non-coordinating phosphonate groups. (c) Top view of the crystal structure showing the cobalt and terbium chains. Colour code: brown - gadolinium, dark red - cobalt, pink - phosphorus, red - oxygen, dark blue - nitrogen, grey - carbon. Hydrogen atoms and solvent molecules have been omitted for clarity.

All three complexes are isostructural and differ only in their 4f element. The lanthanides are coordinated in a for lanthanides rather rare sevenfold coordinated capped trigonal prismatic geometry. <sup>[46]</sup> As expected, the coordination sphere is formed by seven oxygen atoms belonging to different groups. Five of the oxygen atoms belong to five separate phosphonate groups, the remaining two originate from water molecules,

leaving one non-coordinating phosphonate group. Similar to compound **2**, all phosphonates are single protonated as indicated by the P-O bond lengths. One trigonal plane and the cap of the coordination polyhedral is built from four phosphonate oxygen atoms, while the other plane includes both water molecules and one ligand molecule. A comparison of the oxygen-lanthanide bond lengths shows, that the average distance to the water molecules are quiet shorter than the bonds to the ligand (2.291 Å and 2.451 Å, respectively). The second metal is chelated in an  $\eta_2$ -coordination mode comparable to compound **1a** and **1b**, but by three bipyridine coordination sites. They form  $(\text{Co}(\text{H}_2\text{L})_3)_3^-$  building units which connect the incorporated lanthanide ions. The N-Co bond lengths differ significantly from the lengths in the previously described complexes. They range from 1.916(8) Å to 1.950(9) Å with a mean value of 1.933 Å. The origin is found in the oxidation state of the cobalt ion, which oxidizes during the reaction from Co(II) to Co(III). The small differences in bond lengths and the *cis*-angles being close to 90° indicate a good approximation to an ideal octahedral coordination sphere. Figure 2 (b) represents a side view along the b-axis of the two-dimensional layers. It is clearly visible, that only five out of six phosphonate groups are coordinating. The remaining group protrudes above and beneath the layer, connecting it by hydrogen bonds between the phosphonate and crystal water to neighbouring arrays. A closer examination of the arrangement within the layer in figure 2 (c) shows, that the cobalt octahedron form some sort of one-dimensional chain along the b-axis. The distance between two terbium polyhedron is 5.514 Å, which is comparably close to the chain in compound **2**. However, they are connected by hydrogen bonds between the phosphonates and show therefore no direct coordinative or covalent contact. Additionally, the arrangement of the metal centres should rather be described as dimers then chains due to their discontinuous nature: the spacing to the next terbium in the opposite direction is with 11.885 Å much longer.

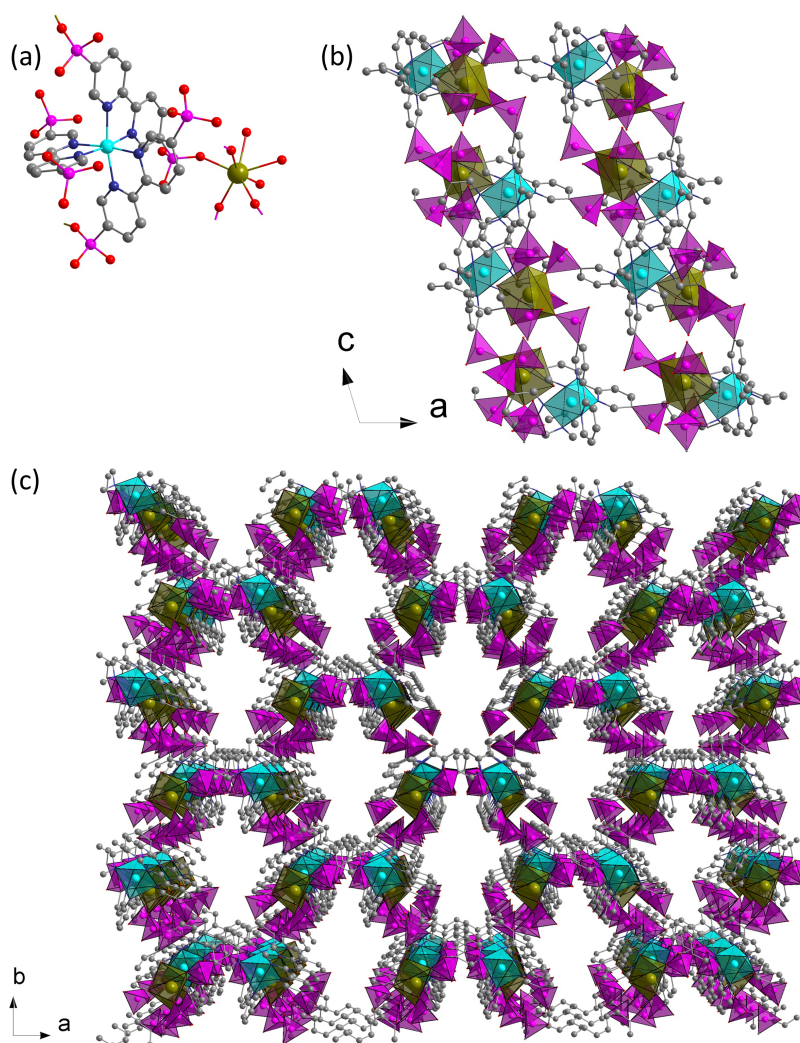


**Figure 3.** (a) Cation of the asymmetric unit of compound **4** with broken off bonds. (b) View along the b-axis showing the connection of the crooked layers by the Ni(H<sub>2</sub>L)<sub>3</sub> units. (c) The view along the c-axis reveals the three-dimensional structure of the compound and the oval motive it is forming. Colour code: brown polyhedron - gadolinium, light blue polyhedron - nickel, pink polyhedron - phosphorus, red - oxygen, dark blue - nitrogen, grey - carbon. Hydrogen atoms and solvent molecules have been omitted for clarity.

The asymmetric unit of compound **4** has the sum formula [GdNi(II)(H<sub>2</sub>L)<sub>3</sub>(H<sub>2</sub>O)<sub>3</sub>]NaCl·6H<sub>2</sub>O. The crystal structure can be solved in the space group *C2* and forms a three-dimensional I<sup>0</sup>O<sup>3</sup> coordination polymer by the  $\mu_2$ -bridging of the gadolinium centres via the ligands. The lanthanide ion has, similar to compounds **3a**, **3b** and **3c**, a coor-



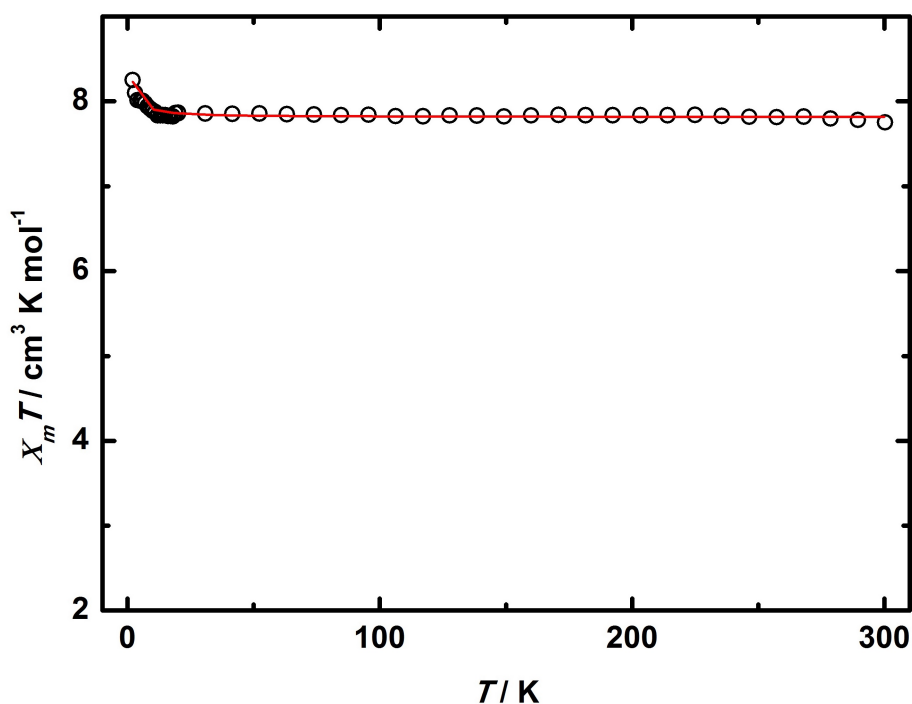
dination number of seven and is in a capped trigonal prismatic coordination environment. But in contrast to the three cobalt complexes, the nickel compound shows three lanthanide-water contacts and only four lanthanide-phosphonate connections, leaving two non-coordinating phosphonate groups. The different connectivity of the phosphonates arises from the different initial pH value due to the use of the chloride metal salt instead of the acetate metal salt and the larger amount of hydrochloric acid which was employed to dissolve the precipitate. As a consequence, the number of phosphonate-metal contacts is reduced. Both trigonal planes of the capped trigonal prism equally consist of two phosphonate groups and one water molecule. The cap is built from a water molecule as well. Again, the nickel ions are coordinated octahedral by the bipyridine coordination sites of the ligand and form building blocks, which connect the gadolinium ions. Due to the different coordination mode of the phosphonates, the motive of a paired chain as in **3a** - **3b** is not present in this compound. Instead, the two different metal ions  $\text{Ni}^{2+}$  and  $\text{Gd}^{3+}$  occur alternating. In figure 3 (c), a view along the c-axis of the crystal structure is shown. It is a representative picture of the three-dimensional structure of this compound and shows the oval pores the structure is forming in this direction.

Table 8.1.: Crystallographic parameters for compounds **3**, **2** and **3**

Compound	2	3a	3b	3c	4
Formula weight	1736.81	1298.08	1300.81	1291.24	1358.75
Crystal system	triclinic	monoclinic	monoclinic	monoclinic	monoclinic
Space group	$P\bar{1}$	$C2/c$	$C2/c$	$C2/c$	$C2$
a / Å	10.362(3)	25.1648(18)	25.1186(12)	25.203(2)	22.6611(11)
b / Å	10.819(3)	17.1628(12)	17.0759(9)	17.0993(14)	16.9747(8)
c / Å	14.686(4)	23.0284(18)	22.9551(14)	22.983(2)	15.2845(7)
$\alpha / ^\circ$	104.138(7)	90	90	90	90
$\beta / ^\circ$	100.605(7)	116.436(2)	116.0600(10)	116.064(2)	106.794(2)
$\gamma / ^\circ$	98.755(7)	90	90	90	90
$V/\text{Å}^3$	1535.5(7)	8905.9(11)	8845.0(8)	8897.4(13)	5628.7(5)
Z	1	8	8	8	4
$\rho_{calc} / \text{g cm}^{-3}$	1.878	1.936	1.954	1.928	1.603
$\mu / \text{mm}^{-1}$	2.572	2.166	2.371	2.265	1.811
$2\theta / ^\circ$	3.968-55.91	2.982-55.892	2.99-55.906	3.946-55.91	3.046-55.7
$F(000)$	854	5140	5136	5112	2680
Data/restraints/parameters	7328/6/406	10663/54/726	10611/96/752	10680/42/688	13356/115/792
GOF $F^2$	1.032	0.975	0.893	1.032	0.947
$R_1, wR_2 [I \geq 2\sigma (I)]$	0.0577, 0.1433	0.0470, 0.1159	0.0524, 0.1029	0.0690, 0.1679	0.0678, 0.1582
$R_1, wR_2$ (all data)	0.0879, 0.1663	0.0718, 0.1263	0.0996, 0.1163	0.1132, 0.1933	0.1152, 0.1783

### 8.4.3. Magnetic Properties

Magnetic measurements at variable temperatures have been carried out for all more-dimensional compounds. All measurements regarding  $\chi_M T$  were conducted under an applied field of 1 kOe in a temperature range between 2 K and 300 K.



**Figure 4.** Temperature dependent measurement of the molar magnetic susceptibility per gadolinium ion for compound **2** in a temperature range between 2 K and 300 K with an applied field of 1 kOe. Black circles represent the experimental data, the red line the simulation with the parameter  $g = 1.992$  and  $J = 0.0076 \text{ cm}^{-1}$ . The inlay shows a more detailed picture of the low temperature region.

For compound **2**, a  $\chi_M T$  value of  $7.76 \text{ cm}^3 \text{K mol}^{-1}$  was observed at room temperature (figure 4), which is in good agreement with the expected values for two uncoupled  $\text{Gd}^{3+}$  ions ( $7.88 \text{ cm}^3 \text{K mol}^{-1}$ ,  $^8\text{S}_{7/2}$ ,  $S = 7/2$ ,  $L = 0$ ,  $g = 2$ ). Upon decreasing the temperature, the value remains almost constant until 10 K, where it increases abruptly. The increase of the magnetic moment can be attributed to several causes. First, it can be the result of a weak ferromagnetic exchange coupling, occurring between neighbouring gadolinium ions, mediated by the phosphonate groups. In order to quantify these

findings, the temperature dependent magnetic molar susceptibility was fitted with the program PHI using an isotropic exchange interaction Hamiltonian  $\hat{H}_{EX} = -2JJ\hat{S}_1 \cdot \hat{S}_2$ .<sup>[47]</sup> For the simulation, the structure was considered as a dimer. The largest congruence of the data was obtained with the parameters  $J = 0.0076 \text{ cm}^{-1}$  and  $g = 1.992$ . The positive sign of the coupling constant indicates that the coupling is indeed of weak ferromagnetic nature. It should be noted, that such small values are more of a qualitative nature. Another reason for the increasing susceptibility at low temperatures could be dipolar coupling. Such magnetic dipole-dipole interaction can occur, when two spin carriers are in very close proximity to each other, which is the case for the gadolinium ions along the  $1^1$  chains in this structure.<sup>[48]</sup> And finally, such an increase of  $\chi_M T$  could arise from a phase transition the compound undergoes at low temperatures.<sup>[39,49]</sup>

Figure 5 shows the magnetic characterization for compounds **3a**, **3b** and **3c** via measurements of the magnetization in a temperature range between 2 K and 10 K with an applied field from 1 kOe to 70 kOe and the magnetic molar susceptibility. The  $\chi_M T$  value at room temperature for the isotropic gadolinium complex in figure 5 (a) is with  $7.90 \text{ cm}^3 \text{ K mol}^{-1}$  close to the expected value for an uncoupled gadolinium ion ( $7.88 \text{ cm}^3 \text{ K mol}^{-1}$ ,  $^8S_{7/2}$ ,  $S = 7/2$ ,  $L = 0$ ,  $g = 2$ ). The susceptibility remains almost constant during the decline of the temperature until 13 K, where it decreases due to small zero field splitting or saturation effects. For quantification, the magnetic data were fitted using the programme PHI.<sup>[47]</sup> The obtained parameters are  $g = 1.980$  and a temperature independent paramagnetism (TIP) of  $3.75 \cdot 10^{-4}$ .

Figure 5 (a) shows the magnetic susceptibility for **3b** and **3c** as well. At room temperature, the values of  $\chi_M T$  are  $14.66 \text{ cm}^3 \text{ K mol}^{-1}$  and  $11.45 \text{ cm}^3 \text{ K mol}^{-1}$ , respectively. This is in good agreement with the expected values of  $14.17 \text{ cm}^3 \text{ K mol}^{-1}$  for **3b** and  $11.82 \text{ cm}^3 \text{ K mol}^{-1}$  for **3c** for uncoupled lanthanides:  $\text{Tb}^{3+}$  ( $^7F_6$ ,  $S = 6$ ,  $L = 3$ ,  $g = 3/2$ ) and  $\text{Dy}^{3+}$  ( $^6H_{15/2}$ ,  $S = 5/2$ ,  $L = 5$ ,  $g = 4/3$ ). Upon cooling, a decrease of the  $\chi_M T$  value is observed, which is attributed to a progressive depopulation of the Stark levels split due to the ligand field.<sup>[48,50,51]</sup>

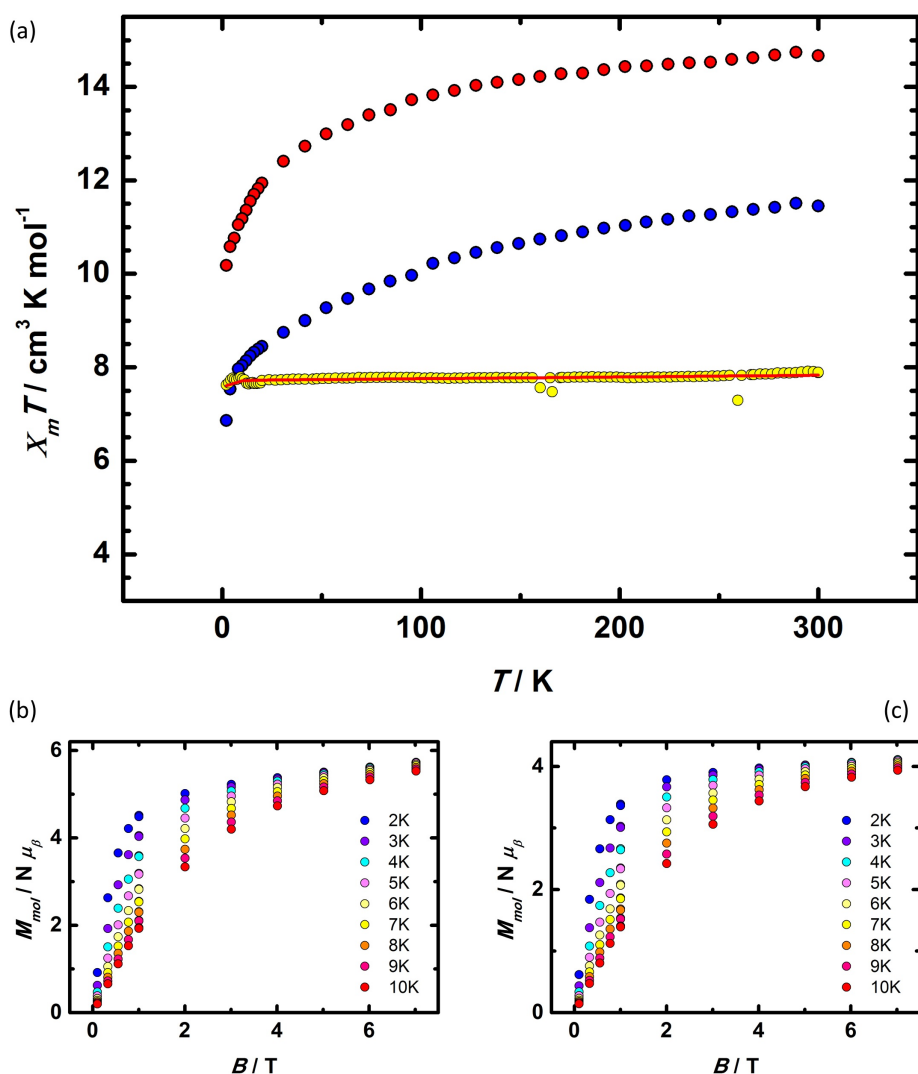


**Figure 5.** (a) Temperature dependent measurement of the molar magnetic susceptibility for compounds **3a** (yellow circles), **3b** (red circles) and **3c** (blue circles). The red line represents the fitted of **3a**. (b) and (c) show the measurement of magnetization at different temperatures for compound **3b** and **3c**, respectively.

In figure 5 (b) and (c), the magnetisation at various temperatures with an applied magnetic field of up to 70 kOe is shown for **3b** and **3c**, respectively. At low fields, a strong increase in the magnetization  $M$  is observed, which slowly reaches for a value near its saturation at high magnetic fields. The highest obtained values for the magnetization at 2 K and 10 K are  $5.73 N\beta$  and  $5.53 N\beta$  for **3b** and  $4.10 N\beta$  and  $3.94 N\beta$  for **3c**. They are quiet lower than the theoretical saturation values one would expect for

an isolated  $\text{Dy}^{3+}$  ion ( $10 N\beta$ ) and  $\text{Tb}^{3+}$  ion ( $9 N\beta$ ). The reason is found again in the magnetic anisotropy with a lower effective spin, and the splitting of the Stark level by the ligand field. [15,52,53]

Compound **4** ( $[\text{GdNi}(\text{II})(\text{H}_2\text{L})_3(\text{H}_2\text{O})_3]\text{NaCl}\cdot 6\text{H}_2\text{O}$ ) shows at room temperature a  $\chi_M T$  value of  $9.04 \text{ cm}^3 \text{ K mol}^{-1}$  (see section 8.4.3), which is in good agreement with the expected values for an uncoupled  $\text{Gd}^{3+}$  ion ( $7.88 \text{ cm}^3 \text{ K mol}^{-1}$ ,  ${}^8S_{7/2}$ ,  $L = 0$ ,  $J = 7/2$ ,  $g = 2$ ) and an uncoupled  $\text{Ni}^{2+}$  ion ( $1.00 \text{ cm}^3 \text{ K mol}^{-1}$ ,  ${}^3A_{2g}$ ,  $L = 0$ ,  $J = 1$ ,  $g = 2$ ).

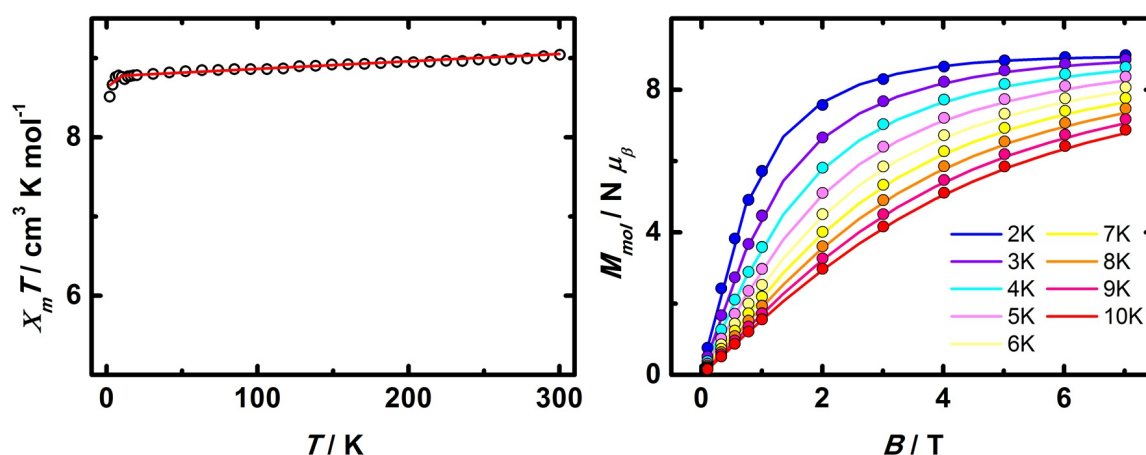


**Figure 6.** Representation of the magnetic properties of compound **4**. Left: variable temperature measurement of the molar susceptibility  $\chi_M$ . Plot shows the product  $\chi_M T$  vs.  $T$ . Circles represent the experimental data, the line the fit obtained by PHI. Right: magnetization at different temperatures in an applied external magnetic field between 1 kOe and 70 kOe.

Upon cooling, the value remains almost constant and decreases only slightly to  $8.76 \text{ cm}^3 \text{ K mol}^{-1}$  at 6 K, where it declines to a final value of  $8.51 \text{ cm}^3 \text{ K mol}^{-1}$  at 2 K, most probably due to zero field splitting. The field dependent magnetization was measured in a temperature range from 2 K up to 10 K. At low fields,  $M$  rapidly increases until a maximum of  $8.97 N\beta$  and  $6.78 N\beta$  is slowly reached at 70 kOe (2 K and 10 K, respectively). Again, the values are in good agreement with the expected values at 2 K and 10 K for an uncoupled  $\text{Gd}^{3+}$  ion ( $6.98 N\beta$  and  $5.73 N\beta$ ) and an uncoupled  $\text{Ni}^{2+}$  ion ( $1.98 N\beta$  and  $1.10 N\beta$ ). The data were fitted using the program PHI. The best accordance of the data was obtained with the fitting parameters  $g_{(\text{Gd}^{3+})} = 1.980$ ,

$g_{(Ni^{2+})} = 2.0438$  and a TIP of  $9.469 \cdot 10^{-4}$ . Due to the similarity of the coordinative environment between compound **3a** and **4**, the  $g_{(Gd^{3+})}$  value from **3a** was used. The magnetic data of compound **4** and compounds **3a**, **3b** and **3c** confirm the oxidation states of the nickel and cobalt ions being +II and +III, respectively. In a strongly split ligand field, Co(III) is found almost exclusively in the diamagnetic low-spin state due to the large ligand field stabilisation energy arising from the electronic configuration  $e_g^0 t_{2g}^6$ . The  $\chi_M T$  value of compound **3a** reflects the absence of another spin carrier additional to the gadolinium ion. The oxidation during the reaction is promoted by two circumstances: first and quite obviously, by the elevated temperature during the crystallization. And second, due to the electronic configuration of  $e_g^1 t_{2g}^6$  in an octahedral coordination environment caused by a strong ligand field, such as from the 2,2'-bipyridine, the Co(II) ion seeks for a Jahn-Teller distortion to remove the degeneracy of the  $e_g$ -orbitals. [54,55] This is hindered by the rigid ligand backbone, which disallows the elongation along a Jahn-Teller axis. For the same reason, the nickel ion is not oxidized during the crystallization. The electronic configuration of an octahedral coordinated Ni(II) ion ( $e_g^2 t_{2g}^6$ ) is much more preferential compared to a Ni(III) ion ( $e_g^1 t_{2g}^6$ ), which would be forced by the Jahn-Teller effect into a for the system not realizable distorted octahedral coordination geometry.

## 8.5. Conclusion

In conclusion, we were able to identify and employ a highly versatile ligand system for the synthesis of several more-dimensional 3d and 4f metal complexes. By taking advantage of the different coordination properties which are offered by the functionalities of the ligand, we prepared several compounds of homometallic and heterometallic nature. In compound **2**, the metal ions are connected by phosphonate groups and form one-dimensional chains. They are tethered via the ligands backbone, which space them by a distance of 11.504 Å. The lanthanides in the heterometallic compounds **3a**, **3b**, **3c** and **4** are in a capped trigonal prismatic coordination geometry and show a rare coordination number of seven. Magnetic measurements were carried out for all the more-dimensional complexes. Compound **2** revealed an interesting behaviour of

the magnetic molar susceptibility at low temperatures, which can be attributed to either small ferromagnetic coupling, dipolar coupling or a phase transition of the compound at low temperatures. Compounds **3a**, **3b**, **3c** and **4** showed that, depending on the metal, an *in situ* oxidation during the synthesis was observed due to the possible occurrence of a Jahn-Teller effect. Studies of the magnetization at various temperatures of compounds **3b** and **3c**, which contain anisotropic lanthanides, showed a split of the Stark level at low temperatures caused by the ligand field. Further syntheses involving the use of various metal/metal/ligand ratios and different reaction conditions are underway in our laboratory to widen the diversity of complexes which can be prepared by employing the ligand system and improve on the magnetic properties.

## 8.6. Experimental

### 8.6.1. General methods and materials

All chemicals were purchased from Alfa Aesar, Deutero, Fisher Chemicals, Sigma-Aldrich and Acros Organics and used without further purification. The NMR spectra were recorded at room temperature by using a Bruker DRX 400 spectrometer and analysed with the program MestReNova.<sup>[56]</sup> Magnetic susceptibility data was collected with a Quantum Design SQUID magnetometer MPMSXL in a temperature range of 2 - 300 K with an applied field of 10 kOe. Elemental analyses (C, H, N and S) were measured at the micro analytical laboratories of the Johannes Gutenberg University Mainz. X-ray diffraction data were collected at 173 K with a Bruker SMART diffractometer and a STOE IPDS 2T at the Johannes Gutenberg University Mainz. The structures were solved with ShelXT and refined with ShelXL 2013 with the program Olex2. CCDC 1477300 (for **1a**), CCDC 1477301 (for **1b**), CCDC 1477302 (for **2**), CCDC 1477303 (for **3a**), CCDC 1477304 (for **3b**), CCDC 1477305 (for **3c**), CCDC 1477306 (for **3a**) and CCDC 1477307 (for **S11**) contain the supplementary crystallographic data for this paper. These data can be obtained free of charge from The Cambridge Crystallographic Data Centre.



### 8.6.2. Synthesis

**Ligand synthesis.** The ligand was prepared as reported in the literature: <sup>[34]</sup> with a selective 5,5'-dibromination of 2,2'-bipyridine hydrobromide, <sup>[57]</sup> followed by a Palladium catalysed phosphonation, the respective phosphonic dialkyl ester 5,5'-bis(diethylphosphonato)-2,2'-bipyridine was obtained as precursor. The desired ligand **H<sub>4</sub>L** (2,2'-bipyridinyl-5,5'-diphosphonic acid) was accessible by hydrolyzation using TMS-Br according to the literature. <sup>[58]</sup> It was isolated as **H<sub>3</sub>H'L** with **H** being a phosphonic acid proton and **H'** being a nitrogen bound proton as depicted in scheme 1. The crystal structure of **H<sub>3</sub>H'L** can be found in the supporting information (figure S1).

**Complex synthesis.** For the preparation of compound **1a**, 0.2 mmol **H<sub>3</sub>H'L** (63.23 mg) were added to a mixture of 3 mL H<sub>2</sub>O and 40  $\mu$ L of concentrated aqueous ammonia. After filtration, a solution of 0.2 mmol Co(Ac)<sub>2</sub>·4H<sub>2</sub>O (49.82 mg) in 3 mL H<sub>2</sub>O was added dropwise and under stirring. An immediate change of colour from pale pink to an intense orange was visible. The viol was left to stand for the solvent to evaporate slowly. Single crystals of orange colour suitable for single crystal XRD (see supporting information figure S2) grew after several days. Yield: 41.57 mg, 46.7%, C<sub>10</sub>H<sub>11</sub>N<sub>2</sub>O<sub>7.5</sub>P<sub>2</sub>Co ([Co(**H<sub>2</sub>L**)]·1.5H<sub>2</sub>O) (400.08): calcd. C 30.02, H 2.77, N 7.00; found C 30.30, H 3.02, N 6.96. Compound **1b** (figure S3) was prepared according to the procedure of **1a** by using 0.2 mmol NiCl<sub>2</sub>·6H<sub>2</sub>O (47.59 mg). Upon addition of ligand and metal, a colour change from pale green to light blue was observed. Yield: 37.72 mg, 42.39%, C<sub>10</sub>H<sub>15</sub>N<sub>2</sub>O<sub>9.5</sub>P<sub>2</sub>Ni ([Ni(**H<sub>2</sub>L**)]·3.5H<sub>2</sub>O) (435.87): calcd. C 27.56, H 3.47, N 6.43; found C 27.74, H 3.43, N 6.47.

Compound **2** was prepared by adding solution of 0.1 mmol Gd(NO<sub>3</sub>)<sub>3</sub>·5 H<sub>2</sub>O (43.33 mg) in 3 mL H<sub>2</sub>O to a mixture of 0.15 mmol **H<sub>3</sub>H'L** (47.42 mg) in 3 mL H<sub>2</sub>O. Immediately, a white solid precipitated. The precipitate was separated from the solution by centrifugation. After the emulsification in 4 mL water, concentrated HCl (0.5 mL) was added to dissolve the solid, giving a clear solution. Acetonitrile (2 mL) was added and the viol was left to stand for six days, giving colourless crystals suitable for single crystal XRD. Yield: 81.51 mg, 58.13% C<sub>30</sub>H<sub>38.5</sub>N<sub>6</sub>P<sub>6</sub>O<sub>23.25</sub>Gd<sub>2</sub>Cl<sub>4</sub> ([Gd<sub>2</sub>(**H<sub>2</sub>H'L**)<sub>2</sub>(**H<sub>2</sub>H'L**)]Cl<sub>4</sub>·5.25H<sub>2</sub>O) (1497.31): calcd. C 24.07, H 2.59, N 5.61; found C 23.81, H 2.74, N 5.91.

Compound **3a**, **3b** and **3c** were prepared by using the following procedure: 0.3 mmol  $\text{H}_3\text{H}'\text{L}$  (94.84 mg) were dissolved in 3 mL  $\text{H}_2\text{O}$  and 40  $\mu\text{L}$  of concentrated ammonia were added. After filtration, 0.1 mmol  $\text{Co}(\text{Ac})_2 \cdot 4\text{H}_2\text{O}$  (24.91 mg) dissolved in 4 mL  $\text{H}_2\text{O}$  were added, whereupon the solution turned orange. The addition of 0.1 mmol  $\text{M}(\text{NO}_3)_3 \cdot x\text{H}_2\text{O}$  (**3a**:  $\text{M} = \text{Gd}$ ,  $X = 5$ ,  $m = 43.33$  mg; **3b**:  $\text{M} = \text{D}$ ,  $X = 1$ ,  $m = 36.65$  mg; **3c**:  $\text{M} = \text{Tb}$ ,  $X = 1$ ,  $m = 36.30$  mg) dissolved in 4 mL  $\text{H}_2\text{O}$  resulted in an immediate precipitation of a white solid, which was dissolved by the addition of 0.5 mL concentrated HCl. The viol was placed in an oven set to  $80^\circ\text{C}$  for 18 h, after which isostructural single crystals suitable for single crystal XRD of orange colour with similar morphology were obtained. **3a**: Yield: 50.17 mg, 43.3%.  $\text{C}_{30}\text{H}_{40}\text{N}_6\text{P}_6\text{O}_{26}\text{CoGd}$  ( $[\text{GdCo}(\text{H}_2\text{L})_3] \cdot 8\text{H}_2\text{O}$ ) (1302.69): calcd. C 27.66, H 3.09, N 6.45; found C 27.64, H 3.20, N 6.45. **3b**: Yield: 54.41 mg, 46.8%,  $\text{C}_{30}\text{H}_{34}\text{N}_6\text{P}_6\text{O}_{23}\text{CoDy}$  ( $[\text{DyCo}(\text{H}_2\text{L})_3] \cdot 5\text{H}_2\text{O}$ ) (1253.89): calcd. C 28.74, H 2.73, N 6.70; found C 28.60, H 2.65, N 6.74. **3c**: Yield: 44.35 mg, 38.2%,  $\text{C}_{30}\text{H}_{38}\text{N}_6\text{P}_6\text{O}_{25}\text{CoTb}$  ( $[\text{DyCo}(\text{H}_2\text{L})_3] \cdot 7\text{H}_2\text{O}$ ) (1286.35): calcd. C 28.01, H 2.98, N 6.53; found C 28.06, H 2.93, N 6.59.

For the preparation of compound **4**, 0.15 mmol  $\text{H}_3\text{H}'\text{L}$  (47.42 mg) were dissolved in 2 mL  $\text{H}_2\text{O}$  and 20  $\mu\text{L}$  of concentrated ammonia were added. After filtration, 0.05 mmol  $\text{NiCl}_2 \cdot 6\text{H}_2\text{O}$  (11.90 mg) dissolved in 2 mL  $\text{H}_2\text{O}$  were added. The addition of 0.05 mmol  $\text{Gd}(\text{NO}_3)_3 \cdot 5\text{H}_2\text{O}$  dissolved in 2 mL  $\text{H}_2\text{O}$  resulted in an immediate precipitation of a white solid, which was dissolved by the addition of 0.4 mL concentrated HCl. The viol was placed in an oven set to  $80^\circ\text{C}$ , where the solvent evaporated and the solution concentrated until a remaining volume of approximately 1.5 mL and then left to stand at room temperature. Single crystals of pale orange suitable for single crystal XRD could be obtained after one day. Yield: 26.58 mg, 43.7%.  $\text{C}_{30}\text{H}_{35}\text{N}_6\text{P}_6\text{O}_{23}\text{NiGdNaCl}$  ( $[\text{GdNi}(\text{H}_2\text{L})_3] \cdot 5\text{H}_2\text{O}$ ) (1307.85): calcd. C 27.55, H 2.70, N 6.43; found C 27.39, H 2.88, N 6.51.

## 8.7. Acknowledgements

Dr. Dieter Schollmeyer and Regine Jung-Pothmann are kindly acknowledged for the support with the crystallographic data.

## 8.8. Notes and references

- [1] J. C. Tan and A. K. Cheetham, *Chem. Soc. Rev.*, **2011**, 40, 1059-1080.
- [2] L. D. Carlos, R. A. Ferreira, V. de Zea Bermudez, B. Julian-Lopez and P. Escribano, *Chem. Soc. Rev.*, **2011**, 40, 536-549.
- [3] M. T. Wharmby, J. P. S. Mowat, S. P. Thompson and P. A. Wright, *J. Am. Chem. Soc.*, **2011**, 133, 1266-1269.
- [4] A. Kondo, T. Satomi, K. Azuma, R. Takeda and K. Maeda, *Dalton Trans.*, **2015**, 44, 12717-12725.
- [5] S. Jones, J. M. Vargas, S. Pellizzeri, C. J. O'Connor and J. Zubieta, *Inorg. Chim. Acta*, **2013**, 395, 44-57.
- [6] M. Pramanik, M. Nandi, H. Uyama and A. Bhaumik, *Cat. Sci. Tech.*, **2012**, 2, 613-620.
- [7] H. Tan, W. Chen, D. Liu, X. Feng, Y. Li, A. Yan and E. Wang, *Dalton Trans.*, **2011**, 40, 8414-8418.
- [8] L. D. Carlos, R. A. S. Ferreira, V. D. Bermudez, B. Julian-Lopez and P. Escribano, *Chem. Soc. Rev.*, **2011**, 40, 536-549.
- [9] K. J. Gagnon, H. P. Perry and A. Clearfield, *Chem. Rev.*, **2012**, 112, 1034-1054.
- [10] K. Maeda, *Microporous Mesoporous Mater.*, **2004**, 73, 47-55.
- [11] K. Maeda, Y. Kiyozumi and F. Mizukami, *J. Phys. Chem. B*, **1997**, 101, 4402-4412.
- [12] Y.-S. Ma, H. Li, J.-J. Wang, S.-S. Bao, R. Cao, Y.-Z. Li, J. Ma and L.-M. Zheng, *Chem. Eur. J.*, **2007**, 13, 4759-4769.
- [13] L. Rosado Piquer and E. C. Sanudo, *Dalton Trans.*, **2015**, 44, 8771-8780.
- [14] M. Andruh, J.-P. Costes, C. Diaz and S. Gao, *Inorg. Chem.*, **2009**, 48, 3342-3359.
- [15] J. Tang, I. Hewitt, N. T. Madhu, G. Chastanet, W. Wernsdorfer, C. E. Anson, R. Sessoli and A. K. Powell, *Angew. Chem. Int. Ed.*, **2006**, 45, 1729-1733.
- [16] G. Novitchi, G. Pilet, L. Ungur, V. V. Moshchalkov, W. Wernsdorfer, L. F. Chibotaru, D. Luneau and A. K. Powell, *Chem. Sci.*, **2012**, 3, 1169-1176.
- [17] J. A. Sheikh, S. Goswami and S. Konar, *Dalton Trans.*, **2014**, 43, 14577-14585.

- [18] J. A. Sheikh, A. Adhikary, H. S. Jena, S. Biswas and S. Konar, *Inorg. Chem.*, **2014**, 53, 1606-1613.
- [19] Y. Bing, N. Xu, W. Shi, K. Liu and P. Cheng, *Chem. Asian. J.*, **2013**, 8, 1412-1418.
- [20] Y. Z. Zheng, M. Evangelisti and R. E. P. Winpenny, *Angew. Chem. Int. Ed.*, **2011**, 50, 3692-3695.
- [21] S. Hu, L. Yun, Y. Z. Zheng, Y. H. Lan, A. K. Powell and M. L. Tong, *Dalton Trans.*, **2009**, 1897-1900.
- [22] C. Janiak, *Dalton Trans.*, **2003**, 2781-2804.
- [23] P. J. Hagrman, D. Hagrman and J. Zubieta, *Angew. Chem. Int. Ed.*, **1999**, 38, 2638-2684.
- [24] A. K. Cheetham, C. N. R. Rao and R. K. Feller, *Chem. Commun.*, **2006**, 4780-4795.
- [25] M. Kurmoo, *Chem. Soc. Rev.*, **2009**, 38, 1353-1379.
- [26] L. J. Murray, M. Dinca and J. R. Long, *Chem. Soc. Rev.*, **2009**, 38, 1294-1314.
- [27] A. Bencini, C. Benelli, A. Caneschi, R. L. Carlin, A. Dei and D. Gatteschi, *J. Am. Chem. Soc.*, **1985**, 107, 8128-8136.
- [28] Z.-G. Gu and S. C. Sevov, *J. Matter. Chem.*, **2009**, 19, 8442-8447.
- [29] B. Zhao, P. Cheng, S. P. Yan, Z. H. Jiang and G. L. Wang, *Angew. Chem. Int. Ed. Engl.*, **2003**, 42, 934-936.
- [30] T. K. Prasad, M. V. Rajasekharan and J. P. Costes, *Angew. Chem. Int. Ed. Engl.*, **2007**, 46, 2851-2854.
- [31] A. C. Rizzi, R. Calvo, R. Baggio, M. T. Garland, O. Pena and M. Perec, *Inorg. Chem.*, **2002**, 41, 5609-5614.
- [32] G. Guerrero, J. G. Alauzun, M. Granier, D. Laurencin and P. H. Mutin, *Dalton Trans.*, **2013**, 42, 12569-12585.
- [33] R. A. Palmer and T. S. Piper, *Inorg. Chem.*, **1966**, 5, 864-878.
- [34] V. Penicaud, F. Odobel and B. Bujoli, *Tetrahedron Lett.*, **1998**, 39, 689-3692.

- [35] E. M. Pineda, F. Tuna, Y.-Z. Zheng, S. J. Teat, R. E. P. Winpenny, J. Schnack and E. J. L. McInnes, *Inorg. Chem.*, **2014**, 53, 3032-3038.
- [36] M. Bartholoma, H. Chueng, S. Pellizzeri, K. Ellis-Guardiola, S. Jones and J. Zubieta, *Inorg. Chim. Acta*, **2012**, 389, 90-98.
- [37] V. Lopez-Diaz, T. M. Smith Pellizzeri, M. D. Lijewski, K. Ruhlandt and J. Zubieta, *Inorg. Chim. Acta*, **2016**, 441, 109-116.
- [38] E. Fernandez-Zapico, J. Montejo-Bernardo, A. Fernandez-Gonzalez, J. R. Garcaa and S. Garca Granda, *J. Solid State Chem.*, **2015**, 225, 285-296.
- [39] A.-M. Pütz, L. M. Carrella and E. Rentschler, *Dalton Trans.*, **2013**, 42, 16194-16199.
- [40] F. Odobel, B. Bujoli and D. Massiot, *Chem. Matter.*, **2001**, 13, 163-173.
- [41] I. Gillaizeau-Gauthier, E. Costa, C. A. Bignozzi, P. Qu and G. J. Meyer, *Inorg. Chem.*, **2001**, 40, 6073-6079.
- [42] H. Zabri, I. Gillaizeau, C. A. Bignozzi, S. Caramori, M.-F. Charlot, J. Cano-Boquera and F. Odobel, *Inorg. Chem.*, **2003**, 42, 6655-6666.
- [43] S. Khanra, S. Konar, A. Clearfield, M. Helliwell, E. J. L. McInnes, E. Tolis, F. Tuna and R. E. P. Winpenny, *Inorg. Chem.*, **2009**, 48, 5338-5349.
- [44] R. Laudise, *Chem. Eng. News*, **1987**, 65, 30-43.
- [45] A. Rajput and R. Mukherjee, *Coord. Chem. Rev.*, **2013**, 257, 350-368.
- [46] J. A. McCleverty and T. J. Meyer, eds., *Comprehensive coordination chemistry II*, Elsevier Pergamon, Amsterdam ; Boston, **2004**.
- [47] N. F. Chilton, R. P. Anderson, L. D. Turner, A. Soncini and K. S. Murray, *J. Comput. Chem.*, **2013**, 34, 1164-1175.
- [48] W. Haase, *Ber. Bunsen-Ges. Phys. Chem.*, **1994**, 98, 1208-1208.
- [49] C. L. Calvin, *Magnetochemistry*, Springer Verlag, Heidelberg, Tokyo, **1986**.
- [50] Y.-L. Hou, G. Xiong, B. Shen, B. Zhao, Z. Chen and J.-Z. Cui, *Dalton Trans.*, **2013**, 42, 3587-3596.

- [51] F. Gao, Y. Li, C. Liu, Z. Li and J. Zuo, *Dalton Trans.*, **2013**, 42, 11043-11046.
- [52] F. Yang, Q. Zhou, G. Zeng, G. Li, L. Gao, Z. Shi and S. Feng, *Dalton Trans.*, **2013**, 43, 1238-1245.
- [53] S. Osa, T. Kido, N. Matsumoto, N. Re, A. Pochaba and J. Mrozinski, *J. Am. Chem. Soc.*, **2004**, 126, 420-421.
- [54] H. A. Jahn and E. Teller, *Proc. R. Soc. London, Ser. A*, **1937**, 161, 220-235.
- [55] H. A. Goodwin, in *Spin Crossover in Transition Metal Compounds I*, Springer Berlin Heidelberg, **2004**, pp. 59-90.
- [56] J. Cobas, F. Sardina, *Concepts in Magnetic Resonance*, **2003**, 19A, 80-96.
- [57] A. B. Zdravkov and N. N. Khimich, *Russ. J. Org. Chem.*, **2006**, 42, 1200-1202.
- [58] C. E. McKenna, M. T. Higa, N. H. Cheung and M.-C. McKenna, *Tetrahedron Lett.*, **1977**, 18, 155-158.

## 8.9. Supporting Information

### *Electronic Supplementary Information*

**Title:** Functionalized phosphonates as building units for multi-dimensional homo- and heterometallic 3d-4f inorganic-organic hybrid-materials and their magnetic characterization.

**Author(s):** Christian Köhler, Eva Rentschler\*

Table 8.2.: Crystallographic parameters for compounds **1a**, **1b** and **H<sub>3</sub>H'L**

Compound	1a	1b	L8
Empirical formula	C <sub>10</sub> H <sub>18</sub> CoN <sub>2</sub> O <sub>12.5</sub> P <sub>2</sub>	C <sub>10</sub> H <sub>19.5</sub> N <sub>2</sub> NiO <sub>12.5</sub> P <sub>2</sub>	C <sub>10</sub> H <sub>10</sub> N <sub>2</sub> O <sub>6</sub> P <sub>2</sub>
Formula weight	487.13	488.42	316.14
Crystal system	monoclinic	monoclinic	orthorhombic
Space group	<i>P2<sub>1</sub>/n</i>	<i>P2<sub>1</sub>/n</i>	<i>Pbcn</i>
a / Å	10.9975(11)	10.9582(16)	13.6133(9)
b / Å	10.0662(10)	10.0015(11)	13.0066(8)
c / Å	18.303(2)	18.204(2)	14.3436(9)
α / °	90	90	90
β / °	105.790(3)	105.491(5)	90
γ / °	90	90	90
Volume / Å <sup>3</sup>	1949.8(4)	1922.6(4)	2539.7(3)
Z	4	4	8
ρ <sub>calc</sub> / g cm <sup>-3</sup>	1.659	1.687	1.654
μ / mm <sup>-1</sup>	1.108	1.241	0.37
2θ / °	3.914-55.992	3.934-55.926	4.332-56.038
F(000)	996	1006	1296
Data/restraints/parameters	4698/0/273	4605/0/277	3074/0/185
GOF F <sup>2</sup>	0.897	0.989	1.059
R <sub>1</sub> , wR <sub>2</sub> [I ≥ 2σ (I)]	0.0388, 0.0792	0.0449, 0.0902	0.0316, 0.0853
R <sub>1</sub> , wR <sub>2</sub> (all data)	0.0771, 0.0867	0.0810, 0.1029	0.0351, 0.0879



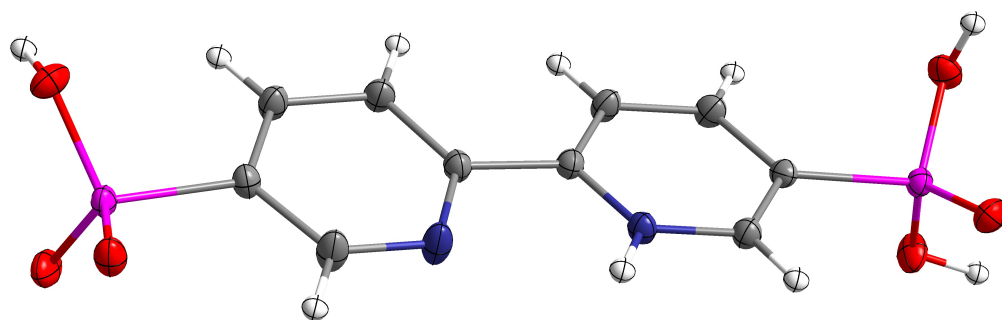


**Figure S1.** Molecular structure of the ligand  $\text{H}_3\text{H}'\text{L}$  with thermal ellipsoids. Colour scheme: pink phosphorus, red - oxygen, dark blue - nitrogen, grey - carbon, white - hydrogen.

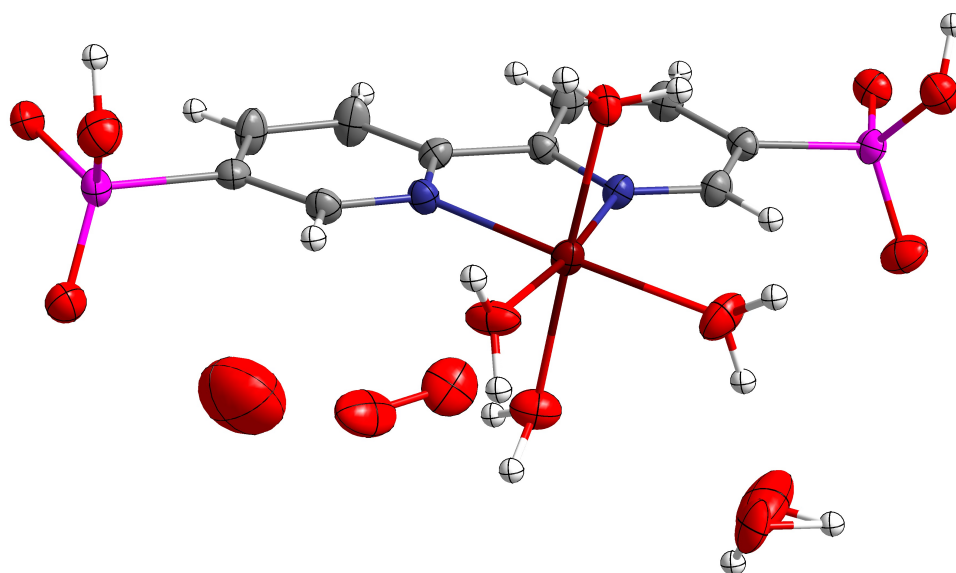


**Figure S2.** Molecular structure of compound **1a** with thermal ellipsoids. Colour scheme: dark red cobalt, pink - phosphorus, red - oxygen, dark blue - nitrogen, grey - carbon, white hydrogen.

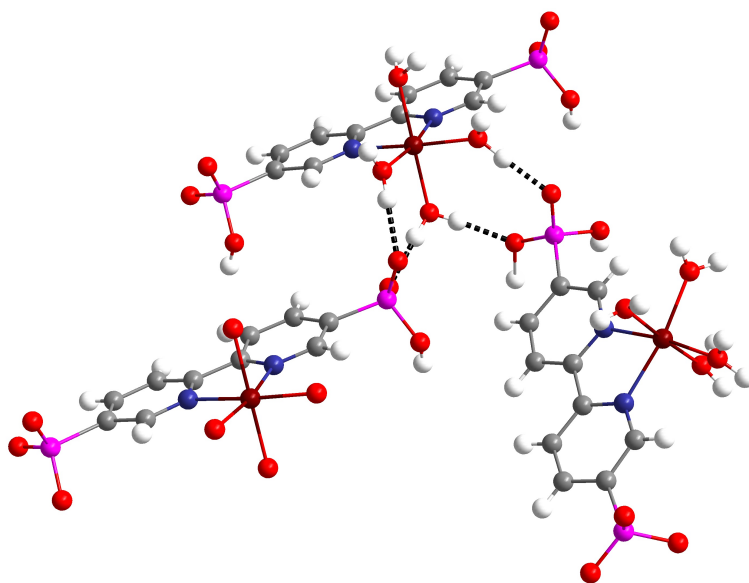


**Figure S3.** Intermolecular connections in compound **1a** mediated by hydrogen bonds between crystal water molecules and phosphonate groups.

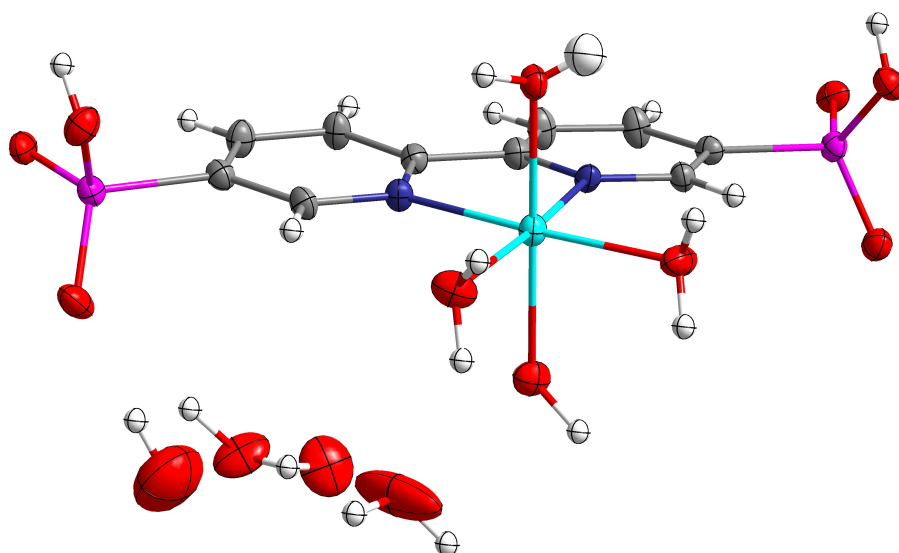


**Figure S4.** Molecular structure of compound **1b** with thermal ellipsoids. Colour scheme: light blue - nickel, pink - phosphorus, red - oxygen, dark blue - nitrogen, grey - carbon, white hydrogen.

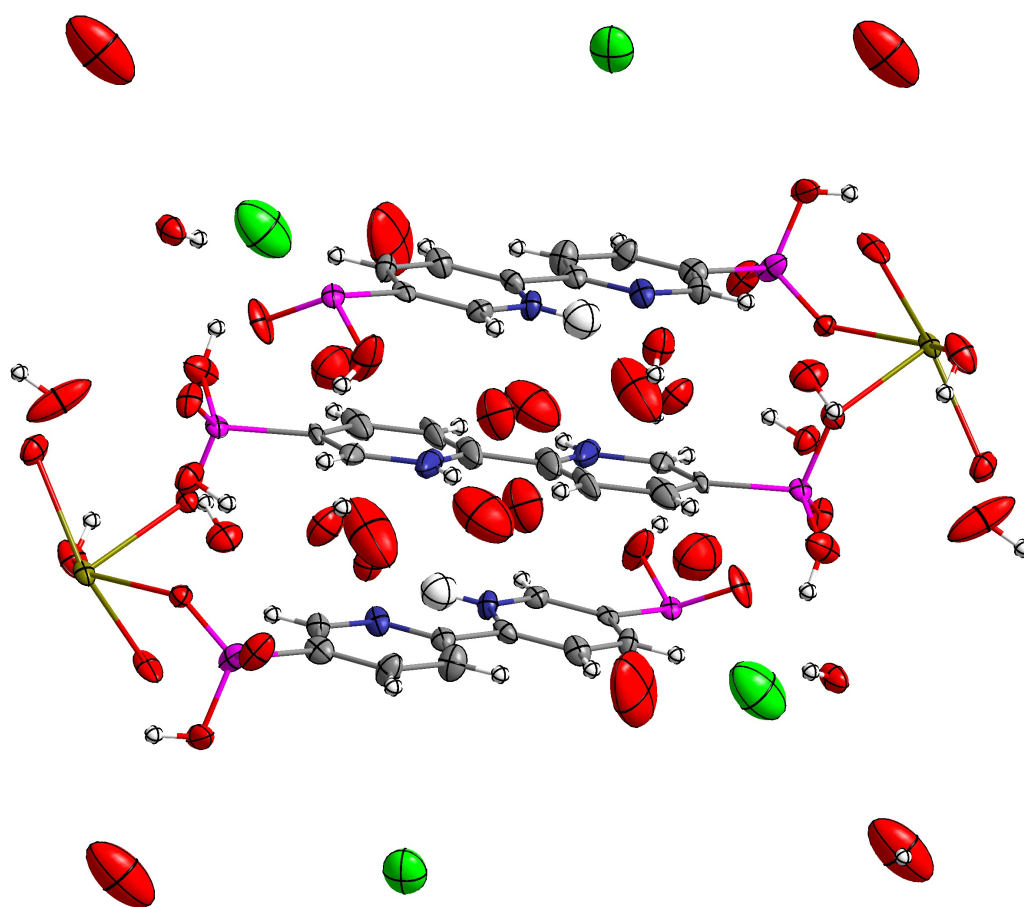


**Figure S5.** Molecular structure of compound **2** with thermal ellipsoids. Colour scheme: brown gadolinium, light green - chlorine, pink - phosphorus, red - oxygen, dark blue - nitrogen, grey - carbon, white hydrogen.

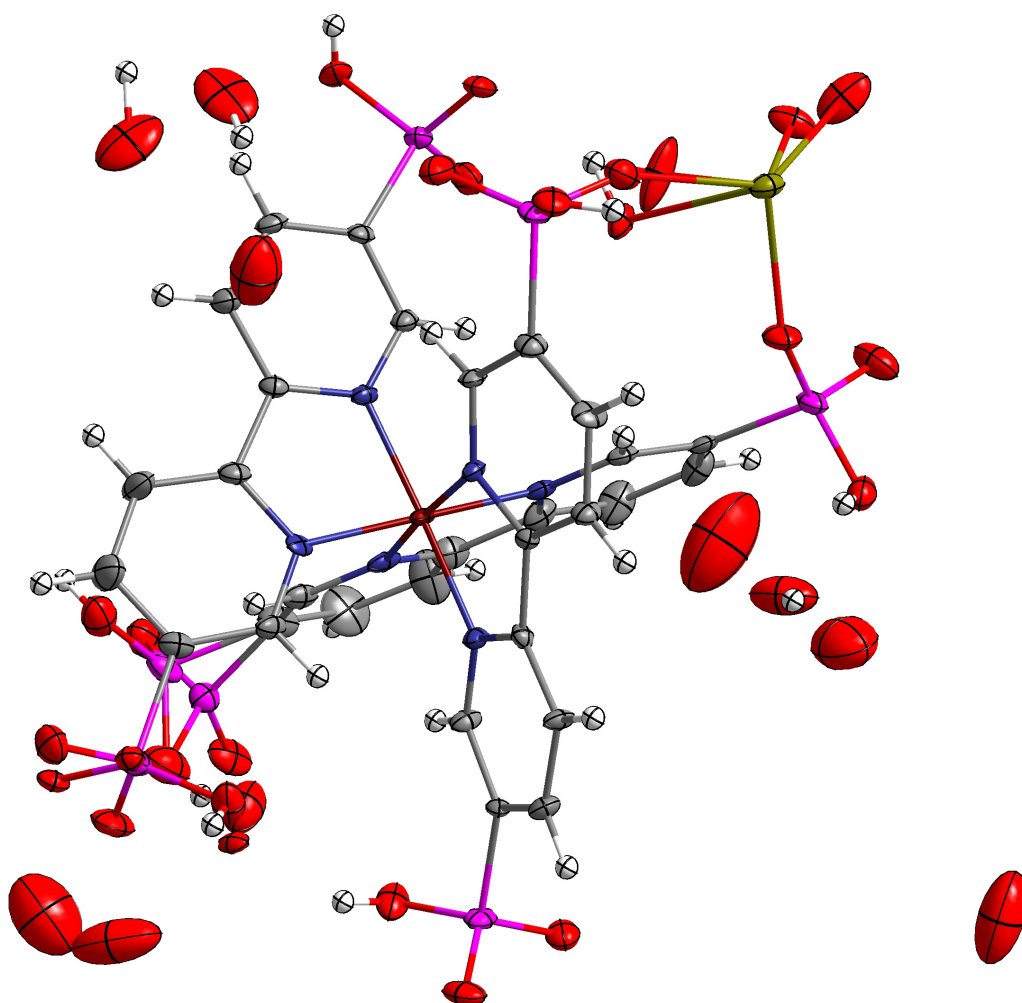


**Figure S6.** Molecular structure of compound **3a** with thermal ellipsoids. Colour scheme: brown gadolinium, dark red - cobalt, pink - phosphorus, red - oxygen, dark blue - nitrogen, grey carbon, white - hydrogen.

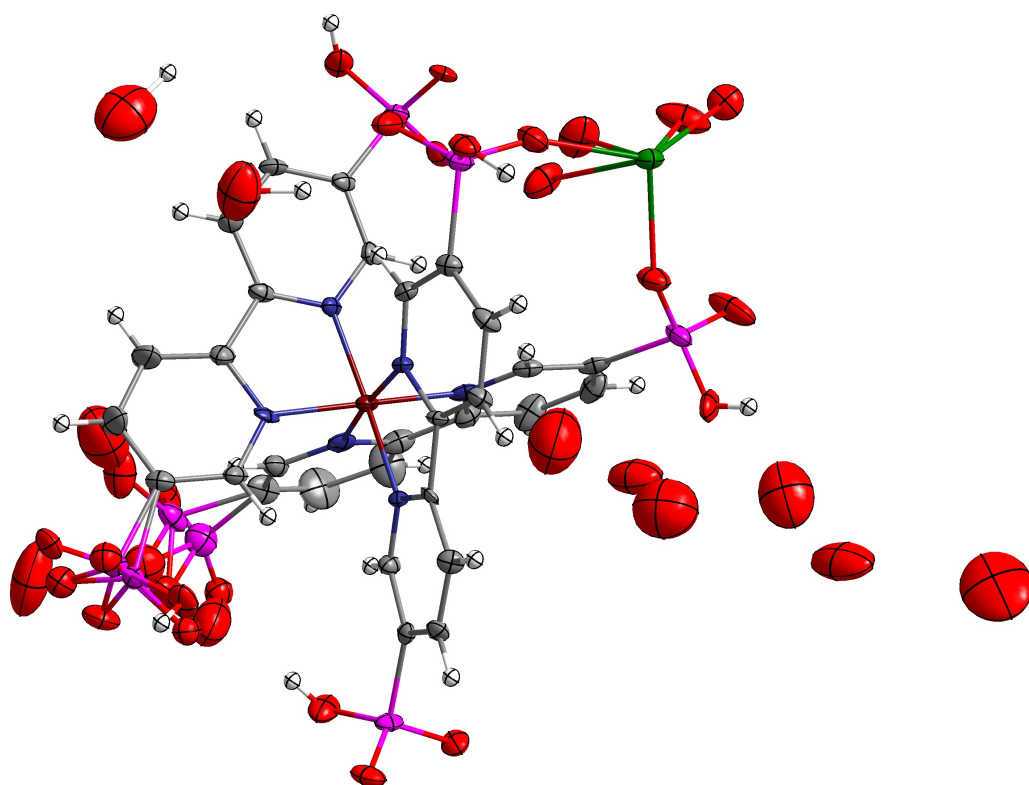


**Figure S7.** Molecular structure of compound **3b** with thermal ellipsoids. Colour scheme: green dysprosium, dark red - cobalt, pink - phosphorus, red - oxygen, dark blue - nitrogen, grey carbon, white - hydrogen.

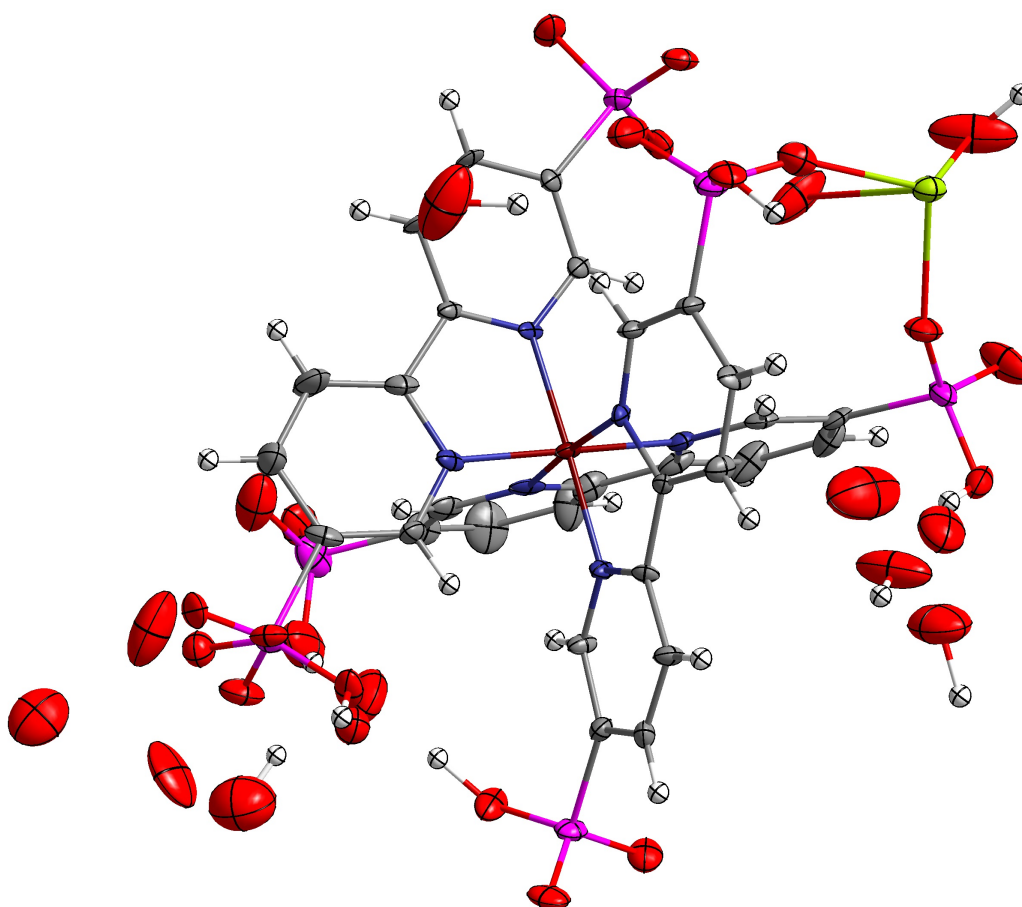


**Figure S8.** Molecular structure of compound **3c** with thermal ellipsoids. Colour scheme: yellow terbium, dark red - cobalt, pink - phosphorus, red - oxygen, dark blue - nitrogen, grey carbon, white - hydrogen.

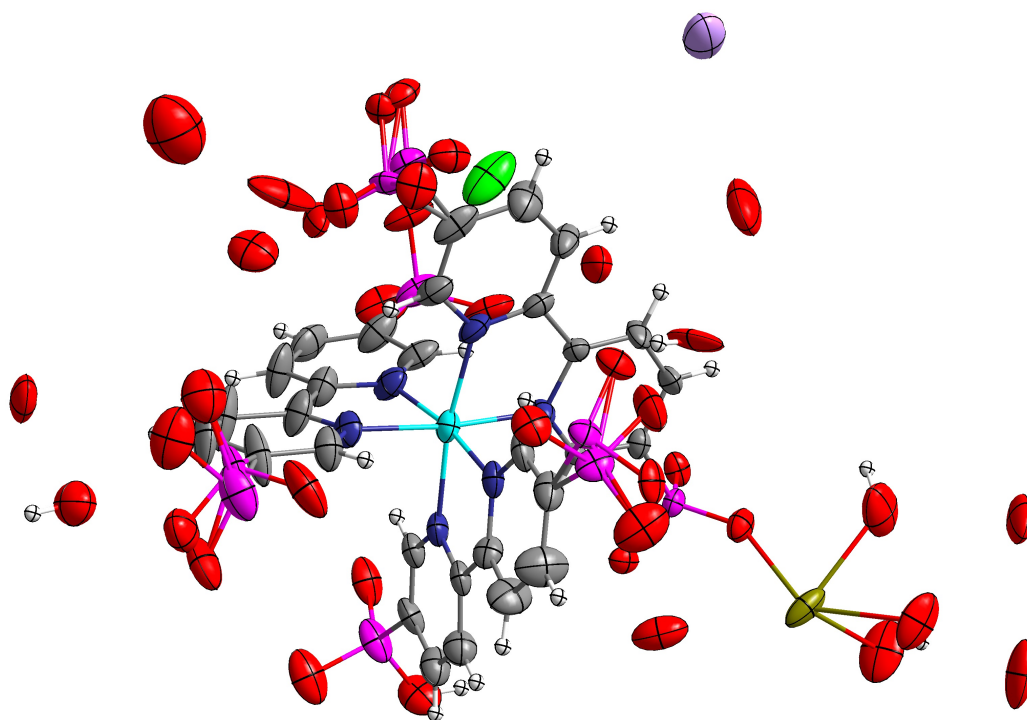


**Figure S9.** Molecular structure of compound **4** with thermal ellipsoids. Colour scheme: brown gadolinium, light blue - nickel, light green - chlorine, pink - phosphorus, purple - sodium, red - oxygen, dark blue - nitrogen, grey - carbon, white - hydrogen.

## 9. Further Investigations

Additional to the extended networks presented in chapter 8, several other complexes were prepared using the ligand  $\text{H}_4\text{L}$ . They vary in their dimensionality, their composition and the used metal ions. To avoid confusion with the systems from part I, the compounds from part II presented so far will be re-indexed as follows:

Table 9.1.: Re-indexed compounds from part II.

Compound index in publication:	<b>1a</b>	<b>1b</b>	<b>2</b>	<b>3a</b>	<b>3b</b>	<b>3c</b>	<b>4</b>
Compound index in this chapter:	<b>6a</b>	<b>6b</b>	<b>7</b>	<b>8a</b>	<b>8b</b>	<b>8c</b>	<b>9</b>

### 9.1. One-Dimensional Cobalt Chain

Due to the successes with the combination of  $\text{H}_4\text{L}$  and cobalt(II) salts, involving a fascinating oxidation which could be observed during the crystallization, further inquiries were undertaken. During the preparation of compounds **8a**, **8b** and **8c**, it caught our attention when the color of an aqueous solution of cobalt(II) acetate changed from a pale pink to an intensive orange upon mixing it with an alkaline aqueous solution of the ligand. The reaction was repeated and instead of adding any lanthanide salts, an excess of acetonitrile was added to precipitate the new system. After filtration, the solid was dissolved in aqueous hydrochloric acid. By using vapor diffusion with acetonitrile, orange single crystals of **10** with the shape of small octahedron (see figure 9.1 (a)) could be obtained. The structure was determined using single crystal XRD.



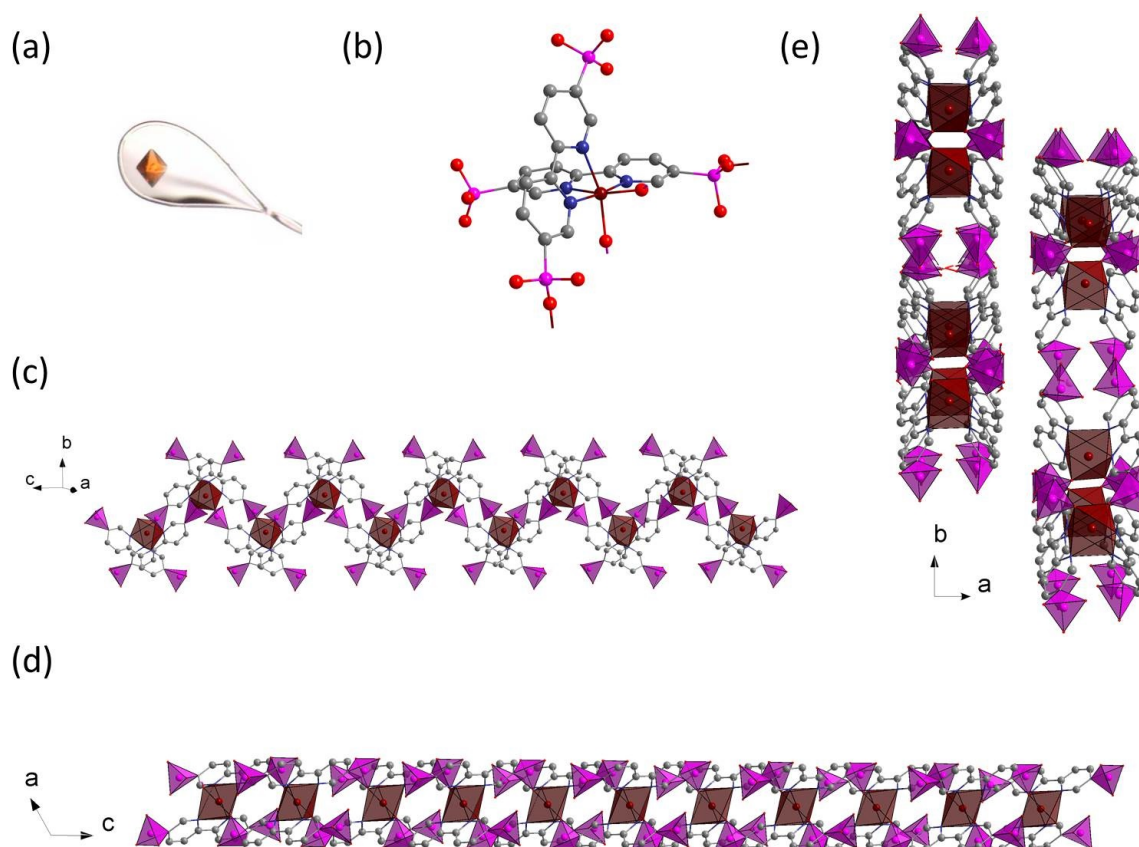


Figure 9.1.: In (a), a picture of the obtained orange crystals is shown. (b) represents the elemental unit of compound **10**. The pictures (c) and (d) are graphical representations of the one-dimensional chain along different crystallographic axis. (e) shows several neighboring chains from a view along the b axis. In all representations, water molecules and hydrogen atoms have been omitted for clarity.

The structure of compound **10** was solved in the space group  $C2/c$ . The elemental unit has the sum formula  $[\text{Co(II)}(\mu_2\text{-}\eta_2\text{-H}_3\text{L})_2] \cdot 6\text{H}_2\text{O}$  (figure 9.1 (b)). The asymmetric unit comprises actually only one ligand and half a cobalt ion, the rest of the elementary cell is generated by symmetry. The structure can be described as a one dimensional homometallic chain. The ligand builds a distorted octahedral coordination geometry, which encloses the cobalt ion. The two bipyridine coordination sites are chelating the cobalt ion in *cis*-configuration, while the remaining coordination sites are occupied by oxygen atoms belonging to one of the two phosphonate groups. The second phosphonate group does not coordinate at all. This gives the ligand a  $\mu_2$ -bridging mode,

which connects the cobalt polyhedrons to a one-dimensional chain (figure 9.1 (c) and figure 9.1 (d)). The metal ions are arranged in a zigzag pattern with a spacing of 7.320 Å and an angle of 115.97° between three metal centers. The chains are connected via hydrogen bonds mediated by water molecules between the phosphonate groups (figure 9.1 (e)). Once again, the oxidation state of the metal can be determined by comparing the metal-nitrogen bond lengths with the literature. They indicate the presence of a cobalt(II) species due to the bond lengths of 2.131 Å, 2.165 Å and 2.055 Å. In contrast to compound **8a** - **8c**, there was no oxidation of the metal ion during the crystallization.

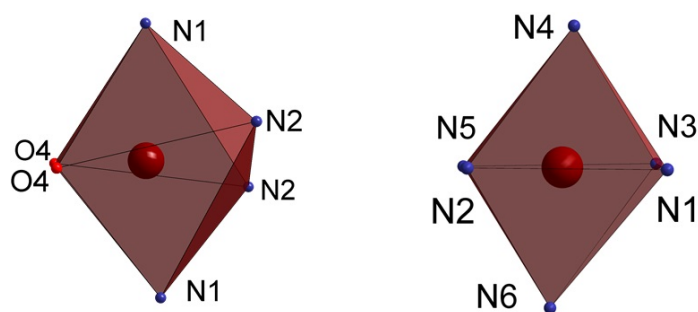


Figure 9.2.: Left: octahedral coordination sphere of **10**. Right: octahedral coordination sphere of **8a**.

The reason for the distinct behavior can be found in the differences in symmetry. As discussed in section 8.4, the  $e_g$ -orbitals of a given metal ion with the electronic configuration  $e_g^1 t_{2g}^6$  are degenerated due to their non-symmetric occupation. This configuration is hence subject to the Jahn-Teller-effect, which enforces the reduction of symmetry in order to resolve the degeneracy. In the heterometallic compounds **8a** - **8c**, the cobalt ions are enclosed by a tris(bipyridine) cage, forcing them into a nearly ideal octahedral coordination geometry (figure 9.2). Their flexibility is much more restrained in comparison to compound **10**, because of the additional phosphonate lanthanide ion connections. Hence, the only way to resolve the degeneracy of the  $e_g$ -orbitals is an oxidation. In compound **10**, every ligand has only three ligand metal contact points instead of four, which gives the system much more flexibility. A reduction of symmetry would resolve the degeneracy of the  $e_g$ -orbitals, preventing an oxidation of the cobalt(II) ion as in the compounds **8a** - **8c**. As a consequence, the octahedral coordination geometry

is very distorted in compound **10**.

The formation of this one-dimensional complex emphasizes once more the tremendous coordination capability of the employed ligand system. However, the synthesis of this complex was hardly reproducible and side products co-crystallized in most cases. Furthermore, the compound was observed as well in reaction mixtures of other synthetic approaches. The reason for these synthetic difficulties is possibly found in the pH value. Since the phosphonic acid groups at a ligand are equivalent, they have initially the same  $pK_a$  value. Due to the connection via a delocalized  $\pi$ -electron system, the deprotonation of one phosphonate group changes the  $pK_a$  value of the other phosphonate group. However, these two values probably are still close together. Unfortunately, the asymmetric protonation is also the premise for the formation of the complex in order to balance the charge. The pH value is changing during the evaporation of the solvent and the hydrochloric acid. Upon reaching the subtle equilibrium, the complex starts to crystallize until the formation of another system is favored. So far, it was not possible to find reaction conditions, which lead to the selective formation of compound **10**.

## 9.2. Two-Dimensional Lanthanides

In an attempt to prepare analogue compounds to **7** with dysprosium and terbium salts, two new species were obtained instead, even though the reaction conditions remained constant. This enforces the earlier statement, that the formation of these systems are subject to a very delicate equilibrium, where even small distortions can lead to novel structures.

### 9.2.1. Terbium Complex

The reaction conditions, that led to the formation of compound **11**, were carried out using terbium nitrate instead of the gadolinium salt. Similar to the known course of the reaction (see section 8.6.2), colorless crystals were obtained after several days. The material was analyzed by single crystal X-ray diffraction and magnetic measurements. It

was surprising to find, that the crystallized product (compound **11**) was of different composition. The asymmetric unit has the formula  $[\text{Tb}(\mu_4\text{-H}_2\text{H}^{\text{M}})(\text{H}_2\text{O})_4]\text{Cl}_2 \cdot \text{H}_2\text{O}$ .

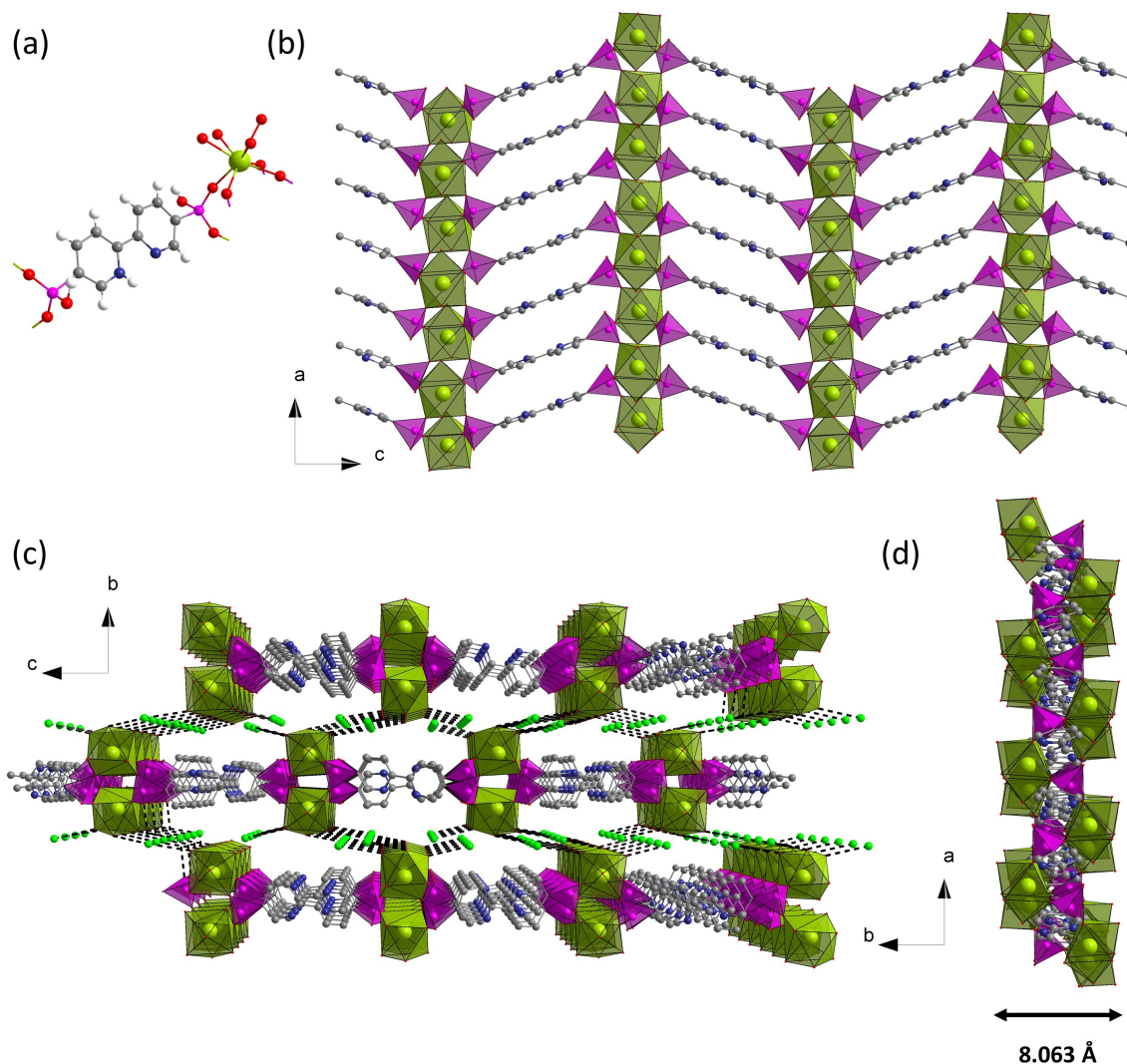


Figure 9.3.: Compound **11**. (a) Shows the complex cation. In (b), the one dimensional terbium ion chains and the bipyridine backbone tethering them are visible. (c) Is a representation, where the interlayer connections via chloride counterions mediated by hydrogen bonds are displayed. (d) Shows a single layer along the bipyridine linkers. Non-coordinating water molecules have been omitted for clarity. Counterions have been omitted in a, b and d. Hydrogen atoms have been omitted in b, c and d.

It is noteworthy, that this compound comprises only one ligand molecule, which bridges four metal ions. The terbium ion is in an eightfold coordinated square antipris-

matic geometry. One of the square planes is built from the crystal water molecules. The second plane is formed by the phosphonate oxygen. Both phosphonate groups are single deprotonated, whereas one of the nitrogen atoms from the bipyridine backbone is protonated. The charge is balanced by two chloride ions.

It is obvious, that the asymmetric unit of compound **11** differs in many ways from the asymmetric unit of compound **7**. Nevertheless, there is quite a structural resemblance between the two systems. The overall dimensionality of this compound is, as in **7**,  $1^1O^1$ . The lanthanide ions form a one-dimensional chain, in which two metal ions are connected by two  $\mu_2$ -connections from both phosphonate groups. The distance between the lanthanides is 5.721 Å. The chains are tethered by the bipyridine backbone. In contrast to compound **7**, where the one-dimensional metal chains were perpendicular to the bipyridine linkers, the tether in the present complex show an alternating angle of 63.6° in regard to the terbium chains. This gives the ligand molecules a wavelike pattern throughout the structure. A view along the chain of bipyridine in figure 9.3 (d) shows, that a single layer is 8.063 Å thick. The perspective reveals as well, that the phosphonate groups are embedded in the middle of the layer, encompassed by the lanthanides. The edges of the layers are built by the crystal water molecules, which prevent a coordinative extension of the network via further phosphonate metal bonds in the third dimension. The delimiting solvent molecules connect individual layers through hydrogen bonds mediated by the chloride counter ions. (see figure 9.3 (c)).

In order to investigate the magnetic properties of this compound, variable temperature measurements of the magnetic molar susceptibility with an applied magnetic field of 1 kOe and the magnetization in a temperature range between 2 K and 10 K with an applied magnetic field between 1 kOe and 70 kOe were conducted. The values and course of the magnetization is very similar to the measurement of compound **8c**: it increases strongly at low fields and slowly reaches for saturation at high magnetic fields with a highest obtained value of 4.60  $N\beta$  at 2 K and 4.50  $N\beta$  at 10 K. They are lower than the expected values because of the anisotropy of the terbium ion and the Stark levels split due to the ligand field.

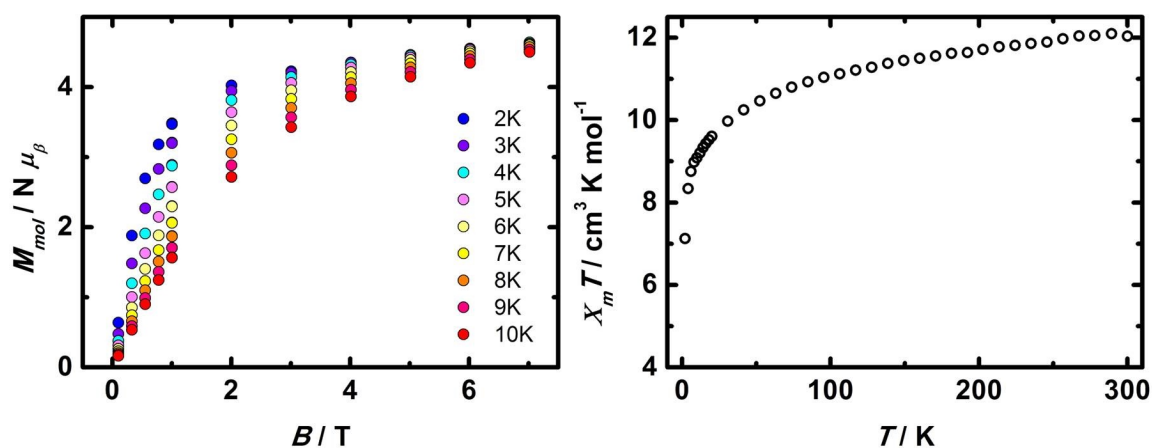


Figure 9.4.: Left: magnetization of compound **11** in a temperature range of 2 K and 10 K in a magnetic field between 1 kOe and 70 kOe. Right:  $\chi_M T$  vs.  $T$  plot in a temperature range between 2 K and 300 K with an applied field of 1 kOe.

The magnetic molar susceptibility shows a value of  $12.03 \text{ cm}^3 \text{ K mol}^{-1}$  at room temperature, which starts to decrease immediately upon cooling. This is again attributed to the progressive depopulation of the split Stark levels. In regard of the findings from compound **7**, a weak increase of the  $\chi_M T$  value was expected at very low temperatures due to their structural resemblance. However, there was no such trend observable. A reason might be the larger distance between the metal ions, which hinders a ferromagnetic or dipolar coupling ( $5.212 \text{ \AA}$  and  $5.721 \text{ \AA}$  for compound **7** and **11**, respectively), or else the absence of a phase transition as described in section 8.4.

### 9.2.2. Dysprosium Complex

A substitution of terbium nitrate by dysprosium nitrate in the reaction led yet to another product (compound **12**). The single crystals suitable for XRD analysis (figure 9.5 (a)) were obtained using similar reaction conditions as for compounds **7** and **10**. Compound **12** has the sum formula  $[\text{Dy}(\text{H}_2\text{H}^M)_2]\text{Cl}\cdot\text{HCl}\cdot 4\text{H}_2\text{O}$  (figure 9.5 (b)). The structure was solved in the space group  $P\bar{1}$ . While the previously described homometallic lanthanide complexes shared several characteristics, the dysprosium compound forms a completely different type of structure. The first major difference is the metal ions coordination number of six, which leads to an octahedral geometry. The coordination sphere

consists solely of phosphonate groups. One similarity is the appearance of the ligand, which provides once more two single deprotonated phosphonate groups and one protonated nitrogen atom. However, in compound **12** they are not equal in terms of their coordination mode. One of the ligands exhibits a  $\mu_2$ -bridging mode due to the two metal contacts from both phosphonate groups. In contrast, the second ligand shows a  $\mu_3$ -bridging mode, because one of the phosphonate groups connects two metal ions additional to the ligand metal contact by the other phosphonate group.

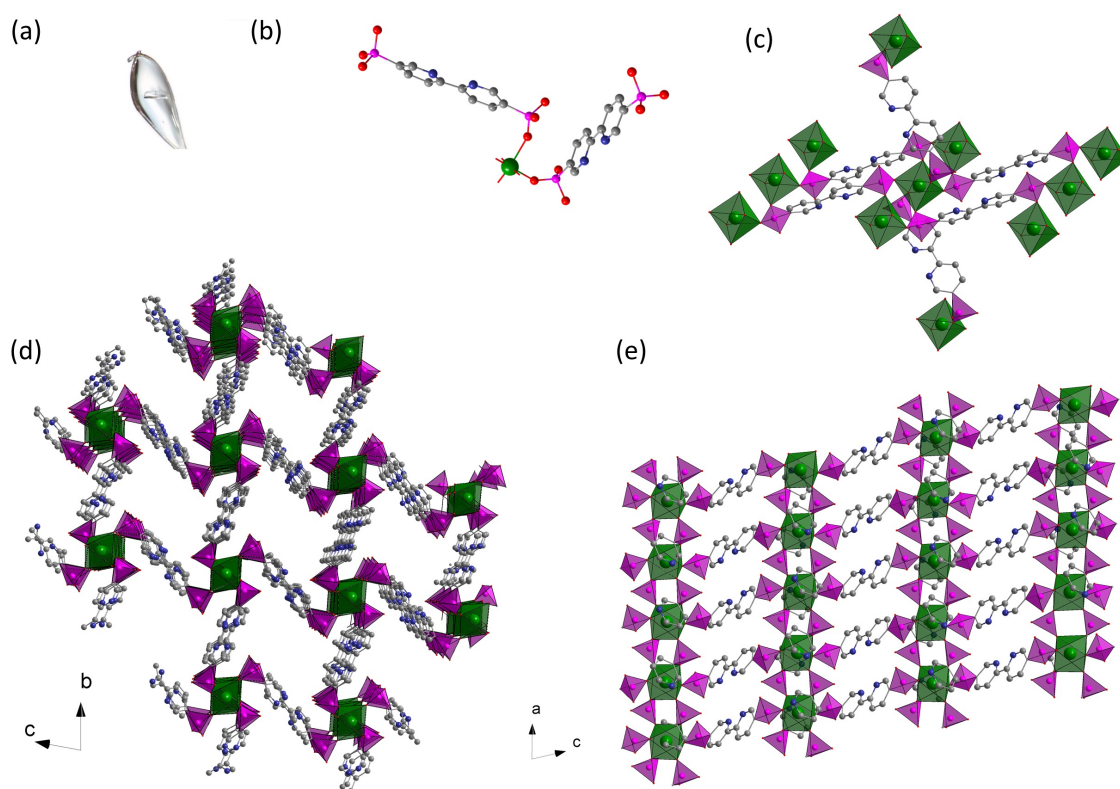


Figure 9.5.: Compound **12**. (a) Shows the single crystal of compound **12**. (b) Displays the complex cation. In (c), a cutout of the overall structure is given, showing the three-dimensional structure. (d) Shows the arrangement of the framework. The one-dimensional terbium chains within the framework are represented in (e). Hydrogen atoms, water molecules and counterions have been omitted for clarity.

This interplay of different bridging modes is the reason for the extraordinary structure of the system. It is a three-dimensional  $I^1O^2$  mixed inorganic-organic framework, in which the dysprosium ions form one dimensional  $I^1$  chains which are  $O^2$ -connected by

the ligand backbone (figure 9.5 (c) - (e)). The distance between the metal ions within the chains is 5.410 Å. The mean distance between individual chains along the b- and c-axis is 12.109 Å and 12.646 Å, respectively. The diagonal spacing is 15.713 Å and 19.137 Å.

Magnetic measurements regarding the magnetic molar susceptibility and the magnetization were conducted. They were performed under the same conditions as for compound **11**. In figure 9.4, the magnetization  $M$  in a temperature range between 2 K and 10 K with an applied field up to 70 kOe is shown.

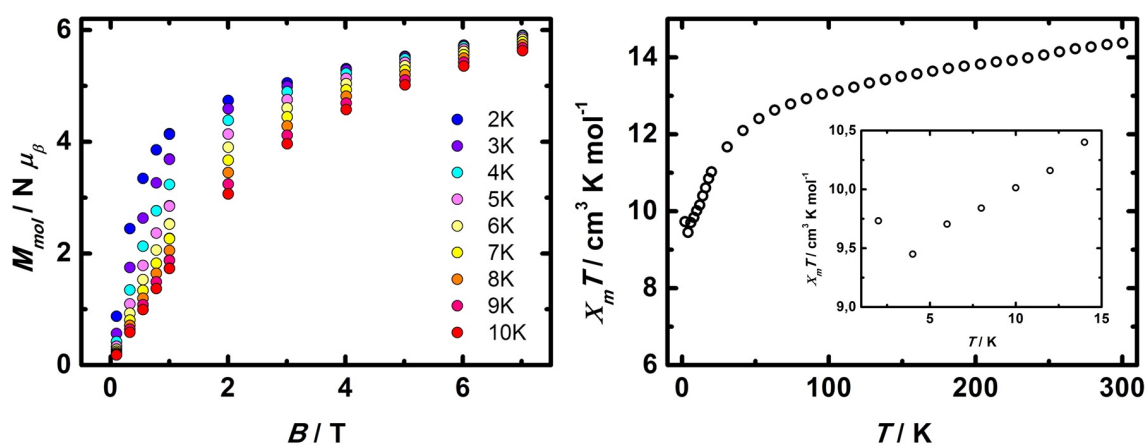


Figure 9.6.: Left: Magnetization of compound **12** in a temperature range of 2 K and 10 K with a magnetic field between 1 kOe and 70 kOe. Right:  $\chi_M T$  vs.  $T$  plot in a temperature range between 2 K and 300 K with an applied field of 1 kOe. The inlay shows a cutout of  $\chi_M T$  at very low temperatures.

At low magnetic fields, a strong increase for  $M$  is observed, which slowly reaches 5.91  $N\beta$  at 2 K and 5.63  $N\beta$  at 10 K for the highest obtained values at high magnetic fields. This is quite lower than the theoretical value one would expect for an isolated  $\text{Dy}^{+3}$  ion (10  $N\beta$ ). The reason is found in the magnetic anisotropy with a lower effective spin, and the splitting of the Stark level by the ligand field. At room temperature, the value of  $\chi_M T$  is with 14.38  $\text{cm}^3 \text{K mol}^{-1}$  in good agreement with the expected value for an uncoupled  $\text{Dy}^{3+}$  ion ( ${}^6H_{15/2}$ ,  $S = 5/2$ ,  $L = 5$ ,  $g = 4/3$ ). Upon cooling, the value decreases because of a progressive depopulation of the Stark level split due to the ligand field. Interestingly, at very low temperature an increase of  $\chi_M T$  can be observed. This might have an origin similar to compound **7** (see section 8.4) and can therefore



be either due to ferromagnetic coupling, dipolar coupling or a phase transition at low temperatures. Even though the complexes share little structural characteristics, the lanthanide ions have comparable distances towards one another (5.212 Å and 5.410 Å for compound **7** and **12**, respectively), and the metal ions are connected via phosphonates as well. It strikes, that the magnetic interaction in compound **12** is much weaker than in compound **7**. This is probably because of the larger distance between the lanthanide ions, which makes dipolar coupling the most likely explanation. Unfortunately, a quantification of the data is not possible due to the magnetic anisotropy and the Stark level split of the used lanthanide.

### 9.3. Other Compounds

Additional to the compounds presented so far, several complexes with different compositions have been isolated. They are summarized in this section because of the inability of reproduction, poor XRD measurement data because of unsatisfying crystal quality or their little relevance to the topic. Nevertheless, their existence emphasize the tremendous variety in compounds, which can be obtained by employing the ligand **H<sub>3</sub>H'L**. The structures are outlined in table 9.2.

Table 9.2.: List of further compounds based on the derivations of **H<sub>4</sub>L**. Crystal structures of the respective compounds can be found in appendix C.

Compound	Composition	SG	a/b/c [Å]	$\alpha/\beta/\gamma$ [°]
<b>13</b>	[Fe(II)(( <b>EtO</b> ) <sub>4</sub> <b>L</b> ) <sub>3</sub> ](BF <sub>4</sub> ) <sub>2</sub>	$R\bar{3}$	17.038 17.038 45.535	90 90 120
<b>14</b>	[LaCo(III)( <b>H<sub>2</sub>L</b> ) <sub>3</sub> (H <sub>2</sub> O) <sub>3</sub> NaCl	<i>C</i> 2	21.568 16.086 15.256	90 107.0 90
<b>15</b>	[GdCo(III)( <b>H<sub>2</sub>L</b> ) <sub>3</sub> (H <sub>2</sub> O) <sub>5</sub> NaCl	<i>C</i> 2/ <i>c</i>	28.198 16.665 26.903	90 121.5 90
<b>16</b> <sup>[a]</sup>	[GdCo(III)( <b>H<sub>2</sub>L</b> ) <sub>3</sub> ] <sub>2</sub>	<i>P</i> 2 <sub>1</sub>	15.30 16.79 22.50	90 106.2 90

[a]: Due to poor quality of diffraction data, a determination of solvent molecules was not possible.

### 9.3.1. Compound 13

The studies with iron(II) complexes in part I have shown, that the metal ion is very eager to be embedded in an octahedral coordination environment. For this reason, several crystallization approaches were conducted using the ligand  $\mathbf{H}_3\mathbf{H}'\mathbf{L}$  and iron(II) salts. Upon mixing of the aqueous solutions, an immediate color change from colorless to a very dark pink was observed. This change in color was already observed for the addition of cobalt and nickel. But especially with iron it was this intense, that even smallest amounts of iron would lead to a visible colorization of a solution. It indicated successful formation of the tris(bipyridine)-iron(II) complex, because this intense color is often found for iron(II) compounds in the *LS*-state (see section 1.1.3), which is expected upon coordination of the used ligand. Unfortunately, it was by no means possible to crystallize the system. This was probably because of the large negative charge the complex would have had with six single deprotonated phosphonate groups. According to the results of compound **7**, the nitrogen of the bipyridine are protonated before the phosphonic acids are completely protonated. This would block the coordination site. Therefore, the bis(diethylester) (figure 9.7, left) was used for crystallization. The only pH sensitive functionality of this ligand species is the bipyridine itself. The mixing of solutions of the ligand and the metal in acetonitrile also led immediately to an intense pink color. Compound **13** was isolated as hexagonal single crystals, which were obtained shortly after adding small amounts of diethyl ether to the reaction mixture. The structure was solved in the space group  $R\bar{3}$  and shows hence a  $c_3$ -symmetry. As expected, the iron center is coordinated in an octahedral geometry by three ligand molecules. The charge is balanced by two tetrafluoroborate ions. Even though three counterions are visible in figure 9.7, their occupational factor is only 2/3. The bond length of 1.960 Å and 1.971 Å indicate, that the metal center is indeed in the *LS*-state. The abrupt change of color and the fast crystallization process confirms the assumption, that the lack of crystallization with  $\mathbf{H}_3\mathbf{H}'\mathbf{L}$  is due to the high charge of the resulting complex. It also confirms, that the change in color upon mixing the ligand with the metal is indeed the result of an immediate complexation.

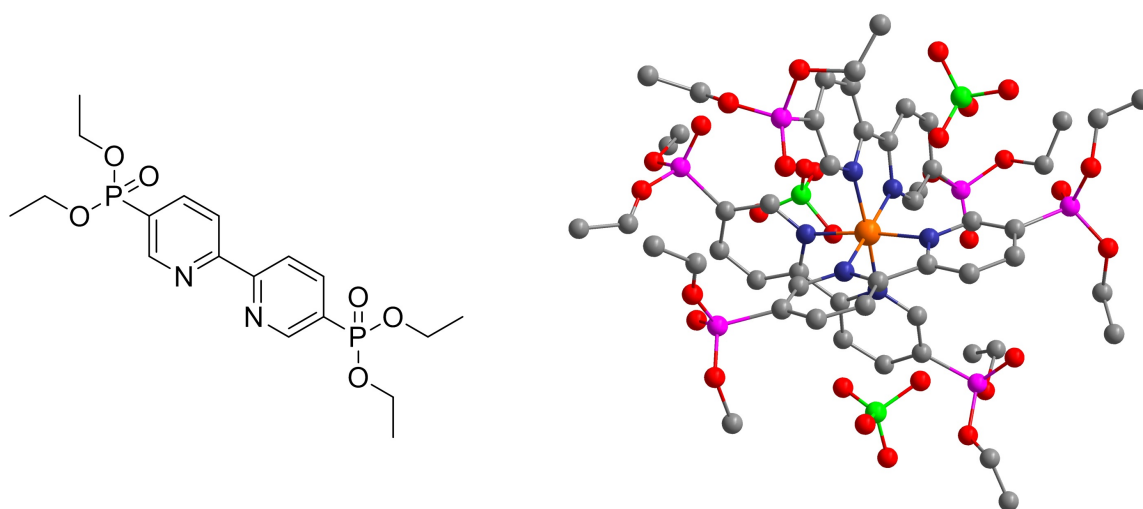


Figure 9.7.: Left: bis(diethylester) compound used for the reaction. Right: molecular structure of compound **13** with  $\text{BF}_4$  counterions.

### 9.3.2. Compounds **14**, **15** and **16**

Compound **14** is in composition and structural aspects very similar to compound **9**. The main differences are found in the metal ions and their oxidation states. Instead of a paramagnetic gadolinium, a diamagnetic lanthanum ion is coordinated by the phosphonate groups. Furthermore, cobalt(II) acetate was used instead of nickel(II) chloride, which was oxidized during the reaction as expected due to the results of compounds **8a** - **8c**. This led to a compound isostructural to **9**. Since compound **14** is diamagnetic, the magnetic properties were not investigated.

Compounds **15** and **16** are essentially of the same composition as compounds **8a** - **8b**, **9** and **14**, but differ in their space group, their lattice parameters and their connectivity. A closer look at the crystal structures reveals, that the number of phosphonate metal contacts in compound **15** is reduced to three and every ligand binds with only one phosphonate group to the lanthanide ion. The remaining coordination sites of the square antiprismatic geometry are occupied by five crystal water molecules. The main difference of compound **16** is the presence of two crystallographic different gadolinium ions. They exhibit both coordinative environments of the lanthanides in compounds **7** and **8a-9**: one of the gadolinium atom is in a square antiprismatic geometry built

by four phosphonate metal contacts and four crystal water molecules, while the second lanthanide ion is in a capped trigonal prismatic coordination environment with only three crystal water molecules. Unfortunately the diffraction data was of poor quality, which made a reliable characterization impossible.

## 10. Summary and Perspective

In conclusion, several homo- and heterometallic more-dimensional extended networks were prepared by using a phosphonate based multi-functional ligand. The obtained complexes were of large structural variety. Magnetic measurements confirmed a structure dependent oxidation of the transition metal ions as well as a weak magnetic interactions in some cases caused most probably by dipolar magnetic coupling.

This part of the work at hand was aiming towards the synthesis of heterometallic compounds, which form extended more-dimensional networks. In order to achieve this goal, a multi-functional ligand was employed, which contained two phosphonate groups as central motive. An aromatic 2,2'-bipyridine unit was chosen as the ligands backbone, which was substituted with two phosphonate acid groups in the 5 and 5' position. This backbone provided several advantages: first of all, it represents a different functionality. The bipyridine coordination site is an excellent group for the coordination of a large number of transition metal ions, including iron(II)-, cobalt(II)- and cobalt(III)- or nickel(II)-ions, which are of special interest regarding their magnetic properties. Second, the aromatic system would be able to mediate any occurring long range magnetic interactions. And finally, there are several promising reports of the homocyclic biphenyl analog, which was deployed successfully in various complex synthesis. The ligand offers in total three, but actually two chemically different coordination sites. Bipyridine is extremely suitable for the coordination of 3d transition metal ions, while the phosphonate groups can coordinate metal ions all across the periodic table, depending on the applied reaction conditions. This diverse coordination behavior made the formation of heterometallic compounds very likely.

In order to prepare extended networks with this ligand, several metal salts containing 3d transition and 4f rare earth elements were used. Mixing aqueous solutions of the respective reagents yielded the novel compounds **6a** - **16**. The dimensionality of the complexes ranged from zero- to three-dimensional. Next to the desired heterometallic structures, which contained various combinations of cobalt(III)-, nickel(II)-,

gadolinium(III)-, dysprosium(III)- and terbium(III)-ions, homometallic compounds were obtained as well. In section 6.6.1 it has been stated, that phosphonate metal bonds generally form by using hydrothermal reaction. We were able to avoid these conditions, which are often afflicted by an uncertainty of the reactions outcome. Instead, we crystallized the products by vapor diffusion, mixing of solvents, slow removal of solvent or the use of elevated temperatures.

We found, that there are several factors which have a large influence on the resulting structure. As expected (see section 6.6), the pH value turned out to take a crucial part in the course of synthesis. By protonating and deprotonating the various functionalities, the compounds could not only be precipitated and re-solved, but also their structures were fine tunable up to a certain degree. Furthermore, the sequence, in which the metal ions were added, had an influence as well: investigations with the esterified ligand and iron(II) revealed, that they reacted immediately to the respective tris(bipyridyl) metal complex, which was reflected by the change of color. A prior coordination of a lanthanide would interfere with the formation of the transition metal complex.

Two sets of heterometallic and more-dimensional structures were obtained. The two-dimensional and isostructural compounds **8a** - **8c** incorporate three ligand molecules and, in respect to the compound, a gadolinium, a dysprosium or a terbium ion. They comprise a cobalt(III) ion as well, even though a cobalt(II) salt was used for the reaction. The asymmetric unit of compound **9** consists of three ligand molecules, a gadolinium ion and a nickel(II) ion. It is almost isostructural, but exhibits one less phosphonate lanthanide connection. This resulted surprisingly in the formation of a three-dimensional structure. Magnetic measurements confirmed the oxidation states of +3 for cobalt and +2 for nickel. The oxidation of the Co ion during the reaction is facilitated by structural aspects: a cobalt(II) would have been forced into a strongly distorted octahedral coordination geometry due to the degeneracy that accompanies the electronic configuration  $e_g^1 t_{2g}^6$ . The rigidity of the complex precluded a Jahn-Teller distortion, which led to the oxidation of the transition metal. Compound **10** and the nickel(II) complex, with an electronic configuration of  $e_g^2 t_{2g}^6$ , were as expected not oxidized.

For the homometallic two-dimensional lanthanide compounds, an unexpected structural variety was observed. Despite the application of similar reaction conditions, three compounds of different composition crystallized in three different structures. The two-dimensional compounds **7** and **11**, which include gadolinium and terbium, respectively, are rather alike. Besides their different composition, they differ slightly in their connectivity. Nevertheless, in both structures, the eightfold coordinated lanthanide ions form one-dimensional metal-chains, which are connected via the organic backbone. In compound **12**, the dysprosium ions built one-dimensional chains as well, but in contrast they were connected in two dimensions, giving a three-dimensional structure. Furthermore, the metal ions showed a rather unexpected octahedral coordination geometry. Measurements of the magnetic molar susceptibility revealed an increasing value of  $\chi_M T$  at low temperatures for compounds **7** and **12**. They could be caused by weak ferromagnetic coupling, a phase transition or dipolar coupling. Comparing the distances between the lanthanide ions and taking into account, that this behavior was not observed for **11**, magnetic dipole-dipole interactions seem to be the most likely explanation.

The large structural differences in the presented compounds, which are all based on the same ligand system, originates from the many coordination modes of which the employed phosphonate groups are capable. Even though the formation of several reaction products could be expected, the enormous variety in the structures was surprising. The number of different complexes with nearly the same composition, and the large range of metal ions, which are readily coordinated, emphasize the potential of the chosen ligand system. A disadvantage are the similar reaction conditions, which lead to the different compounds. This can, in some cases, interfere with the synthesis of a specific compound and hence its reproduction. It stresses the subtle equilibrium of the employed materials, the ratios they are deployed with, the applied pH value and the used crystallization method the expected product is subject to. However, this interplay of reaction conditions has led to many unexpected structures with new and fascinating properties.

Future work with this ligand should focus on the targeted preparation of the reported compounds. A first step to do so would be the crystallographic analysis of the precipitates, which form in the course of synthesis, by e.g. powder X-ray diffraction. The identification of products would allow the conduction of measurements using powder samples. This is preferable for two reasons: first, the recrystallization process is in most cases very time consuming and reduces yields drastically. And second, dissolving the obtained solids involved so far the use of acids, which most likely influenced the structural characteristics of the product. If single crystals are needed, it would facilitate the improvement of recrystallization methods, if a precipitate is known to be the targeting material. Various techniques to re-solve a product without employing acidic compounds could be investigated.

Subsequently, new combinations of different metal ions should be tested. A promising route would be the formation of a 3d transition metal tris(bi-pyridine-diphosphonic acid) complex, which is then used as a precursor. Using hydrothermal reaction, it should be possible to coordinate a second transition metal with the phosphonate groups. Furthermore, the one-dimensional chain of compound **10** might be a good starting material for the preparation of heterometallic complexes. The non-coordinating phosphonate groups, which limit the chain in one direction, could be used for the incorporation of lanthanide ions. Alternatively, unsubstituted 2,2'-bipyridine could be employed as co-ligand in order to prepare  $[M^{x+}(\text{Bipy})_2]\text{Cl}_x$  precursors, with M being any transition metal. In a second step, the chloride ions can be replaced by the ligand **H<sub>2</sub>L**. This way, the dimensionality of the obtained heterometallic compounds might be controlled.

And finally, variations of the presented ligand system should be investigated. The attachment of only one phosphonate group at the bipyridine would therefore be an ideal starting point. The smaller number of pH sensitive groups and coordination sites would allow more control regarding the structural outcome. It could also enable the use of solvents other than water. Again, in part I the impact of solvents has already been discussed in light of the magnetic properties of certain compounds. In this context, a change in solvent might aid the crystallization process.



## 11. Experimental Section

### 11.1. Methods and Materials

#### Materials

All chemicals were purchased from Fisher Chemicals, Sigma-Aldrich, Alfa Aesar, Acros Organics, Deutero, and TCI Chemicals and used without further purification. The solvents for the complex syntheses were degassed with argon.

#### NMR-Spectroscopy

The NMR spectra were recorded at room temperature using a Bruker DRX 400 spectrometer ( $\nu(^1\text{H}) = 400.13$  MHz,  $\nu(^{13}\text{C}) = 100.61$  MHz). The data was processed and analyzed with the programs Bruker TopSpin 1.3 and MestReNova.<sup>[152]</sup>

#### X-ray Crystallography

Single-crystal X-ray diffraction data were collected with a Bruker SMART APEX II CCD and a STOE IPDS 2T diffractometer at the Johannes Gutenberg-University Mainz at 100 K, 173 K and 193 K. The structures were solved with SHELXT and refined with SHELXL and the program Olex2.<sup>[153]</sup>

#### Magnetic Measurements

Magnetic susceptibility data were collected with a Quantum Design SQUID magnetometer MPMSXL (at the Johannes Gutenberg University Mainz). The molar susceptibility was calculated with the program julX 1.4.1 of Eckhard Bill (MPI Mülheim/Ruhr).

The simulation of the magnetic data has been performed with PHI.<sup>[154]</sup> The used Hamiltonian in the program PHI

$$\hat{H} = \hat{H}_{SO} + \hat{H}_{EX} + \hat{H}_{CF} + \hat{H}_{ZEE}$$

contains the spin-orbit coupling Hamiltonian ( $\hat{H}_{SO}$ ), exchange interaction Hamiltonian ( $\hat{H}_{EX}$ ), Crystal Field Hamiltonian ( $\hat{H}_{CF}$ ) and Zeeman Hamiltonian ( $\hat{H}_{ZEE}$ ). It was possible to solely consider the exchange interaction Hamiltonian ( $\hat{H}_{EX}$ ) and Crystal Field Hamiltonian ( $\hat{H}_{CF}$ ) for the treated systems.

$$\hat{H}_{EX} = -2 \sum_{\substack{i,j \in N \\ i < j}} J_{ij} \vec{S}_i \cdot \vec{S}_j \quad \hat{H}_{CF} = \sum_{i=1}^N \sum_{k=2,4,6} \sum_{q=-k}^k B_{k_i}^q \theta_k \hat{O}_{k_i}^q$$

In some cases a temperature independent paramagnetism (TIP) had to be included in the simulation.

### Mössbauer Spectroscopy

<sup>57</sup>Fe Mössbauer spectra were recorded at 85 K and 293 K on a self-made Mössbauer spectrometer with a CryoVac He-Bath-Cryostat. The data was recorded and analyzed by fitting to Lorentzian lines by Sergii I. Shylin and Dr. Vadim Ksenofontov at the Johannes Gutenberg University Mainz.

### Elemental Analysis

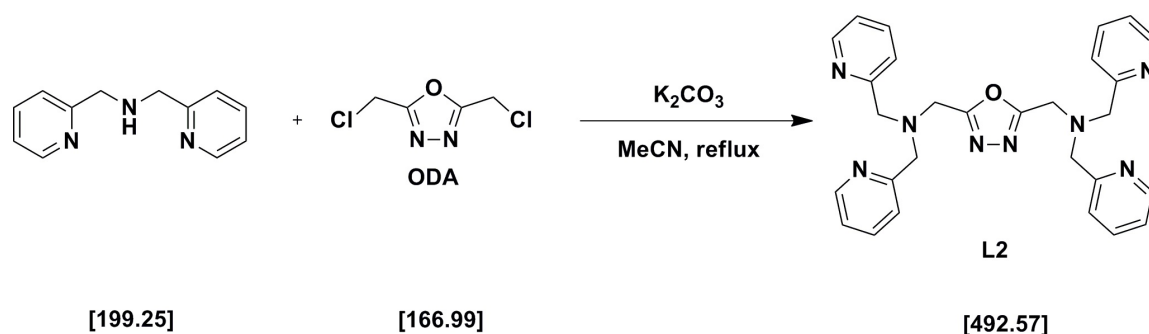
Elemental analyses (C, H, N and S) were measured at the micro-analytical laboratory of the Johannes Gutenberg University Mainz with a Foss Heraeus Vario EL elemental analyzer.

## 11.2. Syntheses

### 11.2.1. Ligands

#### Synthesis of L2

The synthesis of bis(2-pyridylmethyl)amine was carried out according to the literature.<sup>[78]</sup>



Bis(2-pyridylmethyl)amine (4.384 g, 22 mmol) was dissolved in 500 mL acetonitrile. After suspending potassium carbonate (6.910 g, 50 mmol), a solution of 2,5-bis(chloromethyl)-1,3,4-oxadiazole (1.670 g, 10 mmol) in 100 mL acetonitrile was added. The reaction mixture was heated under reflux for 24 h. After cooling to room temperature, the solid was filtered. The solution was concentrated to a volume of 30 mL and stored in the refrigerator overnight. The precipitate was filtered and washed with a small amount of cool acetonitrile. The solid was dissolved in water and extracted with DCM. Finally, the organic phase was dried with magnesium sulfate and the solvent removed to dryness under reduced pressure, giving the pure ligand as a dark red oil.

**Yield:** 5.453 g (11.07 mmol, 50.3 %)

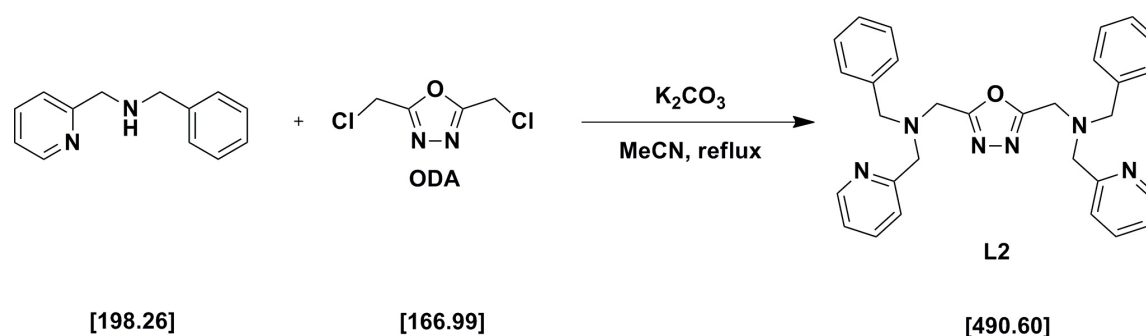
<sup>1</sup>H NMR (400 MHz, CDCl<sub>3</sub>, 25° C): δ = 8.50 (ddd; *J* = 4.9 Hz, 1.7 Hz, 0.9 Hz; 2H; *H*<sub>6</sub>-Py), 7.61 (td; *J* = 7.6 Hz, 1.8 Hz; 2H; *H*<sub>4</sub>-Py), 7.50 (d; *J* = 7.8 Hz; 2H; *H*<sub>3</sub>-Py), 7.12 (ddd; *J* = 7.4 Hz, 4.9 Hz, 1.1 Hz; 2H; *H*<sub>5</sub>-Py), 3.99 (s; 4H; CH<sub>2</sub>-ODA), 3.94 (s; 8H, N-CH<sub>2</sub>-Py).

<sup>13</sup>C NMR (100 MHz, CDCl<sub>3</sub>, 25° C): δ = 164.59 (s; N-C-O), 158.22 (s; C2-Py), 149.21

(s; C6-Py), 136.64 (s; C4-Py), 123.24 (s; C3-Py), 122.31 (s; C5-Py), 59.80 (s; N-CH<sub>2</sub>-Py), 47.71 (s; N-CH<sub>2</sub>-ODA).

### Synthesis of L3

The synthesis of (N-benzyl-N'-pyridin-2-ylmethyl)amine was carried out according to the literature.<sup>[79]</sup>



N-benzyl-N-pyridin-2-ylmethylamine (1.09 g, 5.5 mmol) was dissolved in 125 mL acetonitrile. After suspending potassium carbonate (1.73 g, 12.5 mmol), a solution of 2,5-bis(chloromethyl)-1,3,4-oxadiazole (0.417 g, 2.5 mmol) in 25 mL acetonitrile was added. The reaction mixture was heated under reflux for 4 h. After cooling to room temperature, the solid was filtered. The solvent was removed under reduced pressure, the remaining solid dissolved in dichloromethane. After extraction with water, the organic phase was dried with sodium sulfate and the solvent distilled. The crude product was purified via column chromatography (silica, chloroform), giving the pure product as an orange liquid oil.

**Yield:** 0.634 g (1.29 mmol, 51.6 %)

<sup>1</sup>H NMR (400 MHz, CDCl<sub>3</sub>, 25° C): δ = 8.54 (d; *J* = 4.2 Hz; 2H; H<sub>6</sub>-Py), 7.68 (td; *J* = 7.7 Hz, 1.6 Hz; 2H; H<sub>5</sub>-Py), 7.58 (d; *J* = 7.8 Hz; 2H; H<sub>3</sub>-Py), 7.41 (d; *J* = 7.1 Hz; 4H; H<sub>2</sub>-Ph), 7.31 (t; *J* = 7.3 Hz; 4H; H<sub>3</sub>-Ph), 7.28 - 7.24 (m; 4H; H<sub>3</sub>-Ph), 7.18 (dd; *J* = 6.5 Hz, 5.6 Hz; 2H; H<sub>4</sub>-Py), 3.95 (s; 4H, ODA-CH<sub>2</sub>), 3.94 (s; 4H, Py-CH<sub>2</sub>), 3.78 (s; 4H,

Ph-CH<sub>2</sub>).

<sup>13</sup>C NMR (100 MHz, CDCl<sub>3</sub>, 25° C): δ = 164.74 (s; N-C-O), 158.72 (s; C2-Py), 148.98 (s; C6-Py), 137.99 (s; C1-Ph), 137.05 (s; C5-Ph), 129.13 (s; C2-Ph), 129.13 (s; C3-Ph), 127.57 (s; C4-Ph), 123.27 (s; C3-Py), 122.48 (s; C4-Py), 59.78 (s; N-CH<sub>2</sub>-Py), 58.20 (s; N-CH<sub>2</sub>-Ph), 47.42 (s; N-CH<sub>2</sub>-ODA).

## 11.2.2. Complexes

### 11.2.2.1. Synthesis of [Co<sub>2</sub>(μ<sub>2</sub>-L)<sub>2</sub>](ClO<sub>4</sub>)<sub>4</sub>·4MeCN (4)

A solution of **L** (0.10 mmol, 31 mg) in acetonitrile (4 mL) was added to a solution of Co(ClO<sub>4</sub>)<sub>2</sub>·6H<sub>2</sub>O (0.10 mmol, 37 mg) in acetonitrile (3 mL). An immediate color change from pale pink to orange was observed. After a few hours single crystals suitable for single crystal X-ray diffraction could be obtained. Yield: 42 mg (0.032 mmol, 32 %).

### 11.2.2.2. Synthesis of [NaL2]BPh<sub>4</sub> (5)

A solution of NaBPh<sub>4</sub> (0.50 mmol, 171.1 mg) in methanol (2 mL) was added to a solution of FeSO<sub>4</sub>·7H<sub>2</sub>O (0.20 mmol, 55.6 mg) in methanol (2 mL). Immediately, a precipitation of Na<sub>2</sub>SO<sub>4</sub> formed. After filtering the solid, a solution of **L2** (0.20 mmol, 98.5 mg) in methanol (2 mL) was added. An immediate color change from orange to green was observed. After several days of vapor diffusion with diethyl ether, single crystals suitable for single crystal X-ray diffraction could be obtained.

### 11.2.2.3. Synthesis of [Co(II)(μ<sub>2</sub>-η<sub>2</sub>-H<sub>3</sub>L)<sub>2</sub>]\*6H<sub>2</sub>O (10)

For the preparation of compound **10**, 0.3 mmol **H<sub>3</sub>H'L** (94.8 mg) were dissolved in 4 mL H<sub>2</sub>O and 20 μL of concentrated ammonia were added. After filtration, 0.1 mmol Co(Ac)<sub>2</sub>·4H<sub>2</sub>O (24.9 mg) dissolved in 2 mL H<sub>2</sub>O were added. The addition of 12 mL acetonitrile resulted in an immediate precipitation of a solid of pale orange color. The solid

was resolved in 4 mL H<sub>2</sub>O and a few drops of hydrochloric acid. After several days of vapor diffusion with diethyl ether, single crystals suitable for single crystal X-ray diffraction could be obtained. After several days of vapor diffusion with acetonitrile, single crystals suitable for single crystal X-ray diffraction could be obtained.

#### 11.2.2.4. Synthesis of [Tb( $\mu_4$ -H<sub>2</sub>H<sup>M</sup>)(H<sub>2</sub>O)<sub>4</sub>]Cl<sub>2</sub>·H<sub>2</sub>O (11)

Compound **11** was prepared by adding solution of 0.1 mmol Tb(NO<sub>3</sub>)<sub>3</sub>·H<sub>2</sub>O (36.3 mg) in 3 mL H<sub>2</sub>O to a mixture of 0.15 mmol H<sub>3</sub>H<sup>M</sup>L (47.42 mg) in 3 mL H<sub>2</sub>O. Immediately, a white solid precipitated. The precipitate was separated from the solution by centrifugation. After the emulsification in 4 mL water, concentrated HCl (0.5 mL) was added to dissolve the solid, giving a clear solution. Acetonitrile (2 mL) was added and the vial was left to stand for six days, giving colorless crystals suitable for single crystal XRD.

#### 11.2.2.5. Synthesis of [Dy(H<sub>2</sub>H<sup>M</sup>)<sub>2</sub>]ClHCl·4H<sub>2</sub>O (12)

Compound **12** was prepared by adding solution of 0.1 mmol Dy(NO<sub>3</sub>)<sub>3</sub>·H<sub>2</sub>O (36.7 mg) in 3 mL H<sub>2</sub>O to a mixture of 0.15 mmol H<sub>3</sub>H<sup>M</sup>L (47.42 mg) in 3 mL H<sub>2</sub>O. Immediately, a white solid precipitated. The precipitate was separated from the solution by centrifugation. After the emulsification in 4 mL water, concentrated HCl (0.5 mL) was added to dissolve the solid, giving a clear solution. Acetonitrile (2 mL) was added and the vial was left to stand for six days, giving colorless crystals suitable for single crystal XRD.

#### 11.2.2.6. Synthesis of [Fe(II)((EtO)<sub>4</sub>L)<sub>3</sub>](BF<sub>4</sub>)<sub>2</sub> (13)

Compound **13** was prepared by adding solution of 0.1 mmol Fe(ClO<sub>4</sub>)<sub>2</sub>·H<sub>2</sub>O (27.3 mg) in 3 mL acetonitrile to a mixture of 0.3 mmol (EtO)<sub>4</sub>L (128.5 mg) in 6 mL acetonitrile. Immediately, a change of color from colorless to a deep, intensive pink was observed. Upon the addition of 3 mL diethyl ether, dark hexagonal crystals formed, suitable for single crystal XRD.

**11.2.2.7. Synthesis of [LaCo(III)(H<sub>2</sub>L)<sub>3</sub>(H<sub>2</sub>O)<sub>3</sub>]NaCl (14)**

For the preparation of compound **15**, 0.15 mmol H<sub>3</sub>H'L (47.4 mg) were dissolved in 2 mL H<sub>2</sub>O and 20 μL of concentrated ammonia were added. The addition of 0.1 mmol La(NO<sub>3</sub>)<sub>3</sub>·6H<sub>2</sub>O (43.3 mg) dissolved in 2 mL H<sub>2</sub>O resulted in an immediate precipitation of a white solid. After filtration, the solid was dissolved upon adding 0.5 mL concentrated HCl. 0.15 mmol Co(Ac)<sub>2</sub>·4H<sub>2</sub>O (37.4 mg) dissolved in 2 mL H<sub>2</sub>O were added and the color of the solution changed to a pale orange. 20 mL of acetonitrile were added, and a precipitate formed, which was filtered, emulsified with 4 mL H<sub>2</sub>O and dissolved by the addition of 0.25 mL concentrated HCl. After adding 1 mL of acetonitrile, the viol was left to stand at room temperature. Single crystals of yellow color suitable for single crystal XRD were obtained after 5 days.

**11.2.2.8. Synthesis of [GdCo(III)(H<sub>2</sub>L)<sub>3</sub>(H<sub>2</sub>O)<sub>5</sub>]NaCl (15)**

For the preparation of compound **15**, 0.15 mmol H<sub>3</sub>H'L (47.4 mg) were dissolved in 2 mL H<sub>2</sub>O and 20 μL of concentrated ammonia were added. The addition of 0.1 mmol Gd(NO<sub>3</sub>)<sub>3</sub>·6H<sub>2</sub>O (45.1 mg) dissolved in 2 mL H<sub>2</sub>O resulted in an immediate precipitation of a white solid. After filtration, the solid was dissolved upon adding 0.5 mL concentrated HCl. 0.15 mmol Co(Ac)<sub>2</sub>·4H<sub>2</sub>O (37.4 mg) dissolved in 2 mL H<sub>2</sub>O were added and the color of the solution changed to a pale orange. 20 mL of acetonitrile were added, and a precipitate formed, which was filtered, emulsified with 4 mL H<sub>2</sub>O and dissolved by the addition of 0.25 mL concentrated HCl. After adding 1 mL of acetonitrile, the viol was left to stand at room temperature. Single crystals of yellow color suitable for single crystal XRD were obtained after several days.

**11.2.2.9. Synthesis of [GdCo(III)(H<sub>2</sub>L)<sub>3</sub>]<sub>2</sub> (16)**

For the preparation of compound **15**, 0.15 mmol H<sub>3</sub>H'L (47.4 mg) were dissolved in 2 mL H<sub>2</sub>O and 20 μL of concentrated ammonia were added. The addition of 0.1 mmol Gd(NO<sub>3</sub>)<sub>3</sub>·6H<sub>2</sub>O (45.1 mg) dissolved in 2 mL H<sub>2</sub>O resulted in an immediate precipitation

of a white solid. After filtration, the solid was dissolved upon adding 0.5 mL concentrated HCl. 0.15 mmol  $\text{Co}(\text{Ac})_2 \cdot 4\text{H}_2\text{O}$  (37.4 mg) dissolved in 2 mL  $\text{H}_2\text{O}$  were added and the color of the solution changed to a pale orange. 20 mL of acetonitrile were added, and a precipitate formed, which was filtered, emulsified with 4 mL  $\text{H}_2\text{O}$  and dissolved by the addition of 0.25 mL concentrated HCl. After adding 1 mL of acetonitrile, the viol was left to stand at room temperature. Single crystals of yellow color suitable for single crystal XRD were obtained after several days.



## 12. Bibliography

- [1] L. Cambi, L. Szegö, *Ber. Dtsch. Chem. Ges.* **1931**, *64*, 2591–2598.
- [2] G. Vos, R. A. G. De Graaff, J. G. Haasnoot, A. M. Van der Kraan, P. De Vaal, J. Reedijk, *Inorg. Chem.* **1984**, *23*, 2905–2910.
- [3] P. Gütllich, A. Hauser, H. Spiering, *Angew. Chem. Int. Ed.* **1994**, *33*, 2024–2054.
- [4] P. Gütllich, Y. Garcia, H. A. Goodwin, *Chem. Soc. Rev.* **2000**, *29*, 419–427.
- [5] P. Gütllich, A. B. Gaspar, Y. Garcia, *Beilstein Journal of Organic Chemistry* **2013**, *9*, 342–391.
- [6] H. Bethe, *Ann. Phys.* **1929**, *395*, 133–208.
- [7] B. Neumüller, *Angewandte Chemie* **1990**, *102*, 1411–1412.
- [8] C. K. Jørgensen in *Absorption Spectra and Chemical Bonding in Complexes*, Pergamon, **1962**, S. 107–133.
- [9] C. E. Housecroft, A. G. Sharpe, *Inorganic chemistry*, Pearson Prentice Hall, Upper Saddle River, N.J, 2nd ed, **2005**, 949 S.
- [10] W. Kläui, *Inorg. Chim. Acta* **1980**, *40*, X22–X23.
- [11] W. Kläui, W. Eberspach, P. Guetlich, *Inorg. Chem.* **1987**, *26*, 3977–3982.
- [12] M. Graf, G. Wolmershäuser, H. Kelm, S. Demeschko, F. Meyer, H.-J. Krüger, *Angew. Chem. Int. Ed.* **2010**, *49*, 950–953.
- [13] M. G. Cowan, J. Olguín, S. Narayanaswamy, J. L. Tallon, S. Brooker, *J. Am. Chem. Soc.* **2012**, *134*, 2892–2894.
- [14] A. Hauser in *Spin Crossover in Transition Metal Compounds II*, Topics in Current Chemistry 234, Springer Berlin Heidelberg, **2004**, S. 155–198.
- [15] P. Gütllich, H. A. Goodwin in *Spin Crossover in Transition Metal Compounds I*, (Hrsg.: P. Gütllich, H. A. Goodwin), Topics in Current Chemistry 233, Springer Berlin Heidelberg, **2004**, S. 1–47.
- [16] M. Sorai, S. Seki, *J. Phys. Chem. Solids* **1974**, *35*, 555–570.

- [17] M. Sorai, S. Seki, *J. Phys. Soc. Jpn.* **1972**, *33*, 575–575.
- [18] A. G. Orpen, L. Brammer, F. H. Allen, O. Kennard, D. G. Watson, R. Taylor, *J. Chem. Soc. Dalton Trans.* **1989**, S1–S83.
- [19] A. Hauser in *Spin Crossover in Transition Metal Compounds I*, (Hrsg.: P. Gütlich, H. A. Goodwin), Topics in Current Chemistry 233, Springer Berlin Heidelberg, **2004**, S. 49–58.
- [20] S. Decurtins, P. Gütlich, K. M. Hasselbach, A. Hauser, H. Spiering, *Inorg. Chem.* **1985**, *24*, 2174–2178.
- [21] A. Hauser, *J. Chem. Phys.* **1991**, *94*, 2741–2748.
- [22] A. Hauser, J. Adler, P. Gütlich, *Chem. Phys. Lett.* **1988**, *152*, 468–472.
- [23] C. N. R. Rao, *Int. Rev. Phys. Chem.* **1985**, *4*, 19–38.
- [24] G. A. Craig, J. S. Costa, O. Roubeau, S. J. Teat, H. J. Shepherd, M. Lopes, G. Molnár, A. Bousseksou, G. Aromí, *Dalton Trans.* **2013**, *43*, 729–737.
- [25] Kershaw?Cook, H. J. Shepherd, T. P. Comyn, C. Baldé, O. Cespedes, G. Chastanet, M. A. Halcrow, *Chem. Eur. J.* **2015**, *21*, 4805–4816.
- [26] Y. Hasegawa, R. Sakamoto, K. Takahashi, H. Nishihara, *Inorg. Chem.* **2013**, *52*, 1658–1665.
- [27] T. Tayagaki, A. Galet, G. Molnár, M. C. Muñoz, A. Zwick, K. Tanaka, J.-A. Real, A. Bousseksou, *J. Phys. Chem. B* **2005**, *109*, 14859–14867.
- [28] J. Klingele, D. Kaase, M. H. Klingele, J. Lach, *Dalton Trans.* **2012**, *41*, 1397–1406.
- [29] J. Klingele, D. Kaase, M. Schmucker, Y. Lan, G. Chastanet, J.-F. Létard, *Inorg. Chem.* **2013**, *52*, 6000–6010.
- [30] J. A. Kitchen, N. G. White, G. N. L. Jameson, J. L. Tallon, S. Brooker, *Inorg. Chem.* **2011**, *50*, 4586–4597.
- [31] M. P. Shores, C. M. Klug, S. R. Fiedler in *Spin-Crossover Materials*, (Hrsg.: L. a. Halcrow), John Wiley & Sons Ltd, **2013**, S. 281–301.
- [32] R. Kulmaczewski, J. Olguín, J. A. Kitchen, H. L. C. Feltham, G. N. L. Jameson, J. L. Tallon, S. Brooker, *J. Am. Chem. Soc.* **2014**, *136*, 878–881.

- [33] S. Brooker, *Chem. Soc. Rev.* **2015**, *44*, 2880–2892.
- [34] G. S. Matouzenko, J.-F. Létard, S. Lecocq, A. Bousseksou, L. Capes, L. Salmon, M. Perrin, O. Kahn, A. Collet, *Eur. J. Inorg. Chem.* **2001**, *2001*, 2935–2945.
- [35] J. A. Real, H. Bolvin, A. Bousseksou, A. Dworkin, O. Kahn, F. Varret, J. Zarembowitch, *J. Am. Chem. Soc.* **1992**, *114*, 4650–4658.
- [36] G. Ritter, E. Koenig, W. Irlner, H. A. Goodwin, *Inorg. Chem.* **1978**, *17*, 224–228.
- [37] M. G. B. Drew, C. J. Harding, V. McKee, G. G. Morgan, J. Nelson, *J. Chem. Soc. Chem. Commun.* **1995**, 1035–1038.
- [38] P. Gütlich, *Eur. J. Inorg. Chem.* **2013**, *2013*, 581–591.
- [39] J. F. Létard, *J. Mater. Chem.* **2006**, *16*, 2550–2559.
- [40] P. Gütlich, H. A. Goodwin in *Spin Crossover in Transition Metal Compounds I*, (Hrsg.: P. Gütlich, H. A. Goodwin), Topics in Current Chemistry 233, Springer Berlin Heidelberg, **2004**, S. 1–47.
- [41] A. B. Gaspar, G. Levchenko, S. Terekhov, G. Bukin, J. Valverde-Muñoz, F. J. Muñoz-Lara, M. Seredyuk, J. A. Real, *Eur. J. Inorg. Chem.* **2014**, *2014*, 429–433.
- [42] J.-F. Létard, G. Chastanet, O. Nguyen, S. Marcén, M. Marchivie, P. Guionneau, D. Chasseau, P. Gütlich, *Monatsh. Chem.* **2003**, *134*, 165–182.
- [43] E. König in *Complex Chemistry, Structure and Bonding* 76, Springer Berlin Heidelberg, **1991**, S. 51–152.
- [44] I. Gudyma, A. Maksymov, C. Enachescu, *Phys. Rev. B* **2014**, *89*, 224412.
- [45] M. H. Klingele, B. Moubaraki, J. D. Cashion, K. S. Murray, S. Brooker, *Chem. Commun.* **2005**, 987–989.
- [46] V. Ksenofontov, H. Spiering, S. Reiman, Y. Garcia, A. Gaspar, N. Moliner, J. Real, P. Gütlich, *Chem. Phys. Lett.* **2001**, *348*, 381–386.
- [47] E. König, K. Madeja, *Chem. Commun. (London)* **1966**, 61–62.
- [48] P. Gütlich, *Z. anorg. allg. Chem.* **2012**, *638*, 15–43.

- [49] P. Gütlich, R. Link, A. X. Trautwein in *Mössbauer Spectroscopy and Transition Metal Chemistry*, Inorganic Chemistry Concepts, Springer Berlin Heidelberg, Berlin, Heidelberg, **1978**.
- [50] L. G. Lavrenova, O. G. Shakirova, *Eur. J. Inorg. Chem.* **2013**, *2013*, 670–682.
- [51] A. Gaspar, M. Seredyuk, P. Gütlich, *Coord. Chem. Rev.* **2009**, *253*, 2399–2413.
- [52] M. J. O'Neill, *Anal. Chem.* **1964**, *36*, 1238–1245.
- [53] B. Weber in *Spin-Crossover Materials*, (Hrsg.: L. a. Halcrow), John Wiley & Sons Ltd, **2013**, S. 55–76.
- [54] C. Baldé, W. Bauer, E. Kaps, S. Neville, C. Desplanches, G. Chastanet, B. Weber, J. F. Létard, *Eur. J. Inorg. Chem.* **2013**, *2013*, 2744–2750.
- [55] B. Weber, *Coord. Chem. Rev.* **2009**, *253*, 2432–2449.
- [56] V. Petrouleas, J. .-P. Tuchagues, *Chem. Phys. Lett.* **1987**, *137*, 21–25.
- [57] J. S. Costa, C. Balde, C. Carbonera, D. Denux, A. Wattiaux, C. Desplanches, J.-P. Ader, P. Gütlich, J.-F. Létard, *Inorg. Chem.* **2007**, *46*, 4114–4119.
- [58] L. A. Barrios, E. Peyrecave-Lleixà, G. A. Craig, O. Roubeau, S. J. Teat, G. Aromí, *Eur. J. Inorg. Chem.* **2014**, *2014*, 6013–6021.
- [59] W. A. Baker, H. M. Bobonich, *Inorg. Chem.* **1964**, *3*, 1184–1188.
- [60] N. Moliner, M. C. Muñoz, S. Létard, J.-F. Létard, X. Solans, R. Burriel, M. Castro, O. Kahn, J. A. Real, *Inorg. Chim. Acta* **1999**, *291*, 279–288.
- [61] S. Zheng, M. A. Siegler, O. Roubeau, S. Bonnet, *Inorg. Chem.* **2014**, *53*, 13162–13173.
- [62] R. W. Hogue, R. G. Miller, N. G. White, H. L. C. Feltham, G. N. L. Jameson, S. Brooker, *Chem. Commun.* **2014**, *50*, 1435–1437.
- [63] J.-F. Létard, G. Chastanet, P. Guionneau, C. Desplanches in *Spin-Crossover Materials*, (Hrsg.: L. a. Halcrow), John Wiley & Sons Ltd, **2013**, S. 475–506.
- [64] K. S. Murray in *Spin-Crossover Materials*, (Hrsg.: L. a. Halcrow), John Wiley & Sons Ltd, **2013**, S. 1–54.
- [65] S. Hayami, Z.-z. Gu, M. Shiro, Y. Einaga, A. Fujishima, O. Sato, *J. Am. Chem. Soc.* **2000**, *122*, 7126–7127.

- [66] M. W. Meisel, A. Hauser, C. Achim, M. Shatruk, *Chem. Eur. J.* **2012**, *18*, 15805–15815.
- [67] R. W. Hogue, R. G. Miller, N. G. White, H. L. C. Feltham, G. N. L. Jameson, S. Brooker, *Chem. Commun.* **2013**, *50*, 1435–1437.
- [68] A. B. Gaspar, V. Ksenofontov, J. A. Real, P. Gütlich, *Chem. Phys. Lett.* **2003**, *373*, 385–391.
- [69] J. Krober, E. Codjovi, O. Kahn, F. Groliere, C. Jay, *Journal of the American Chemical Society* **1993**, *115*, 9810–9811.
- [70] J. A. Real, I. Castro, A. Bousseksou, M. Verdaguer, R. Burriel, M. Castro, J. Linares, F. Varret, *Inorg. Chem.* **1997**, *36*, 455–464.
- [71] A. B. Gaspar, V. Ksenofontov, H. Spiering, S. Reiman, J. A. Real, P. Gütlich, *Hyperfine Interactions* **2002**, *144-145*, 297–306.
- [72] M. H. Klingele, B. Moubaraki, K. S. Murray, S. Brooker, *Chem. Eur. J.* **2005**, *11*, 6962–6973.
- [73] C. F. Herold, L. M. Carrella, E. Rentschler, *Eur. J. Inorg. Chem.* **2015**, *2015*, 3632–3636.
- [74] M. H. Klingele, S. Brooker, *Coord. Chem. Rev.* **2003**, *241*, 119–132.
- [75] International Tables for Crystallography, (Hrsg.: T. Hahn, International Union of Crystallography), Springer, Dordrecht, 5. ed., reprinted with corrections, **2005**, 911 S.
- [76] S. Brooker, R. G. Miller, S. Narayanaswamy, J. Tallon, *New J. Chem.* **2014**, DOI 10.1039/C3NJ01451G.
- [77] C. Ambrus, P. Tregenna-Piggott, N. Amstutz, E. Krausz, A. Hauser, *Coord. Chem. Rev.* **2007**, *251*, 364–378.
- [78] J. N. Hamann, M. Rolf, F. Tuczek, *Dalton Trans.* **2015**, *44*, 3251–3258.
- [79] A. Requet, O. Colin, F. Bourdreux, S. M. Salim, S. Marque, C. Thomassigny, C. Greck, J. Farjon, D. Prim, *Magn. Reson. Chem.* **2014**, *52*, 273–278.
- [80] A. Kondo, T. Satomi, K. Azuma, R. Takeda, K. Maeda, *Dalton Trans.* **2015**, *44*, 12717–12725.

- [81] K. Maeda, Y. Kiyozumi, F. Mizukami, *J. Phys. Chem. B* **1997**, *101*, 4402–4412.
- [82] H. Tan, W. Chen, D. Liu, X. Feng, Y. Li, A. Yan, E. Wang, *Dalton Trans.* **2011**, *40*, 8414–8418.
- [83] E. Fernández-Zapico, J. Montejo-Bernardo, A. Fernández-González, J. R. García, S. García-Granda, *J. Solid State Chem.* **2015**, *225*, 285–296.
- [84] P. J. Hagrman, D. Hagrman, J. Zubieta, *Angew. Chem. Int. Ed.* **1999**, *38*, 2638–2684.
- [85] A. K. Cheetham, C. N. R. Rao, R. K. Feller, *Chem. Commun.* **2006**, 4780–4795.
- [86] G. Alberti, U. Costantino, S. Allulli, N. Tomassini, *J. Inorg. Nucl. Chem.* **1978**, *40*, 1113–1117.
- [87] C. Janiak, *Dalton Trans.* **2003**, 2781–2804.
- [88] A. K. Cheetham, G. Férey, T. Loiseau, *Angew. Chem. Int. Ed.* **1999**, *38*, 3268–3292.
- [89] T. Yamase, H. Naruke, *J. Chem. Soc. Dalton Trans.* **1991**, 285–292.
- [90] A.-M. Pütz, Diss., Universitätsbibliothek Mainz, **2010**.
- [91] M. Andruh, J.-P. Costes, C. Diaz, S. Gao, *Inorg. Chem.* **2009**, *48*, 3342–3359.
- [92] J.-W. Cheng, J. Zhang, S.-T. Zheng, M.-B. Zhang, G.-Y. Yang, *Angew. Chem. Int. Ed.* **2006**, *45*, 73–77.
- [93] L. Bogani, C. Sangregorio, R. Sessoli, D. Gatteschi, *Angew. Chem. Int. Ed.* **2005**, *44*, 5817–5821.
- [94] B. Zhao, X.-Y. Chen, P. Cheng, D.-Z. Liao, S.-P. Yan, Z.-H. Jiang, *J. Am. Chem. Soc.* **2004**, *126*, 15394–15395.
- [95] Y. Bing, N. Xu, W. Shi, K. Liu, P. Cheng, *Chem. Asian J.* **2013**, *8*, 1412–1418.
- [96] S. Jones, J. M. Vargas, S. Pellizzeri, C. J. O'Connor, J. Zubieta, *Inorg. Chim. Acta* **2013**, *395*, 44–57.
- [97] O. Kahn, *Science* **1998**, *279*, 44–48.
- [98] A. J. Blake, N. R. Champness, M. Crew, S. Parsons, *New J. Chem.* **1999**, *23*, 13–15.

- [99] N. Masciocchi, F. Castelli, P. M. Forster, M. M. Tafoya, A. K. Cheetham, *Inorg. Chem.* **2003**, *42*, 6147–6152.
- [100] A. de Bettencourt-Dias, *Inorg. Chem.* **2005**, *44*, 2734–2741.
- [101] R. W. Gable, B. F. Hoskins, R. Robson, *Chem. Commun.* **1990**, 762.
- [102] L. Carlucci, G. Ciani, D. M. Proserpio, A. Sironi, *Angew. Chem. Int. Ed.* **1995**, *34*, 1895–1898.
- [103] M. Eddaoudi, D. B. Moler, H. Li, B. Chen, T. M. Reineke, M. O’Keeffe, O. M. Yaghi, *Acc. Chem. Res.* **2001**, *34*, 319–330.
- [104] Y. Pei, M. Verdaguer, O. Kahn, J. Sletten, J. P. Renard, *Inorg. Chem.* **1987**, *26*, 138–143.
- [105] P. M. Forster, P. M. Thomas, A. K. Cheetham, *Chem. Mater.* **2002**, *14*, 17–20.
- [106] N. Stock, T. Bein, *J. Mater. Chem.* **2005**, *15*, 1384–1391.
- [107] P. M. Forster, A. R. Burbank, C. Livage, G. Férey, A. K. Cheetham, *Chem. Commun.* **2004**, 368–369.
- [108] R. A. LAUDISE, *Chem. Eng. News Archive* **1987**, *65*, 30–43.
- [109] T.-H. Zhou, Z.-Z. He, X. Xu, X.-Y. Qian, J.-G. Mao, *Cryst. Growth Des.* **2012**.
- [110] C. A. Merrill, A. K. Cheetham, *Inorg. Chem.* **2005**, *44*, 5273–5277.
- [111] R. Sessoli, *Angew. Chem. Int. Ed.* **2012**, *51*, 43–45.
- [112] D. Gatteschi, R. Sessoli, J. Villain, *Molecular Nanomagnets*, OUP Oxford, **2011**, 762 S.
- [113] Z. Wang, B. Zhang, H. Fujiwara, H. Kobayashi, M. Kurmoo, *Chem. Commun.* **2004**, 416–417.
- [114] M. Kurmoo, *Chem. Soc. Rev.* **2009**, *38*, 1353–1379.
- [115] L. D. Carlos, R. A. S. Ferreira, V. d. Z. Bermudez, B. Julián-López, P. Escribano, *Chem. Soc. Rev.* **2011**, *40*, 536–549.
- [116] M. Pramanik, M. Nandi, H. Uyama, A. Bhaumik, *Catal. Sci. Technol.* **2012**, *2*, 613–620.

- [117] K. Maeda, *Microporous Mesoporous Mater.*, Metal-Organic Open Frameworks **2004**, *73*, 47–55.
- [118] Q. Fang, G. Zhu, M. Xue, J. Sun, F. Sun, S. Qiu, *Inorg. Chem.* **2006**, *45*, 3582–3587.
- [119] X. Guo, G. Zhu, Q. Fang, M. Xue, G. Tian, J. Sun, X. Li, S. Qiu, *Inorg. Chem.* **2005**, *44*, 3850–3855.
- [120] A. Michaelis, R. Kaehne, *Ber. Dtsch. Chem. Ges.* **1898**, *31*, 1048–1055.
- [121] P.-A. Jaffrès, N. Bar, D. Villemin, *J. Chem. Soc. Perkin Trans. 1* **1998**, 2083–2090.
- [122] V. Penicaud, F. Odobel, B. Bujoli, *Tetrahedron Lett.* **1998**, *39*, 3689–3692.
- [123] G. Guerrero, J. G. Alauzun, M. Granier, D. Laurencin, P. H. Mutin, *Dalton Trans.* **2013**, *42*, 12569–12585.
- [124] P. DeBurgomaster, H. Liu, C. J. O'Connor, J. Zubieta, *Inorg. Chim. Acta* **2010**, *363*, 1654–1658.
- [125] A. Rabenau, *Angew. Chem. Int. Ed. Engl.* **1985**, *24*, 1026–1040.
- [126] J. Gopalakrishnan, *Chem. Mater.* **1995**, *7*, 1265–1275.
- [127] J. Gopalakrishnan, N. S. Bhuvanesh, K. K. Rangan, *Curr. Opin. Solid State Mater. Sci.* **1996**, *1*, 285–294.
- [128] T.-T. Wang, M. Ren, S.-S. Bao, M. Zheng, *Eur. J. Inorg. Chem.* **2014**, *2014*, 1042–1050.
- [129] V. Chandrasekhar, D. Sahoo, R. S. Narayanan, R. J. Butcher, F. Lloret, E. Pardo, *Dalton Trans.* **2013**, *42*, 8192.
- [130] V. Chandrasekhar, T. Senapati, A. Dey, S. Hossain, *Dalton Trans.* **2011**, *40*, 5394.
- [131] V. Chandrasekhar, T. Senapati, A. Dey, E. C. Sañudo, *Inorg. Chem.* **2011**, *50*, 1420–1428.
- [132] V. Chandrasekhar, L. Nagarajan, *Dalton Trans.* **2009**, 6712.
- [133] S. Khanra, S. Konar, A. Clearfield, M. Helliwell, E. J. L. McInnes, E. Tolis, F. Tuna, R. E. P. Winpenny, *Inorg. Chem.* **2009**, *48*, 5338–5349.



- [134] S. Langley, M. Helliwell, R. Sessoli, S. J. Teat, R. E. P. Winpenny, *Inorganic Chemistry* **2008**, *47*, 497–507.
- [135] G. Cao, V. M. Lynch, J. S. Swinnea, T. E. Mallouk, *Inorg. Chem.* **1990**, *29*, 2112–2117.
- [136] Y.-S. Ma, H. Li, J.-J. Wang, S.-S. Bao, R. Cao, Z. Li, J. Ma, M. Zheng, *Chem. Eur. J.* **2007**, *13*, 4759–4769.
- [137] H. Ma, O. Acton, D. O. Hutchins, N. Cernetic, A. K.-Y. Jen, *Phys. Chem. Chem. Phys.* **2012**, *14*, 14110–14126.
- [138] M. L. Jespersen, C. E. Inman, G. J. Kearns, E. W. Foster, J. E. Hutchison, *J. Am. Chem. Soc.* **2007**, *129*, 2803–2807.
- [139] H. Klauk, U. Zschieschang, J. Pflaum, M. Halik, *Nature* **2007**, *445*, 745–748.
- [140] Y. Zhou, J. W. Shim, C. Fuentes-Hernandez, A. Sharma, K. A. Knauer, A. J. Giordano, S. R. Marder, B. Kippelen, *Phys. Chem. Chem. Phys.* **2012**, *14*, 12014–12021.
- [141] D. Kälblein, R. T. Weitz, H. J. Böttcher, F. Ante, U. Zschieschang, K. Kern, H. Klauk, *Nano Lett.* **2011**, *11*, 5309–5315.
- [142] S. Tanase, J. Reedijk, *Coord. Chem. Rev.* **2006**, *250*, 2501–2510.
- [143] A. Bencini, C. Benelli, A. Caneschi, R. L. Carlin, A. Dei, D. Gatteschi, *J. Am. Chem. Soc.* **1985**, *107*, 8128–8136.
- [144] J. A. Sheikh, S. Goswami, S. Konar, *Dalton Trans.* **2014**, *43*, 14577–14585.
- [145] K. Liu, W. Shi, P. Cheng, *Coord. Chem. Rev.*, Progress in Magnetochemistry **2015**, *289?290*, 74–122.
- [146] A. Clearfield, Z. Wang, *Dalton Trans.* **2002**, 2937–2947.
- [147] K. D. Paul DeBurgomaster, *Inorg. Chim. Acta* **2010**, *364*, 150–156.
- [148] R. A. Palmer, T. S. Piper, *Inorg. Chem.* **1966**, *5*, 864–878.
- [149] F. Odobel, B. Bujoli, D. Massiot, *Chem. Mater.* **2001**, *13*, 163–173.
- [150] I. Gillaizeau-Gauthier, F. Odobel, M. Alebbi, R. Argazzi, E. Costa, C. A. Bignozzi, P. Qu, G. J. Meyer, *Inorg. Chem.* **2001**, *40*, 6073–6079.

- [151] H. Zabri, I. Gillaizeau, C. A. Bignozzi, S. Caramori, M.-F. Charlot, J. Cano-Boquera, F. Odobel, *Inorg. Chem.* **2003**, *42*, 6655–6666.
- [152] J. C. Cobas, F. J. Sardina, *Concepts Magn. Reson.* **2003**, *19A*, 80–96.
- [153] O. V. Dolomanov, L. J. Bourhis, R. J. Gildea, J. A. K. Howard, H. Puschmann, *J. Appl. Cryst.* **2009**, *42*, 339–341.
- [154] N. F. Chilton, R. P. Anderson, L. D. Turner, A. Soncini, K. S. Murray, *J. Comput. Chem.* **2013**, *34*, 1164–1175.

## A. Abbreviations

SCO	Spin crossover
ST	Spin transition
LS	low-spin
HS	high-spin
$\Delta$	Ligand field splitting
$\Delta_{crit}$	Critical ligand field splitting
$P$	Spin pairing energy
$\Delta E_{HL}^0$	Zero-point energy difference
$\Delta G$	Gibbs free energy difference
$\Delta H$	Enthalpy difference
$\Delta S$	Entropy difference
$T_{1/2}$	Transition temperature
LIESST	Light-Induced Excited Spin-State Trapping
$\gamma_{HS}$	High-spin fraction
$\chi(T)$	Magnetic susceptibility as a function of the temperature
SQUID	Superconducting QUantum Interference Device
phen	1,10-Phenanthroline
NCS	Thiocyanate
NCSe	Selenocyanate
$CN^-$	Cyanide
SMMs	Single-molecule magnets
$\Gamma$	Lorentzian line width
bt	2,2'-bi-2-thiazoline
K	Kelvin

## Appendix A. Abbreviations

---

DSC	Differential scanning calorimetry
UV/Vis	Ultraviolet/visible
IR	Infrared
cm <sup>-1</sup>	Wavenumber
PMAT	4-Amino-3,5-bis{[(2-pyridylmethyl)amino]methyl}- 4H-1,2,4-triazole
PMATS	2,5-bis{[(2-pyridylmethyl)amino]methyl}- 4H-1,3,4-thiadiazole
PMAP	3,5-Bis{[(2-pyridylmethyl)amino]methyl}-pyrazole
$\Sigma$	Octahedral distortion parameter
NMR	Nuclear magnetic resonance
ppm	Parts per million (10 <sup>-6</sup> )
ESI-MS	Electrospray ionization mass spectrometry
FD-MS	Field desorption mass spectrometry
MeOH	Methanol
DMSO	Dimethylsulfoxide
DMF	N,N-Dimethylformamide
MeCN	Acetonitrile
THF	Tetrahydrofuran
m/z	Mass-to-charge ratio
<i>g</i> -value	Landé factor
<i>J</i>	Exchange parameter
<i>D</i>	Zero-field splitting parameter
<i>TIP</i>	Temperature independent paramagnetism
py	pyridine
MOF	Metal organic framework
CP	Coordination polymer
SBU	Secondary building unit
H <sub>4</sub> L	2,2'-bipyridinyl-5,5'-diphosphonic acid
(CN) <sub>2</sub> N <sup>-</sup>	Dicyanamide
$\delta$	Isomer shift
$\Delta E_Q$	Quadrupole splitting

## B. NMR Spectra

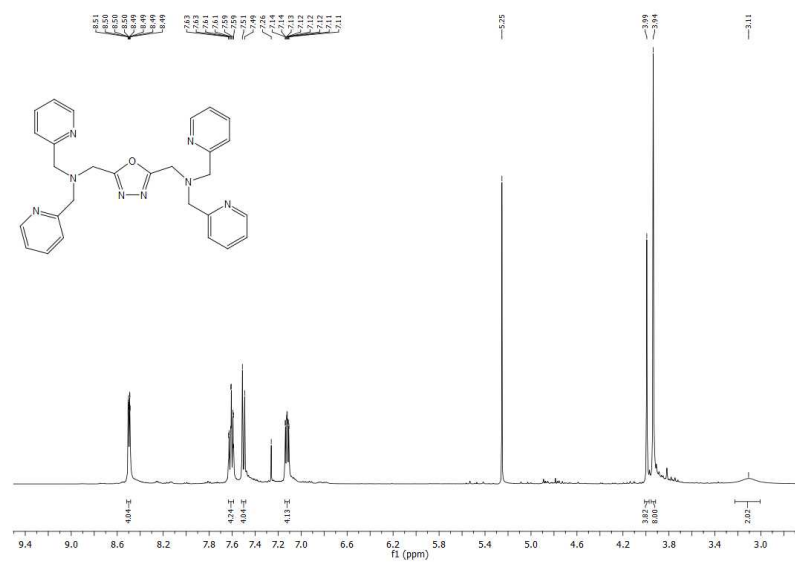


Figure B.1.: <sup>1</sup>H-NMR spectrum of **L2** 2,5-bis([N-(dipyridin-2-ylmethyl)amino]methyl)-1,3,4-oxadiazole

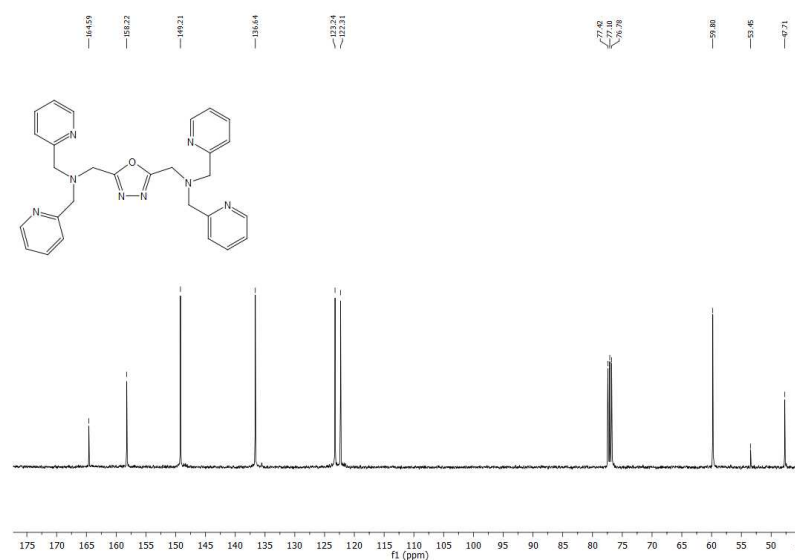


Figure B.2.: <sup>13</sup>C-NMR spectrum of **L2** 2,5-bis([N-(dipyridin-2-ylmethyl)amino]methyl)-1,3,4-oxadiazole

## Appendix B. NMR Spectra

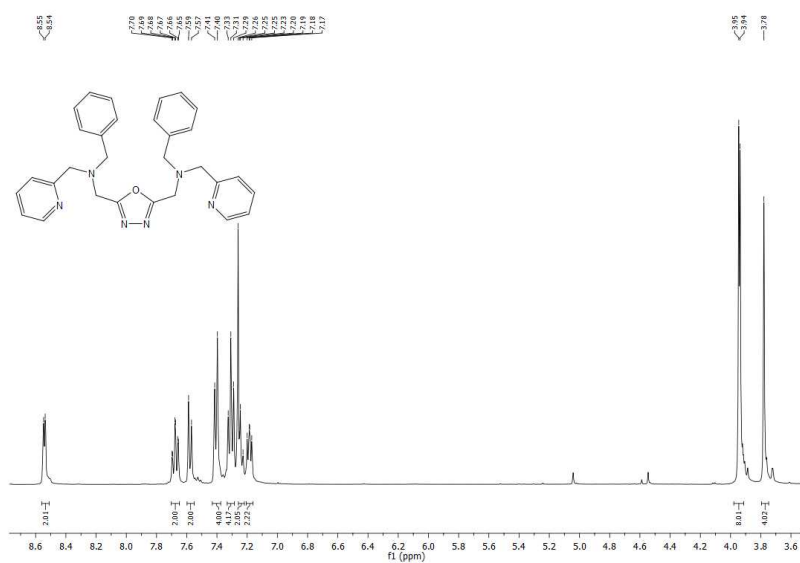


Figure B.3.:  $^1\text{H-NMR}$  spectrum of **L3** 2,5-bis([(N-benzyl-N-pyridin-2-ylmethyl)-amino]methyl)-1,3,4-oxadiazole

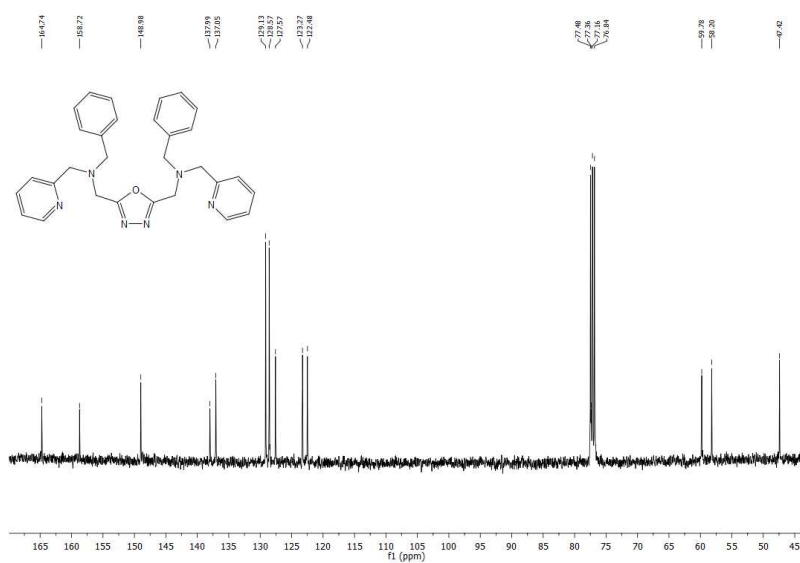


Figure B.4.:  $^{13}\text{C-NMR}$  spectrum of **L3** 2,5-bis([(N-benzyl-N-pyridin-2-ylmethyl)-amino]methyl)-1,3,4-oxadiazole

## **C. Crystallographic Parameters**

Table C.1.: Crystallographic parameters for compounds **10** - **12**

Compound	<b>10</b>	<b>11</b>	<b>12</b>
Empirical formula	C <sub>30</sub> H <sub>23</sub> ClCoLaN <sub>6</sub> NaO <sub>28.25</sub> P <sub>6</sub>	C <sub>10</sub> H <sub>15</sub> Cl <sub>2</sub> N <sub>2</sub> O <sub>11</sub> P <sub>2</sub> Tb	C <sub>20</sub> H <sub>23</sub> Cl <sub>2</sub> DyN <sub>4</sub> O <sub>16</sub> P <sub>4</sub>
$F_W$	1361.64	631	932.7
$T / K$	173.15	173.15	173.15
Crystal system	monoclinic	orthorhombic	triclinic
Space group	C2	Pcab	P-1
$a / \text{Å}$	21.568(2)	8.011(5)	10.9249(14)
$b / \text{Å}$	16.0857(13)	17.701(5)	12.1090(15)
$c / \text{Å}$	15.2558(14)	28.300(5)	12.6462(16)
$\alpha / ^\circ$	90	90	78.765(3)
$\beta / ^\circ$	107.000(3)	90	75.628(3)
$\gamma / ^\circ$	90	90	85.502(3)
$V / \text{Å}^3$	5061.5(8)	4013(3)	1588.8(3)
$Z$	4	8	2
$\rho_{calc} / \text{g cm}^3$	1.787	2.089	1.972
$\mu / \text{mm}^{-1}$	1.506	4.006	2.705
$F(000)$	2692	2448	918
$2\theta / ^\circ$	2.792-55.752	2.878-56.126	3.38-55.922
GOF $F^2$	0.984	1.285	0.914
Final $R (I \geq 2\sigma(I))$	$R_1 = 0.0691, wR_2 = 0.1375$	$R_1 = 0.0548, wR_2 = 0.1078$	$R_1 = 0.0439, wR_2 = 0.0902$
Final $R$ (all data)	$R_1 = 0.1213, wR_2 = 0.1627$	$R_1 = 0.0695, wR_2 = 0.1113$	$R_1 = 0.0820, wR_2 = 0.0982$



Table C.2.: Crystallographic parameters for compounds **13** - **15**

Compound	<b>13</b>	<b>14</b>	<b>15</b>
Empirical formula	C <sub>54</sub> H <sub>69</sub> Cl <sub>1.98</sub> FeN <sub>6</sub> O <sub>25.92</sub> P <sub>6</sub>	C <sub>30</sub> H <sub>23</sub> ClCoLaN <sub>6</sub> NaO <sub>28.25</sub> P <sub>6</sub>	C <sub>240</sub> Co <sub>8</sub> Gd <sub>8</sub> N <sub>48</sub> Na <sub>4</sub> O <sub>232</sub> P <sub>48</sub> ClH
$F_W$	1528.73	1361.64	10611.3
$T/K$	363.15	173.15	296.15
Crystal system	trigonal	monoclinic	monoclinic
Space group	R-3	C2	C2/c
$a / \text{Å}$	17.0378(14)	21.568(2)	28.1024(15)
$b / \text{Å}$	17.038	16.0857(13)	16.8298(8)
$c / \text{Å}$	45.535(4)	15.2558(14)	26.7835(14)
$\alpha / ^\circ$	90	90	90
$\beta / ^\circ$	90	107.000(3)	121.5220(10)
$\gamma / ^\circ$	120	90	90
$V / \text{Å}^3$	11447(2)	5061.5(8)	10798.2(10)
$Z$	6	4	1
$\rho_{calc} / \text{g cm}^3$	1.331	1.787	1.632
$\mu / \text{mm}^{-1}$	0.467	1.506	1.802
$F(000)$	4752	2692	5142
$2\theta / ^\circ$	2.684-55.902	2.792-55.752	2.958-56.02
GOF $F^2$	0.961	0.984	1.042
Final $R (I \geq 2\sigma(I))$	$R_1 = 0.0825, wR_2 = 0.2392$	$R_1 = 0.0691, wR_2 = 0.1375$	$R_1 = 0.0830, wR_2 = 0.2373$
Final $R$ (all data)	$R_1 = 0.1739, wR_2 = 0.2776$	$R_1 = 0.1213, wR_2 = 0.1627$	$R_1 = 0.1172, wR_2 = 0.2705$

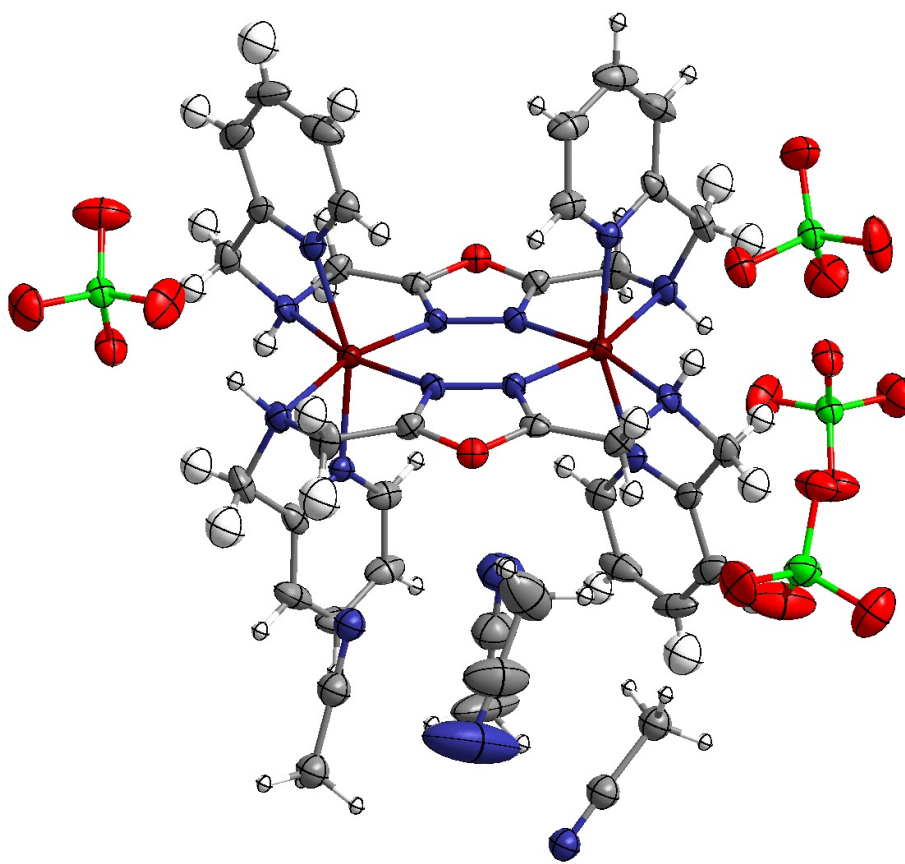


Figure C.1.: Molecular structure of **C4** ( $[\text{Co}(\text{II})_2\mu_2\text{L}_2](\text{ClO}_4)_4 \cdot 4\text{MeCN}$ ) at 193 K with thermal ellipsoids. Colour scheme: dark red - Co(II), red - O, blue - N, gray - C, white - H, green - Cl

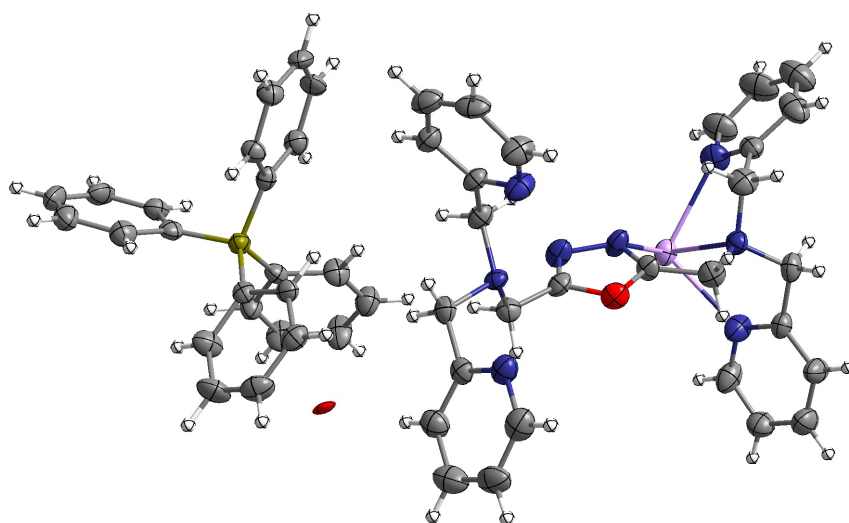


Figure C.2.: Molecular structure of **C4** ( $[\text{NaL}_2]\text{BPh}_4 \cdot 0.25\text{H}_2\text{O}$ ) at 173 K with thermal ellipsoids. Color code: purple - sodium, red - oxygen, deep blue - nitrogen, gray - carbon, dark yellow - boron.

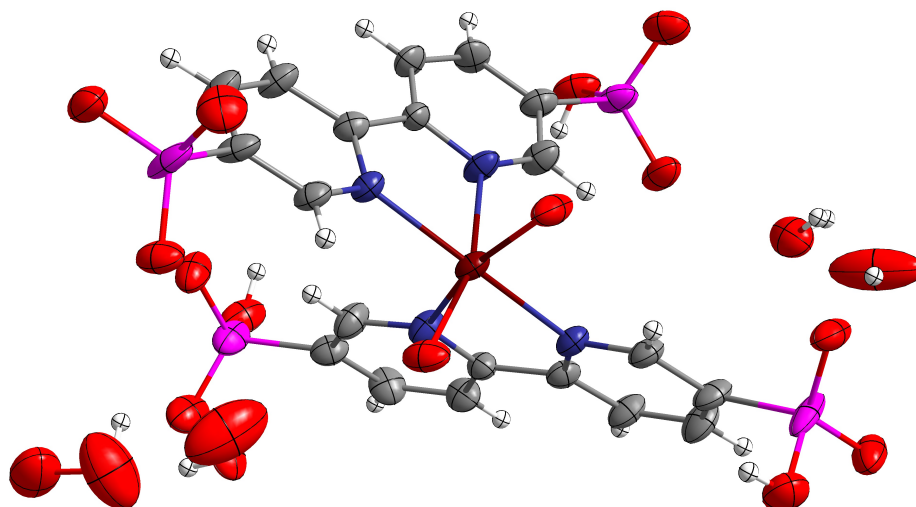


Figure C.3.: Molecular structure of **10** ( $[\text{Co}(\text{II})(\mu_2\text{-}\eta_2\text{-H}_3\text{L})_2] \cdot 6\text{H}_2\text{O}$ ) at 173 K with thermal ellipsoids. Color code: dark red - cobalt, pink - phosphorus, red - oxygen, dark blue - nitrogen, gray - carbon, white - hydrogen.

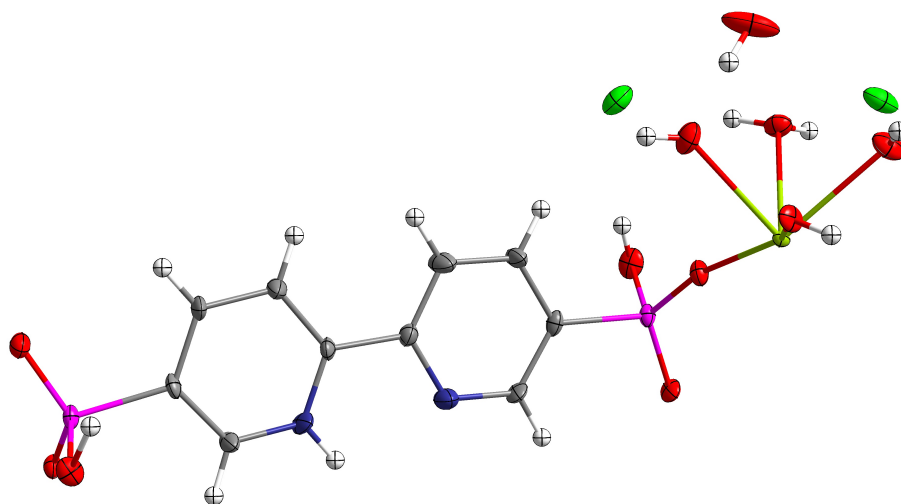


Figure C.4.: Molecular structure of **11** ( $[\text{Tb}(\mu_4\text{-H}_2\text{H}^M)(\text{H}_2\text{O})_4]\text{Cl}_2 \cdot \text{H}_2\text{O}$ ) at 173 K with thermal ellipsoids. Color code: yellow - terbium, green - chlorine, pink - phosphorus, red - oxygen, dark blue - nitrogen, gray - carbon, white - hydrogen.

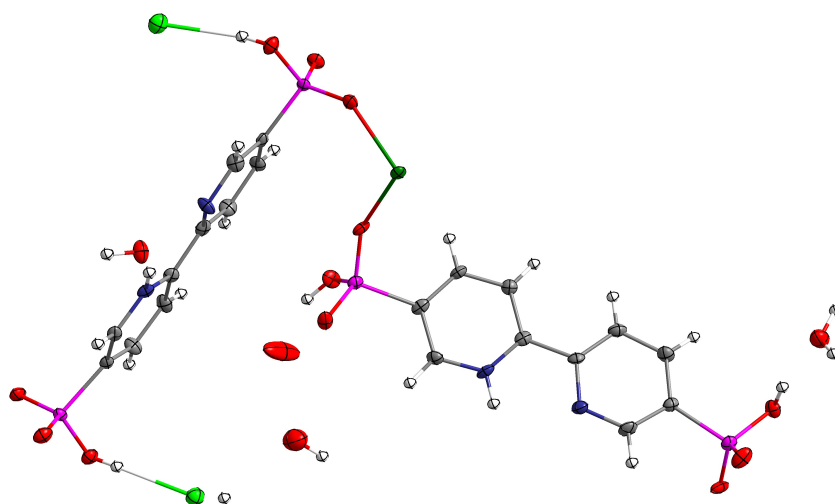


Figure C.5.: Molecular structure of **12** ( $[\text{Dy}(\text{H}_2\text{H}^M)_2]\text{ClHCl} \cdot 4\text{H}_2\text{O}$ ) at 173 K with thermal ellipsoids. Color code: dark green - dysprosium, green - chlorine, pink - phosphorus, red - oxygen, dark blue - nitrogen, gray - carbon, white - hydrogen.

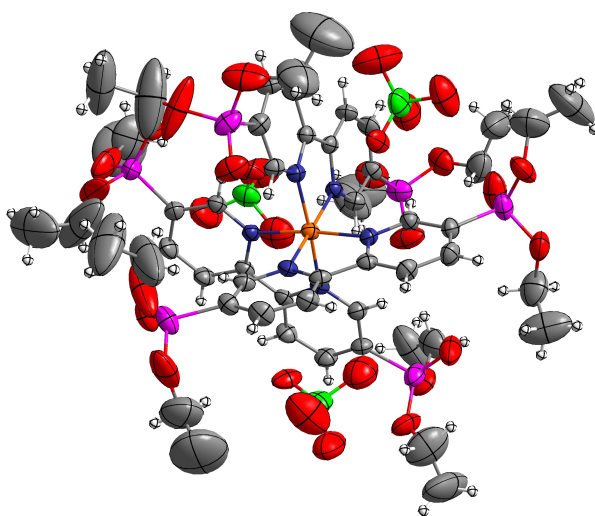


Figure C.6.: Molecular structure of **13** ( $[\text{Fe}(\text{II})((\text{EtO})_4\text{L})_3](\text{BF}_4)_2$ ) at 173 K with thermal ellipsoids. Color code: orange - iron, green - chlorine, pink - phosphorus, red - oxygen, dark blue - nitrogen, gray - carbon, white - hydrogen.

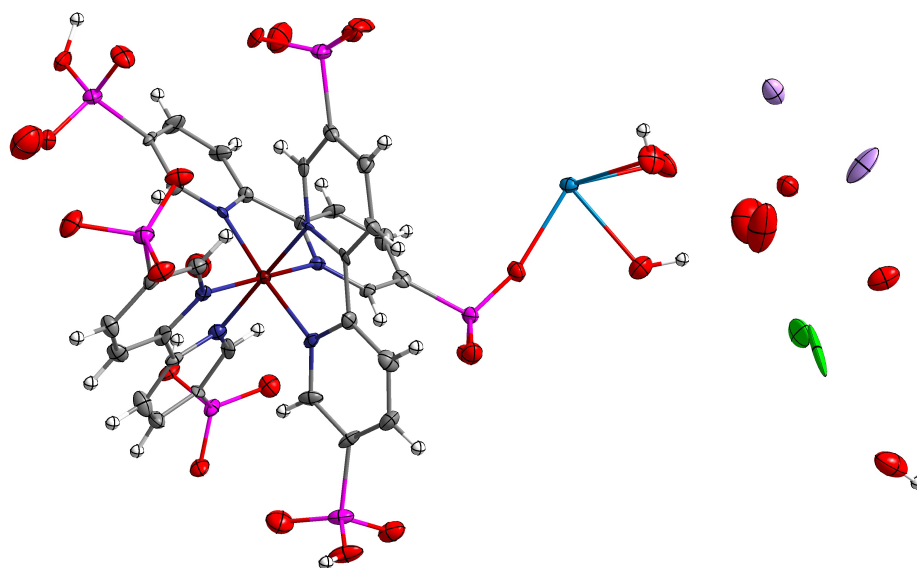


Figure C.7.: Molecular structure of **14** ( $[\text{LaCo}(\text{III})(\text{H}_2\text{L})_3(\text{H}_2\text{O})_3]\text{NaCl}$ ) at 173 K with thermal ellipsoids. Color code: blue - lanthanum, dark red - cobalt, green - chlorine, purple - sodium, pink - phosphorus, red - oxygen, dark blue - nitrogen, gray - carbon, white - hydrogen.

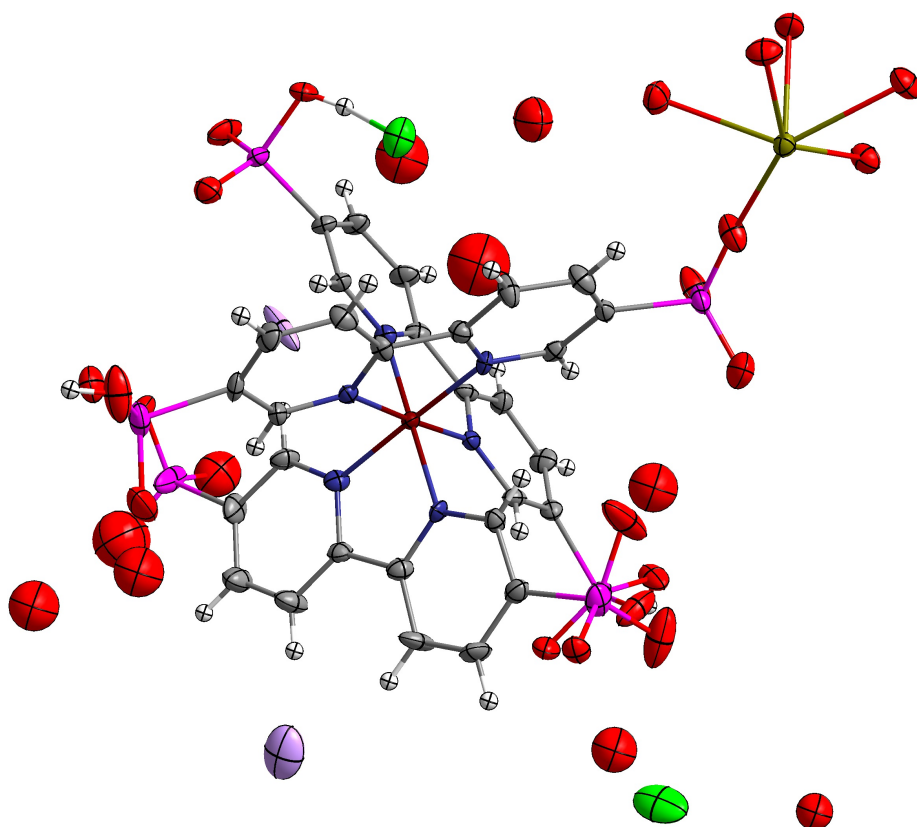


Figure C.8.: Molecular structure of **15** ( $[\text{GdCo(III)}(\text{H}_2\text{L})_3(\text{H}_2\text{O})_5]\text{NaCl}$ ) at 173 K with thermal ellipsoids. Color code: brown - gadolinium, dark red - cobalt, green - chlorine, purple - sodium, pink - phosphorus, red - oxygen, dark blue - nitrogen, gray - carbon, white - hydrogen.

## D. Curriculum Vitae

Name: Christian Köhler



[REDACTED]

[REDACTED]

### Education:

04/2013 - present **Doctoral Studies in Chemistry**

Doctoral Studies in the group of Prof. Dr. Eva Rentschler at the Institute of Inorganic and Analytical Chemistry at the Johannes Gutenberg University Mainz.

Topic of the Dissertation:

'Spin Crossover Behavior of 1,3,4-Oxadiazole Based Dinuclear Iron(II) Complexes' and 'Functionalized Phosphonates as Bridging Ligands in Inorganic-Organic Hybrid-Materials'

07/2012 - 03/2013 **Diploma thesis** [REDACTED]

[REDACTED]

[REDACTED]

04/2007 - 03/2013 **Chemistry Studies**

[REDACTED]  
[REDACTED]

04/2006 - 12/2006 **Military Service**

[REDACTED]

03/2006 **School**

[REDACTED]  
[REDACTED]

**Publications:**

- 11/2015 'The First 1,3,4-Oxadiazole Based Dinuclear Iron(II) Complexes Showing Spin Crossover Behavior With Hysteresis' by Christian Köhler and Eva Rentschler. European Journal of Inorganic Chemistry, DOI:10.1002/ejic.2015012786
- 05/2016 'Functionalized Phosphonates as Building Units for Multi-Dimensional Homo- and Heterometallic 3d-4f Inorganic-Organic Hybrid-Materials and their Magnetic Characterization' by Christian Köhler and Eva Rentschler. Dalton Transactions (submitted)